

**THE PHARMACOKINETICS AND PHARMACODYNAMICS
OF CNS-ACTING AGENTS**

by

Mohamed A. Kamal

A dissertation submitted in partial fulfillment
of the requirements for the degree of
Doctor of Philosophy
(Pharmaceutical Sciences)
in the University of Michigan
2008

Doctoral Committee:

Professor David E. Smith, Chair
Professor Richard F. Keep
Professor Victor C. Yang
Daniele Ouellet, Glaxo Smith-Kline
Jack A. Cook, Pfizer
Douglas Feltner, Pfizer

© Mohamed A. Kamal
All Rights Reserved
2008

PREFACE

“The greatest glory in living lies not in never falling but in rising every time we fall”

-Nelson Mandela, South African President and Human Rights Activist

The significance of this quote is that it defines greatness and success in how we as human beings handle hardship, failure, or unexpectedness in life. Persistence and perseverance are important qualities in a scientist, since the essence of scientific research almost always implies that our hypothesis may not be right the first time around. Moreover, these qualities are not only important for the success of a scientist in the workplace but for any human being in his or her personal life since life is unforeseeable and unpredictable.

The thesis presented herein has been completed in the Department of Pharmaceutical Sciences, College of Pharmacy, at the University of Michigan, Ann Arbor. The thesis is unique in that it has allowed me to explore and learn various aspects of drug disposition (pharmacokinetics) and drug action (pharmacodynamics), broadening my exposure to basic science aspects of pharmacology and the quantitative science aspects of clinical pharmacology. The half of the thesis related to the PEPT2 transporter system has enhanced my understanding of drug transporters and how a transporter may modulate the disposition of a drug substrate systemically or locally and how such modulation may translate to significant changes of drug pharmacodynamics at the biophase. Moreover, it has provided me with the experience in designing

pharmacokinetic studies and working with experimental animal models in the laboratory, the latter which I had not learned before.

The half of the thesis related to the utility of subjective continuous and ordinal pharmacodynamic scales in early CNS drug development has allowed me to build on the pharmacokinetic/pharmacodynamic (PK/PD) principles I learned while completing my PharmD at the University at Buffalo, extending my training in the pharmacostatistical and population aspects of PK/PD modeling and simulation. While different in theme, both sections of the split thesis cover an in-depth study of the pharmacokinetics and pharmacodynamics of Central Nervous System (CNS) agents.

TABLE OF CONTENTS

| | |
|--------------------------------|-------------|
| PREFACE..... | ii |
| LIST OF TABLES..... | viii |
| LIST OF FIGURES..... | ix |
| LIST OF APPENDICES..... | xii |

I. PHARMACOMETRIC UTILITY OF ORDERED CATEGORICAL AND CONTINUOUS PHARMACODYNAMIC SCALES IN EVALUATING LORAZEPAM SLEEPINESS AND DIZZINESS

CHAPTER 1- INTRODUCTION TO PART I

| | |
|-----------------------------------------------------------------|-----------|
| Subjective Pharmacodynamic Scales..... | 1 |
| Visual Analog Scale (VAS)..... | 1 |
| The Ordered Categorical (Ordinal) Scale..... | 4 |
| Comparison of Ordinal and Continuous Scales..... | 6 |
| Pharmacokinetic/Pharmacodynamic Applications..... | 7 |
| Nonlinear Mixed Effect Modeling (NONMEM)..... | 8 |
| SPLUS..... | 9 |
| Modeling Continuous versus Ordinal Data..... | 9 |
| Preliminary Pharmacodynamic Differentiation Profile..... | 11 |
| Pharmacokinetic Models..... | 14 |

| | |
|------------------------------|-----------|
| Study Rationale..... | 17 |
| Study Objectives..... | 18 |
| Tables..... | 19 |
| Figures..... | 22 |
| References..... | 27 |

**CHAPTER 2- UTILITY OF AN ORDERED CATEGORICAL
PHARMACODYNAMIC SCALE TO EVALUATE LORAZEPAM SLEEPINESS
AND DIZZINESS**

| | |
|--------------------------|-----------|
| Abstract..... | 30 |
| Introduction..... | 31 |
| Methods..... | 33 |
| Results..... | 41 |
| Discussion..... | 46 |
| Tables..... | 55 |
| Figures..... | 59 |
| References..... | 65 |

**CHAPTER 3- PHARMACOMETRIC ANALYSES OF A CONTINUOUS VISUAL-
ANALOG MEASURE OF LORAZEPAM SLEEPINESS**

| | |
|--------------------------|-----------|
| Abstract..... | 67 |
| Introduction..... | 68 |
| Methods..... | 70 |
| Results..... | 74 |
| Discussion..... | 76 |
| Tables..... | 80 |
| Figures..... | 82 |
| References..... | 88 |

CHAPTER 4- CONCLUSION TO PART I

| | |
|-------------------------------------|-----------|
| Major Findings..... | 90 |
| Proposed Future Studies..... | 91 |

II. ROLE OF PEPT2 SYSTEM IN NEUROPEPTIDE DISPOSITION, DYNAMICS, AND TOXICITY.

CHAPTER 5- INTRODUCTION TO PART II

| | |
|-----------------------------------------------------------------------------------|------------|
| Proton-Coupled Oligopeptide Transporters (POTs)..... | 93 |
| POT Tissue and Cellular Localization..... | 95 |
| PEPT2 Transport Models..... | 97 |
| General Substrate Structure..... | 98 |
| Choroid-Plexus and the Blood-CSF Barrier..... | 99 |
| Structure and Function of the Choroid Plexus..... | 100 |
| Potential For Drug Delivery..... | 102 |
| Transporter Distribution at Choroid Plexus..... | 104 |
| Role of PEPT2 in Choroid Plexus Whole Tissue: <i>In Vitro</i> Studies..... | 105 |
| Role of PEPT2 in Peptide/Mimetic Disposition: <i>In Vivo</i> Studies..... | 106 |
| Figures..... | 109 |
| References..... | 114 |

CHAPTER 6- A PHYSIOLOGICAL PERSPECTIVE OF PEPT2: THE DISPOSITION OF L-CARNOSINE IN WILD-TYPE AND PEPT2 KNOCKOUT MICE

| | |
|-----------------------------------|------------|
| Abstract..... | 117 |
| Introduction..... | 118 |
| Materials and Methods..... | 120 |

| | |
|---------------------------------------------|----------------|
| Results..... | 125 |
| Discussion..... | 127 |
| Tables..... | 131 |
| Figures..... | 133 |
| References..... | 137 |
| CHAPTER 7- CONCLUSION TO PART II | |
| Major Findings..... | 139 |
| Proposed Future Studies..... | 140 |
| APPENDICES..... | 141 |

LIST OF TABLES

Table

| | |
|-----------------------------------------------------------------------------------------------------------------------------------------------------------------------------------------------------------------------------------------|-----|
| 1.1 Summary of noncompartmental pharmacokinetic parameter values (% CV) following administration of single dose of atomoxetine 80 mg, paroxetine 20 mg, olanzapine 10 mg and lorazepam 2 mg after single oral dose administration | 19 |
| 1.2 Summary of statistically significant results of the ANOVA analysis on VAS TACB (Time Average 0-12 hr Change from Baseline) endpoint of pairwise comparisons with placebo..... | 20 |
| 1.3 Summary of statistically significant results of the ANOVA analysis on Categorical TACB (Time Average 0-12 hr Change from Baseline) endpoint of pairwise comparisons with placebo..... | 21 |
| 2.1 Subject Demographics (n=20)..... | 55 |
| 2.2 Pharmacokinetic Parameters in Healthy Volunteers after a 2 mg Oral Dose of Lorazepam..... | 56 |
| 2.3 Categorical Sleepiness and Dizziness Pharmacodynamic Parameters in Healthy Volunteers after a 2 mg Oral Dose of Lorazepam or Placebo (n=20)..... | 57 |
| 2.4 Relationship of Data-Derived and Model-Derived PD Parameters to the Label Incidence of Sleepiness and Dizziness in Healthy Volunteers after Administration of a 2 mg Oral Dose of Lorazepam..... | 58 |
| 3.1 Subject Demographics (n=20)..... | 80 |
| 3.2 Pharmacodynamic Parameters in Healthy Volunteers after a 2 mg Oral Dose of Lorazepam..... | 81 |
| 6.1 Pharmacokinetic parameter estimates of L-carnosine after an IV bolus dose administration of drug at 1 nmol/g in PEPT2 ^{+/+} and PEPT2 ^{-/-} mice (n=10)..... | 131 |
| 6.2 Renal pharmacokinetics of L-carnosine in PEPT2 ^{+/+} and PEPT2 ^{-/-} mice (n=7)..... | 132 |
| H.1 Table of Final PK Parameter Estimates of Four Study CNS Drugs..... | 187 |

LIST OF FIGURES

Figure

- 1.1 Illustration of continuous Visual Analog Scales (VAS).....22
- 1.2 Illustration of 7- point ordered categorical scales.....23
- 1.3 The mean plasma concentration vs. time plots of the four study CNS drugs (Lorazepam 2 mg, Olanzapine 10 mg, Paroxetine 20 mg, and Atomoxetine 80 mg) after single oral dose administration in twenty healthy volunteers.....24
- 1.4 Mean VAS effect vs. time pharmacodynamic profiles of sleepiness, dizziness, nausea, and blurred vision measured in 20 healthy volunteers after administration of single oral dose of Lorazepam 2 mg, Olanzapine 10 mg, Paroxetine 20 mg, Atomoxetine 80 mg, and placebo.....25
- 1.5 Mean ordered categorical effect vs. time pharmacodynamic profiles of sleepiness, dizziness, nausea, and blurred vision measured in 20 healthy volunteers after administration of single oral dose of Lorazepam 2 mg, Olanzapine 10 mg, Paroxetine 20 mg, Atomoxetine 80 mg, and placebo.....26
- 2.1 Left Panel: Observed mean \pm SD and predicted mean plasma concentrations versus time after a 2mg oral dose of lorazepam in healthy volunteers (n=20). Right Panel: Observed Individual, mean, and predicted mean plasam concentrations versus Time.....59
- 2.2 Cumulative probability plots of reporting sleepiness and dizziness. $P_{\geq 1-5}$ is the cumulative probability of reporting an effect of at least minimum, mild, moderate, significant, and severe intensity on the categorical scale.....60
- 2.3 Ninety percent prediction intervals of sleepiness and dizziness scores in healthy volunteers as a function of time (n=20). Panel one shows lorazepam and placebo sleepiness, panel two lorazepam and placebo dizziness , and panel three lorazepam sleepiness and dizziness. Symbols indicate observed data, middle line indicates simulated data, and lower and upper lines indicate lower and upper prediction interval bounds.....61
- 2.4 Posterior distributions of MaxS and AUEC for lorazepam sleepiness and dizziness in healthy volunteers after a 2 mg oral dose of lorazepam(n=20). Line indicates mean observed value. MaxS is the maximum reported categorical score,

| | |
|------------------------------------------------------------------------------------------------------------------------------------------------------------------------------------------------------------------------------------------------------------------------------------------------------------------------------------------------------------------------------------------------------------------------------------|------------|
| AUEC is the area under the effect curve from 0h-24h..... | 63 |
| 2.5 Relationship between the probability and logistic domains..... | 64 |
| 3.1 A modified Visual Analog Scale used to measure sleepiness..... | 82 |
| 3.2 The time course of Lorazepam plasma concentrations after oral administration of a 2 mg dose in twenty healthy volunteers. B : Time course of Sleepiness measured on the VAS after administration of 2 mg Lorazepam. C : Counter-Clockwise Hystereisis on the Effect-Concentration plot denoting the lag in Sleepiness effect compared to plasma lorazepam concentrations..... | 83 |
| 3.3A Histograms showing the right skewed distribution of VAS sleepiness scores reported by 20 healthy subjects after after oral administration of a 2 mg dose at various time points (Time = 0, 0.5, 3, 4, 6, 12 hr)..... | 84 |
| 3.3B Histograms showing distribution of transformed VAS sleepiness scores reported by 20 healthy subjects after after oral administration of a 2 mg dose at various time points (Time = 0, 0.5, 3, 4, 6, 12 hr)..... | 85 |
| 3.4 Concordance and Residual Plots. (Top panel: Model applied to VAS Scores in the Untransformed Domain. Bottom Panel: Model applied to Transformed VAS scores in the Logistic Domain). A Predicted (PRED) VAS scores versus Observed (OBS). B Individual Predicted VAS Scores (IPRED) versus Observed (OBS) C Weighted Residuals (WRES) versus time. D Individual Weighted residuals versus Time..... | 86 |
| 3.5 Monte-Carlo Simulations of the VAS untransformed scores and transformed scores converted to the original scale..... | 87 |
| 5.1 Sequential models of peptide/ mimetic transport in the choroid plexus [A] and renal proximal tubule epithelium [B] by PEPT2 showing the concerted action of apical and basolateral transporters in creating the acidic microenvironment at the apical interface..... | 109 |
| 5.2 Schematic of the kidney and nephron functional unit. PEPT1 is localized in the S1 segment of the cortex (convoluted proximal tubule), while PEPT2 is localized in the later segment of the proximal tubule (corresponding to theS2-S3 segments of the outer medulla)..... | 110 |
| 5.3 Sites of the barriers of the nervous system. Specialized endothelial cells with tight junctions form the blood-brain barrier (BBB). Tight junctions of the choroidal epithelium and the arachnoid epithelium forms the blood-CSF barrier (BCSFB). ECF = extracellular fluid; CSF CSF=cerebrospinal fluid..... | 111 |

| | | |
|-----|-------------------------------------------------------------------------------------------------------------------------------------------------------------------------------------------------------------------------------------------------------------------------------------------------------------------------------------------------------------------------------------------------------------------------------------------|------------|
| 5.4 | Illustration of the the Blood-Brain and Blood-CSF Barriers. The leaky ependyma separates the CSF and extracellular fluid surrounding the brain parenchymal cells. PEPT2 (shown as P2) is localized on the apical side of the choroid plexus epithelium and acts to remove peptides/mimetics from the CSF into the choroid plexus..... | 112 |
| 5.5 | Structures of various substrates of PEPT2 under study. Glysar is a synthetic dipeptide, while L-carnosine, 5-ALA, and L-Kyotorphin are physiologically relevant dipetides. Cefadroxil is a peptide-mimetic amino-chehalosporin..... | 113 |
| 6.1 | The Plasma concentration-time profile of L-carnosine after IV bolus administration of drug at 1 nmol/g (mean ± SE, n=10) in PEPT2 ^{+/+} and PEPT2 ^{-/-} mice..... | 133 |
| 6.2 | Tissue-to-blood concentration ratios of L-carnosine in PEPT2 ^{+/+} and PEPT2 ^{-/-} mice as observed 30 min after IV bolus administration of drug at 1 nmol/g (mean ± SE, n=7)..... | 134 |
| 6.3 | L-Carnosine stability in kidney, urine and plasma samples from PEPT2 ^{+/+} and PEPT2 ^{-/-} mice as observed 30 min after IV bolus administration of drug at 1 nmol/g (mean ± SE, n=4)..... | 135 |
| 6.4 | Renal clearance of L-carnosine in PEPT2 ^{+/+} and PEPT2 ^{-/-} mice as observed 30 min after IV bolus administration of drug at 1 nmol/g (mean ± SE, n=7). The estimated GFR of 250 µl/min is indicated by a dashed line..... | 136 |
| A.1 | Top panel: cerebrospinal fluid (CSF)-to-plasma concentration ratios in PEPT2 null mice were 4.2, 5.6 and 7.3 times that of values in wild-type mice for glycylsarcosine (GlySar), cefadroxil and 5-aminolevulinic acid (ALA), respectively. Bottom panel: choroid plexus-to- CSF concentration ratios in PEPT2 null mice were 0.3, 0.07 and 0.09 times that of values in wild-type mice for GlySar, cefadroxil and ALA, respectively..... | 154 |
| A.2 | Schematic of how the proton-coupled oligopeptide transporter SLC15A2 (PEPT2 displayed as PT2) affects the distribution of 5-aminolevulinic acid (ALA) in different compartments of the brain The top-half of the figure represents a scenario in wild- type (WT) mice while the bottom-half of the figure represents a scenario in PEPT2-deficient (Null) mice..... | 155 |
| I.1 | PK model goodness-of-fit plots..... | 188 |

LIST OF APPENDICES

Appendix

| | |
|----------------------------------------------------------------------------------------------------|-----|
| A. Role and relevance of PEPT2 in Drug Disposition, Dynamics, and Toxicity... | 141 |
| B. NONMEM control streams for paroxetine, atomoxetine, lorazepam, and olanzapine PK models..... | 159 |
| C. NONMEM control streams of lorazepam sleepiness and dizziness categorical models..... | 163 |
| D. NONMEM control stream of VAS Sleepiness model..... | 167 |
| E. SPLUS nonparametric bootstrap code..... | 169 |
| F. Categorical sleepiness simulation code (SPLUS)..... | 170 |
| G. Categorical dizziness simulation code (SPLUS)..... | 179 |
| H. Table of final PK parameter estimates of four study CNS drugs..... | 187 |
| I. PK model goodness-of-fit plots..... | 188 |

PART I

**PHARMACOMETRIC UTILITY OF ORDERED CATEGORICAL AND
CONTINUOUS PHARMACODYNAMIC SCALES IN EVALUATING
LORAZEPAM SLEEPINESS AND DIZZINESS**

CHAPTER 1

INTRODUCTION TO PART I

Subjective Pharmacodynamic Scales

Subjective pharmacodynamic scales become important in drug development when a clinical effect of interest has no alternative objective measure. A good example is pain which has been measured in several analgesic trials using ordered categorical (e.g. none, mild, moderate or severe) and continuous subjective scales (marking a line with none on one end and worst imaginable on the other). In CNS drug development the reliance on subjective pharmacodynamic scales increases as clinical endpoints such as anxiety, mood, depression and sleepiness, for example are difficult to measure objectively. Examples of commonly used subjective scales in CNS drug development are Likert questionnaires which use a categorical scale and the continuous visual analog scale both of which can be modified to measure a number of subjective effects.

The Visual Analogue Scale

The Visual Analogue scale (VAS) is a continuous scale typically consisting of a 10-centimeter line anchored at both ends with words descriptive of the maximal and minimal extremes of the dimension being measured. Subjects are asked to indicate

specific feelings at the time by marking the line at the appropriate point between the two extreme statements. The scale is scored by measuring the distance from the minimal endpoint to the mark, on a predetermined measurement interval. The most commonly chosen interval is millimeters with a 10 centimeter line, producing a 100- point scale (McCormack et al, 1988). Although verbal labels define the endpoints of VAS, neither numbers nor intermediate labels are used to define intermediate points, as this may cause clustering of scores around a preferred digit leading to bias (Scott and Huskisson, 1974). Figure 1.1 shows a representation of the VAS scale.

The VAS is not a novel scale and was first used in psychological research as early as the 1920's (Hayes M. et al, 1921; Freyd M; 1923). Its widespread use in clinical research was stimulated by the work of Aitken & Zealley who used it to construct single item mood scales (Aitken and Zealley, 1970). They argued that words may fail to describe the 'exactness of the subjective experience' and that verbal rating scales imposed artificial categories on the continuous phenomena of feelings. They proposed that VAS offered a sensitivity of scoring which was impossible with digital and ordinal rating scales (Aitken et al 1969).

Most reports describing the use of VAS in the literature are validation studies. The majority of these studies focus on VAS developed to measure either mood or pain and assess validity by correlating VAS scores with the scores of an established scale (McCormack et al, 1988).

The re-test reliability of VAS was also established. Robinson et al (1975) asked subjects to rate their hunger on two occasions separated by a one hour interval, during a

fasting period in their study of the reliability of VAS-Hunger. The correlation between the two rating periods was very high ($r=0.92$, $P<0.001$).

The apparent simplicity of the VAS and its adaptability to a wide range of research settings has made it an attractive measurement option. Among its advantages proponents have claimed that VAS: 1) is simple and quick to construct (Ahles et al, 1984); 2) quick and easy to administer and score (Rampling et al, 1977); 3) suitable for frequent and repeated use (Rampling et al, 1977); 4) is easily understood by subjects (Morrison, 1983); 5) is very sensitive with a discriminating capacity superior to other scales (Scott & Huskisson, 1976); 5) require little motivation for completion by subjects (Rampling et al, 1977); 6) is suitable for use by untrained staff (Folstein & Luria, 1973); and 7) allows the use of numerical values suitable for statistical analysis (Robinson et al, 1975).

Despite the studies that advocate VAS as a valid, reliable, sensitive, and robust measurement instrument, some have highlighted difficulties associated with its use. Carlsson et al (1983) questioned the assumption that VAS is an easy scale to use by subjects pointing out that the VAS requires an ability to transform a complex subjective experience into a visuo-spatial display, involving perceptual judgment and accuracy. Older age and the loss of ability to think abstractly (Kremer et al, 1981), mental disorganization and confusion (Hornblow, 1976), and decline of perceptual skills and memory (Carlsson, 1983) have all been suggested as factors, which may contribute to respondent error. The reliability of the VAS may even change as a study progresses. For example, results of a study (Hornblow and Kidson, 1976) suggest that the ability to use VAS-Anxiety as a continuum and as a valid scale decreases as the psychiatric symptoms

of subjects become more severe. In contrast, when Carlsson (1983) explored the impact of learning, memory, and perceptual judgment on the reliability and validity of VAS, no relationship between these variables and the subject's ability to make reliable assessments on VAS-Pain were found. However these two studies measured different effects (anxiety versus pain), therefore alluding to the possibility that, depending on the effect measured as well as study conditions (i.e. absence or presence of altering medications and disease progression), and the reliability of VAS may be quite different.

Moreover, certain studies demonstrated that the same VAS could be treated differently by different populations. In their comparison of psychiatric patients and medical students on the VAS-Anxiety, Hornblow and Kidson (1976) found that, while medical students treated the scale as a continuum, patient scores were tri-modal, with clusters at the midpoint and extremes of scales, suggesting interpretation of the scale instructions may be different between varying populations.

Little and McPhail (1973) also pointed out that patients, while using the VAS-Depression as a repeated measure, scored the VAS to the maximum before completion of the study, leaving themselves no room to record a higher score should their mood worsen.

The above studies emphasize the importance of testing the suitability of VAS for the population to be assessed prior to application of the technique.

The Ordered Categorical (Ordinal) Scale

The ordered categorical or ordinal scale sorts and ranks the dimension to be measured in non-overlapping categories, which usually have a numerical rating scale, attached. While the magnitude of change in going from category to category is unknown

the direction of change is (Stevens S, 1946; Merbitz C et al, 1989). The ordered categorical scale was included in the aforementioned study and was part of a 69-item questionnaire called the Subject Rated Drug Effect Questionnaire (SRDEQ, developed by Pfizer Inc) that measures subjective effects in 7 distinct ordered categories. As shown the categories are described by verbal adjectives that describe an ascending order in effect intensity.

Ordinal scales have been used in a variety of clinical settings as an instrument measuring subjective phenomena, otherwise difficult to measure using objective tests. Such phenomena as Pain (Ahles et al, 1984; Seymour et al, 1982; Jensen et al, 1986; Sheiner , 1994; Gupta et al; 1999; Mandema et al, 1996; Lundeberg et al, 2001), mood (Folstein and Luria, 1973), sleepiness (Mitsutomo et al, 2000), health perception and quality of life (Cox et al, 1992; Spilker et al, 1996) and have all been measured using single- and multi-item categorical scales. Moreover, the validity (McCormack et al, 1988; Jensen et al, 1986) and reliability (Jensen et al, 1986; Lundeberg et al, 2001) of many ordinal scales have been established in a number of studies.

Some of the advantages of ordinal scales are their: 1) simplicity, ease of use and administration (Merbitz et al, 1989; Jensen et al, 1986); 2) ease of comprehension providing definite tangible descriptors that require less imagination (Joyce et al, 1975, Merbitz et al, 1989); 3) requirement of little training and motivation for the subject to complete (Joyce et al, 1975); 4) suitability for frequent and repeated use (Deyo et al, 1986, 1991; Lundeberg et al, 2001). The reported disadvantages of ordinal scales are their: 1) placement of artificial boundaries on subjective dimensions (Aitken & Zealley, 1970); 2) decreased sensitivity, responsiveness and discriminating capacity (due to fewer

categories) to detect small clinically relevant changes (Joyce et al, 1975; Ohnhaus & Adler, 1975; Seymour et al, 1982; McCormack et al, 1988; Svensson et al, 2000); 3) inability to quantify change in going from category to category (Merbitz et al, 1989); 4) difficulty in manipulating ordinal data for statistical analysis leading to sometimes misuse and misinference (Merbitz et al, 1989;Svensson et al, 1998, 2000).

Comparison of Ordinal and Continuous Scales

A number of comparative studies between continuous scales and ordinal scales measuring various types of variables have been performed, however no consensus has been reached as to the superiority of one over the other.

Ohnhaus & Adler (1975) found their VAS -Pain was more sensitive to increases and decreases in reported pain than the five point verbal ordinal (ordered categorical) scale that they compared it to. Similar conclusions were reported by Joyce et al (1975) that compared a 4-point ordinal scale to a VAS measuring chronic pain and Seymour et al that compared the VAS to a 4-point ordinal scale measuring post-operative dental pain. While one might logically conclude that the VAS is the more sensitive scale than the ordinal scale, which has a small number of response categories, Jensen et al (1986) pointed out that scales with more response categories have only the potential to be more sensitive, but are not necessarily more sensitive when used in a given study. Moreover, sensitivity to detect treatment effects is not necessarily associated with greater construct validity.

Lundeberg et al (2001) reported that the VAS produced significantly greater systematic discrepancies than the categorical scale, the reason being that subjects tended to overestimate their baseline pain on the VAS while discrepancies on the verbal scale

occurred in both directions.

Jaeshke et al (1990) recommended a 7-point ordinal scale over the VAS while Mckelvie et al (1978) recommended scales with five or six categories. In a study comparing a 7 point ordinal and VAS measures of muscle soreness Vickers et al (2000), found that VAS scores plotted recorded concurrently with each Likert score (a categorical scale) varied enormously and that there was significant overlap in the VAS scores, depicting a high variability in VAS measures. However their deduction that the Likert scale is more responsive must be considered with caution as the statistical approaches used assume normally continuous distributions and ignore the rank-invariant properties of ordinal data

In another study highlighting the superiority of the ordered categorical scale, Svensson (2000) presented a rank-invariant approach to evaluate the parallel reliability of intra-rater assessments made of a VAS scale, a 5-point ordinal scale, and a graphical rating scale. The latter is a hybrid of the ordinal and continuous scales consisting of a continuous line land marked with verbal categories. Overlapping of the VAS assessments on the discrete categories was observed and it was concluded that both ordinal scale and graphical rating scale displayed higher intra-scale stability (defined as intra -rater agreement and lack of systematic disagreement in assessments between two occasions) than the VAS.

Pharmacokinetic/Pharmacodynamic Applications

As mentioned previously, continuous and ordinal scales have been used in a variety of clinical PK/PD applications. They have been used extensively as biomarkers in clinical pharmacology studies assessing efficacy, safety, comparative efficacy, effect of

formulation on pharmacodynamics, and pharmacodynamic interaction studies. To highlight some examples: 1) A 5 point ordered categorical scale was used to measure efficacy of ketorolac as an analgesic for postoperative pain after administration of various intramuscular doses. (Mandema et al, 1996); 2) The safety of oxybutynin was investigated where the undesirable effect of dry mouth was measured using a 4 point categorical scale (Gupta et al, 1999); 3) In another study by Mitsutomo et al (2000), a 7-point ordinal scale called the Stanford Sleepiness Scale and a multi-item visual analogue scale measuring various dimensions of mood were used to measure and compare the residual effects of standard clinical doses of Zolpidem and Zopiclone (two hypnotics) on daytime sleepiness and psychomotor function; 4) The time course of sleepiness in 6 male subjects was assessed on the Stanford sleepiness scale and a nurse rating sedation scale (both ordinal scales) to compare the pharmacodynamics of an intravenous and orally administered 1mg dose of alprazolam (Smith R et al 1984); 5) In a pharmacodynamic drug-drug interaction study, the VAS scale was used to measure the effect of coadministration of nimodipine on diazepam induced tiredness (Heine R et al, 1994).

NonLinear Mixed Effects Modeling (NONMEM)

NONMEM (Beal and Sheiner, 1982) is a computer program, written in using Abbreviated Fortran, designed to fit general statistical (nonlinear) regression models to data. Proper modeling of such data involves accounting for both unexplainable inter- and intra-subject effects (random effects), as well as measured concomitant effects (fixed effects). NONMEM allows for this 'mixed effects modeling'.

In population PK/PD modeling one attempts to describe or model exposure/response data obtained from a sample that one believes represents the population. The model allows us to make inferences of the population as a whole. Fixed effects are estimated with THETA parameters that measure the typical population value or central tendency. The random effects consist of two parameter types. Omega parameters quantify the magnitude of interindividual or between-subject variability in the population, whereas Epsilon parameters quantify the magnitude of residual error (a measure of intraindividual variability, measurement error and model misspecification).

SPLUS

SPLUS is a statistical software package used for data visualization and exploration and statistical programming and simulation, and as such is used frequently in the area of pharmacometrics. In the current thesis, S- Plus has been used mostly for creating graphics, bootstrapping, and simulation based on bootstrap estimates.

Modeling Continuous versus Ordinal Data

Modeling ordered categorical data poses a challenge as this data is not continuous and thus cannot be modeled using conventional linear and nonlinear regression techniques. The outcome variable (in this case effect) is polytomous (many discrete outcome categories) and has a polynomial distribution. The simplest case of an ordinal variable is a dichotomous or binary variable, which has a binomial distribution.

Statistically, the polynomial distribution is different from the continuous distribution in that outcome categories may not be equidistant and hence homogeneity of variance does not hold in such a case. For example, on the continuous VAS, going from 5mm to 10mm is the same change in effect as going from 10mm to 15mm, whereas in the

ordinal scale, the change in effect in going from mild to moderate is not necessarily the same as going from moderate to significant. Only the direction of change is known but not the magnitude. This essentially highlights what statisticians refer to as the rank invariant property of ordinal data or that the data remains invariant in all order-preserving transformations, which means that the category labels do not represent any mathematical value other than the order of responses (McCullagh et al, 1980).

This is why modeling ordinal data requires a special type of regression known as logistic regression. If we convert ordinal pharmacodynamic data into probabilities of scoring a particular category as a function of time we can then use the logit transformation as follows:

$$g\{P(Y_t \leq m)\} = \log \frac{P}{1-P} \quad \text{Equation 1}$$

Where m represents the effect category (i.e. 0=none, 1=minimum, 2=mild, etc), P is the probability (ranging from 0 to 1) of reporting that effect category at time t and $g(x)$ is the function in logits.

The logit domain is an infinitely continuous domain ranging from $-\infty$ to $+\infty$, and so now the data can be manipulated using techniques that apply to continuous data and can be modeled using similar principles to those that apply to linear and nonlinear regression. However one drawback with the logistic function (and hence ordinal data) is that the final model can give information only about the population as a whole. Individual estimates, however, cannot be obtained and so information (which may be valuable) is lost at the individual level.

Preliminary Pharmacodynamic Differentiation Profile

It is clear that continuous and ordered categorical scales have been used as measurement instruments in a variety of clinical studies and that they each have advantages and disadvantages. However, their standard use and relative suitability for measuring pharmacodynamics and subjective experiences in relation to pharmacokinetic profiles have not been examined closely in the context of PK-PD modeling analysis, especially in smaller study settings. Use of timed assessments with VAS or ordered categorical scales to measure commonly occurring adverse events and other drug effects may provide useful information from small samples of healthy volunteers. This would help in creating a Preliminary Pharmacodynamic Differentiation Profile (PPDP) to evaluate new compounds (Moton et al, 2005). While the PPDP would not be a definitive assessment of tolerability or other important drug effects, it would be used to provide a preliminary characterization of several effects of leading marketed compounds for a comparison of those of new compounds in early development. This profile amongst other factors, may also be used to identify doses of the drug candidate that are unlikely to achieve a profile of adverse events or other drug effects that are equal to or better than a particular drug currently marketed for the same indication.

Pharmacometric utility of these psychometric scales in small pharmacology studies will depend on the feasibility of pharmacokinetic-pharmacodynamic (PK-PD) modeling to develop reliable population models that can accurately compare the relative potency of different compounds based on various measures of CNS effects which would be used to: 1) characterize the time course of pharmacodynamic response in relation to the PK profile 2) identification of PD parameters that can be modeled for several compounds

or used in clinical trial simulation studies. Pharmacokinetics and pharmacodynamic effects measured using both a continuous and ordered categorical scales were obtained in a study designed to assess the feasibility of using different subjective scales as biomarkers of pharmacodynamic response using model CNS drugs (Moton et al, 2005). This study was conducted in 20 healthy volunteers using a randomized, double-blind, single dose, 5-way crossover design. Each subject received 5 treatments administered approximately 1 week apart for 5 consecutive weeks. The regimens under investigation were: 1) Olanzapine 10mg, 2) Atomoxetine 80mg, 3) Paroxetine 40 mg, 4) Lorazepam 2 mg, and 5) Placebo. These are prescribed for a spectrum of CNS therapeutic indications-atomoxetine for attention deficit hyperactivity disorder, olanzapine for schizophrenia, lorazepam for anxiety and insomnia, and paroxetine for depression and Obsessive Compulsive Disorder. These model drugs were selected in the study because they: 1) have distinct pharmacologies and as such would produce different AE profiles and 2) would produce measurable CNS symptoms with single doses. The doses selected represent the maximum recommended clinical doses of each drug.

Blood concentrations (PK) were measured at various intervals spanning 72 hours post dose. As originally reported per protocol analysis (Pfizer Report, data on file), the PK profiles of the 4 model CNS drugs are shown below in Figure 1.3. As seen these drugs have distinct PK properties, with Atomoxetine possessing rapid absorption and disposition kinetics, lorazepam rapid absorption and slower disposition kinetics, olanzapine and paroxetine showing slow absorption and disposition kinetics. The distinct PK properties of the model CNS drugs are reflected in the noncompartmental estimates shown in Table 1.1. Atomoxetine and lorazepam both showed the shortest Tmax (1.14 hr

and 1.71 hr respectively) while olanzapine and paroxetine concentrations peaked at later times (7.32 and 6.83 hr respectively). Olanzapine had the longest biological half life followed by lorazepam, paroxetine and atomoxetine.

The Preliminary Pharmacodynamic Differentiation Profiles (PPDP) of these four CNS drugs was created by administering a battery of various instruments after single dose administration. These including the VAS; 7 point ordered categorical scales, 4 point Likert scales measuring drug strength and likeness, the Digit Symbol Substitution Test (DSST) measuring cognition, a test for extrapyramidal signs and symptoms, and a glucose and prolactin assay to measure any hyperglycemic and hyperprolactenemic effects was also applied. The Modified VAS administered was a 9-item VAS measuring the following effects (sleepiness, dizziness, nausea, anxiety, forgetfulness, confusion, fatigue/weakness, stiffness, blurred vision). The ordered categorical scale as shown in Figure 1.2 was administered as a 7-point Likert questionnaire consisting of 69 statements, which assessed the subject's intensity of drug effect experienced, ranging from none to extreme, after test drug administration using an ordered categorical scale. The questionnaire included a list of statements about various complaints, symptoms, or feelings the subjects have experienced.

Tables 1.2 and 1.3, shows the VAS effects measured and some of the 69 categorical effects measured respectively, including p values for significant and highly significant differences obtained from an ANOVA analysis of the Time-Averaged Change from Baseline (TACB) endpoint when compared with placebo. Due to the number of test employed some effects may be significant by chance. No correction for Type I error such as a Bonferroni or Tukey's correction was applied. Bonferroni which involves

determining the actual p-value using the product of the number of tests and the observed p-value would disqualify most effects as non-significant due to the large number of tests employed. However the procedure is very conservative and assumes independence of tests and since most tests employed were dependent (e.g. sleepiness and dizziness) a Tukey's correction would be more appropriate, however this would require measurement of dependence between tests which is difficult to perform. Therefore only those effects with the lowest p-values ($p < 0.0001$) were considered viable for any further pharmacometric analysis. Differential pharmacodynamic (PD) profiles shown in Figures 1.4 and 1.5 shows the onset and offset of some of the more pronounced PD signals recorded on the VAS and ordered categorical scale respectively as well as their relationship to plasma concentrations. For example lorazepam shows fast onset of sleepiness and slow offset of effect consistent with its rapid absorption kinetics and slower disposition kinetics.

Pharmacokinetic Models

The time course of drug concentrations of the 4 compounds, lorazepam 2 mg, paroxetine 40 mg, atomoxetine 80 mg, and olanzapine 10 mg, were structurally modeled using either 1 or 2 compartments with first order absorption with or without a lag time of absorption. For olanzapine and lorazepam, a 2-compartment model with and without a lag time for absorption respectively, adequately described the time course of drug concentrations while paroxetine and atomoxetine PKs were described with a 1-compartment model with and without an absorption lag time respectively. A summary of the final PK parameter estimates is provided in Appendix H. The NONMEM control

are provided in Appendix B.. Residual variability was modeled by a combined additive/proportional model for olanzapine, atomoxetine, and paroxetine and with a proportional model for lorazepam. As a measure of the goodness of fit of the final models, different plots were generated (Appendix I) including observed concentrations (CONC) versus population predicted (PRED) and versus individual predicted (IPRED), weighted residuals (WRES) versus population predicted concentrations, individual weighted residuals (IWRES) versus individual predicted concentrations, and weighted residuals versus time. In general, for all 4 drugs studied, a good correlation between the predicted values and the measured drug concentrations was observed both at the population level and with the individual predicted concentrations however, some underestimation was seen in the atomoxetine and paroxetine plots at higher concentrations. Generally, the weighted residuals were randomly scattered across the range of predicted concentrations with the exception of atomoxetine and paroxetine plots. For atomoxetine data, WRES were above the line of concordance at time = 0.5 and 1 hr ($t_{max} = 1.14$ hr from noncompartmental analysis). Similarly for paroxetine data, IWRES were above the line of concordance at time = 6 and 8 hr ($t_{max} = 6.83$ hr), supporting the finding that peak concentrations are slightly underestimated by the model. Certain outliers are visible in the residual plots. On the WRES versus PRED and Time plots, for olanzapine PK data, Subjects 14 and 20 showed abnormally higher positive residuals at a time of 1 hour. For atomoxetine, Subject 20 was an outlier in the IWRES versus IPRED and Time plots with a large negative residual at time = 0.5 hour. For lorazepam, Subject 5 showed an extremely lower residual on the WRES versus PRED and TIME plots at time = 0.5 hour. Subject 20 showed a larger negative residual on the IWRES versus

IPRED plot and Subjects 1 and 5 showed large negative residuals on the IWRES versus TIME plots at time = 72 and 0.5 hour, respectively.

Although not the primary purpose of the PK analysis, further analysis of the effect of covariates on interindividual random effects (unexplained variability) and hence model goodness of fit was performed. Despite the few subjects that were studied, certain covariates were observed to be significant and included in the final PK models. In the final olanzapine model, the effect of gender on volume of distribution was significant and hence kept in the final model. For lorazepam, CL_{cr} on clearance and weight on volume of distribution were significant and for atomoxetine, a significant effect of gender on volume of distribution was observed. No covariate effects were observed with the paroxetine PK data.

Study Rationale

Upon inspection of the pharmacodynamic profiles in Figures 1.4 and 1.5 and their relationship to the pharmacokinetic signature profiles in Figure 1.3, the following questions were of interest:

1. Is it feasible to model these PD measures using a mixed effects population approach?
2. If so, which PD measures would be appropriate for modeling?
3. Can clinically relevant PD parameters be identified and related to a tangible known quantity, e.g. using label incidence rates as a benchmark.

The categorical and VAS PD measures of lorazepam sleepiness and dizziness were chosen to initiate an exploratory pharmacometric analysis. These effects were of interest because they: 1) showed relatively high signal amplitude on both scales as indicated by maximum mean differences from placebo ($VAS_{\text{sleep}}=30.2$ mm, $VAS_{\text{dizz}}=9.1$ mm and $\text{Categorical}_{\text{Sleep}}=1.6$, $\text{Categorical}_{\text{Dizz}}= 1.2$) showed high statistical significance in ANOVA analyses of TACB, 3) their reported label incidence rates are different and based on data from healthy volunteers, i.e., Sleepiness (15.7%) has a higher incidence than dizziness (6.9%), 4) there are no PD data published contrasting these effects of lorazepam. In addition, their pharmacology is thought to be conferred by benzodiazepine receptor activity in distinctly different areas of the brain (Volkow et al) and this may further differentiate these two symptoms.

Mean olanzapine (difference from placebo) sleepiness signal was also high on

both scales (Maximum VAS=35.1 mm, Maximum Categorical Score=2.1) however was excluded from the analysis since label incidence data was based on schizophrenic patients and not healthy volunteers as in the current study. Atomoxetine and paroxetine were not included in the analysis as they showed no strong signals on both the VAS and categorical scale (with Atomoxetine nausea showing the largest signal yet recorded very modestly on both scales, Maximum Mean VAS Score=15.3 mm, Maximum Average Categorical Score=1.57).

Study Objectives

The objectives of the pharmacometric analyses described in the following chapters are to:

- 1) **Determine** the feasibility of modeling the categorical and VAS endpoints of Lorazepam Sleepiness and Dizziness using a population mixed effect approach, thereby assessing the pharmacometric utility of these measures using the current study design.
- 2) **Assess** the performance of proposed population models using simulation and posterior predictive checking.
- 3) **Relate** data-derived (e.g. Maximum Score) and model-derived (e.g. slope, EC50) pharmacodynamic parameters to the label incidence of lorazepam sleepiness and dizziness (15.7% and 6.9%, respectively).

Table 1.1 Summary of noncompartmental pharmacokinetic parameter values (%CV) following administration of single dose of atomoxetine 80 mg, paroxetine 20 mg, olanzapine 10 mg and lorazepam 2 mg after single oral dose administration in twenty healthy volunteers (data on file, Pfizer report).

| Pharmacokinetic Parameter | Olanzapine 10 mg | Atomoxetine 80 mg | Paroxetine 20 mg | Lorazepam 2 mg |
|----------------------------------|-----------------------------|------------------------------|-----------------------------|---------------------------|
| Tmax (hr) | 7.32 (35.8) | 1.14 (67.9) | 6.83 (17.0) | 1.71 (40.8) |
| Cmax (ng/mL) | 16.4 (31.5) | 624 (31.1) | 21.5 (38.6) | 26.8 (22.9) |
| AUC(0-tlqc), ng·hr/mL | 502 (28.8) | 3233 (42.4) | 484 (50.2) | 517 (29.3) |
| AUC(0-∞), ng·hr/mL | 668 (28.0) | 3343 (41.7) | 514 (51.9) | 551 (31.0) |
| t_{1/2}, hr | 35.6 (17.2) | 3.49 (30.0) | 14.6 (27.0) | 16.8 (21.3) |

Table 1.2. Summary of statistically significant results of the ANOVA analysis on TACB (Time Average 0-12 hr Change from Baseline) endpoint of pairwise comparisons with placebo. The VAS was applied as a 9 item instrument. Blank cells indicate the absence of a statistically significant result (alpha = 0.05). **(data on file, Pfizer report)**..

| Question | Olanzapine | Atomoxetine | Paroxetine | Lorazepam |
|----------------------|------------|-------------|------------|-----------|
| | 10 mg | 80 mg | 20 mg | 2 mg |
| VAS - Sleepy | p<0.001 | | | p<0.001 |
| VAS - Dizzy | | | | p<0.001 |
| VAS - Nauseous | | p=0.047 | | |
| VAS - Anxious | | p=0.009 | | |
| VAS - Forgetful | | | | p=0.067 |
| VAS - Confused | | | | p<0.001 |
| VAS - Fatigued/Weak | p=0.014 | | | p=0.004 |
| VAS - Stiff | | | | p=0.003 |
| VAS - Blurred Vision | p=0.017 | | | p<0.001 |

Table 1.3. Summary of statistically significant results of the ANOVA analysis on TACB (Time Average 0-12 hr Change from Baseline) endpoint of pairwise comparisons with placebo. The 7 point Ordered Categorical Scale was applied as a questionnaire measuring 69 items measuring various effects, subject complaints and feelings of which 30 items are shown below. Blank cells indicate the absence of a statistically significant result (alpha = 0.05). **(data on file, Pfizer report)**..


| Question | Olanzapine 10 mg | Atomoxetine 80 mg | Paroxetine 20 mg | Lorazepam 2 mg |
|---------------------------------|-----------------------------|------------------------------|-----------------------------|---------------------------|
| Q1 - Arousing or Stimulating | | | | |
| Q2 - Depressing or Sedating | p=0.035 | | | p<0.001 |
| Q3 - Headache | | | | |
| Q4 - Confused or Disoriented | p=0.006 | | | p<0.001 |
| Q5 - Sleepy | p<0.001 | p=0.053 | | p<0.001 |
| Q6 - Blurred Vision | | | | p<0.001 |
| Q7 - Dry Mouth | p<0.001 | p=0.012 | | |
| Q8 - Drooling | | | | |
| Q9 - Difficulty Swallowing | p=0.045 | | | |
| Q10 - Sweating | | p=0.005 | | |
| Q11 - Limp or Loose | | | | p<0.001 |
| Q12 - Rapid Heart Rate | | p=0.037 | | |
| Q13 - Problem Walking | p=0.039 | | | p<0.001 |
| Q14 - Poor Balance | p=0.029 | | | p<0.001 |
| Q15 - Lightheaded or Dizzy | p=0.013 | | | p<0.001 |
| Q16 - Queasy or Sick to Stomach | | p=0.006 | p=0.001 | |
| Q17 - Vomiting or Throwing Up | | p=0.041 | | |
| Q18 - Stomach Pain | | | | |
| Q19 - Lost Appetite | | p=0.05 | p=0.035 | |
| Q20 - Diarrhea | | | p<0.001 | |
| Q21 - Fatigued or Weak | p=0.013 | | | p=0.001 |
| Q22 - Unsteady | p=0.013 | | | p<0.001 |
| Q23 - Hot or Flushed | | p=0.001 | | |
| Q24 - Difficulty Urinating | | | | |
| Q25 - Difficulty Concentrating | p=0.007 | | | p=0.006 |
| Q26 - Slurred Speech | p=0.050 | | | p=0.005 |
| Q27 - Mentally Slowed Down | p=0.011 | | | p<0.001 |
| Q28 - Muscle Stiffness | | | | |
| Q29 - Body or Limb Shaking | | p=0.031 | | |
| Q30 - Slowing of Movement | p=0.023 | | | p<0.001 |

INSTRUCTIONS:

- For each of the following questions, place a slash (/) across the line in the position that best describes your response.

1. How sleepy do you feel right now?


Not at All Extremely



Score in mm
(Investigator's use only)

2. How dizzy do you feel right now?


Not at All Extremely



Score in mm
(Investigator's use only)

3. How nauseous do you feel right now?

Not at All Extremely



Score in mm
(Investigator's use only)

Figure 1.1. An illustration of continuous Visual Analog Scales (VAS). Subjects make a visual analogy of the dimension being measured by placing a slash on the 10 cm line anchored by words descriptive of the dimension being measured. The score is recorded as the distance in mm from the slash to the minimum anchor point of the scale.

INSTRUCTIONS

The following questionnaire includes a list of statements about various complaints, symptoms, or feelings you may have experienced during this study. For each statement, please answer how strongly you have felt the complaint, symptom, or feeling. If you did not feel the effect, ✓ the "None" box.

| <input type="checkbox"/> 3 Not Done | None | Minimum | Mild | Moderate | Significant | Severe | Extreme |
|-------------------------------------|----------------------------|----------------------------|----------------------------|----------------------------|----------------------------|----------------------------|----------------------------|
| 1. Arousing or stimulating effect | <input type="checkbox"/> 0 | <input type="checkbox"/> 1 | <input type="checkbox"/> 2 | <input type="checkbox"/> 3 | <input type="checkbox"/> 4 | <input type="checkbox"/> 5 | <input type="checkbox"/> 6 |
| 2. Depressing or sedating effect | <input type="checkbox"/> 0 | <input type="checkbox"/> 1 | <input type="checkbox"/> 2 | <input type="checkbox"/> 3 | <input type="checkbox"/> 4 | <input type="checkbox"/> 5 | <input type="checkbox"/> 6 |
| 3. Headache | <input type="checkbox"/> 0 | <input type="checkbox"/> 1 | <input type="checkbox"/> 2 | <input type="checkbox"/> 3 | <input type="checkbox"/> 4 | <input type="checkbox"/> 5 | <input type="checkbox"/> 6 |
| 4. Confused or disoriented | <input type="checkbox"/> 0 | <input type="checkbox"/> 1 | <input type="checkbox"/> 2 | <input type="checkbox"/> 3 | <input type="checkbox"/> 4 | <input type="checkbox"/> 5 | <input type="checkbox"/> 6 |
| 5. Sleepy | <input type="checkbox"/> 0 | <input type="checkbox"/> 1 | <input type="checkbox"/> 2 | <input type="checkbox"/> 3 | <input type="checkbox"/> 4 | <input type="checkbox"/> 5 | <input type="checkbox"/> 6 |

Figure 1.2. An illustration of 7- point ordered categorical scales. These scale measure the pharmacodynamic dimension of interest using non-overlapping categories with a numerical rating scale attached (0-6).

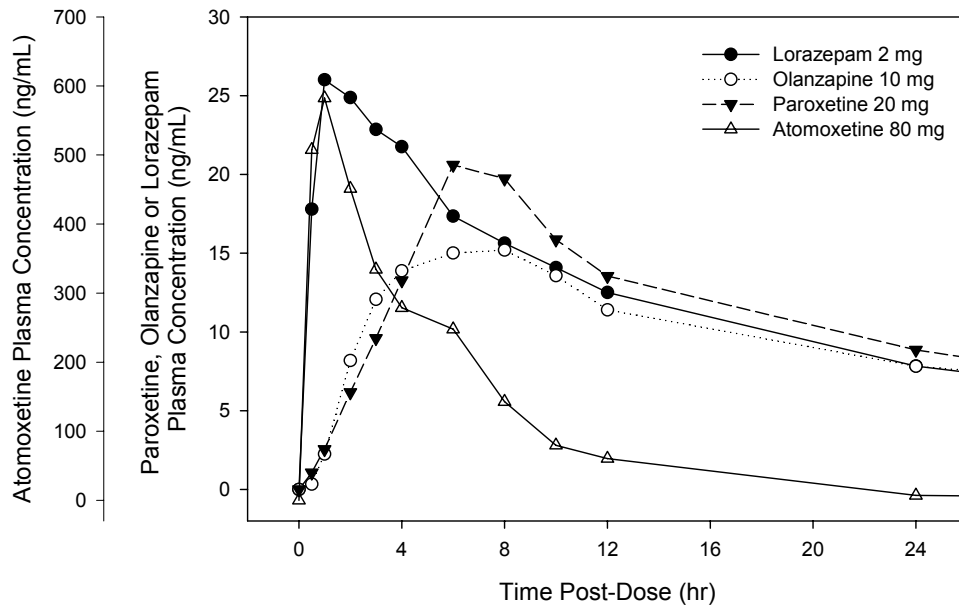


Figure 1.3. The mean plasma concentration vs. time plots of the four study CNS drugs (Lorazepam 2 mg, Olanzapine 10 mg, Paroxetine 20 mg, and Atomoxetine 80 mg) after single oral dose administration in twenty healthy volunteers (data on file, Pfizer report).

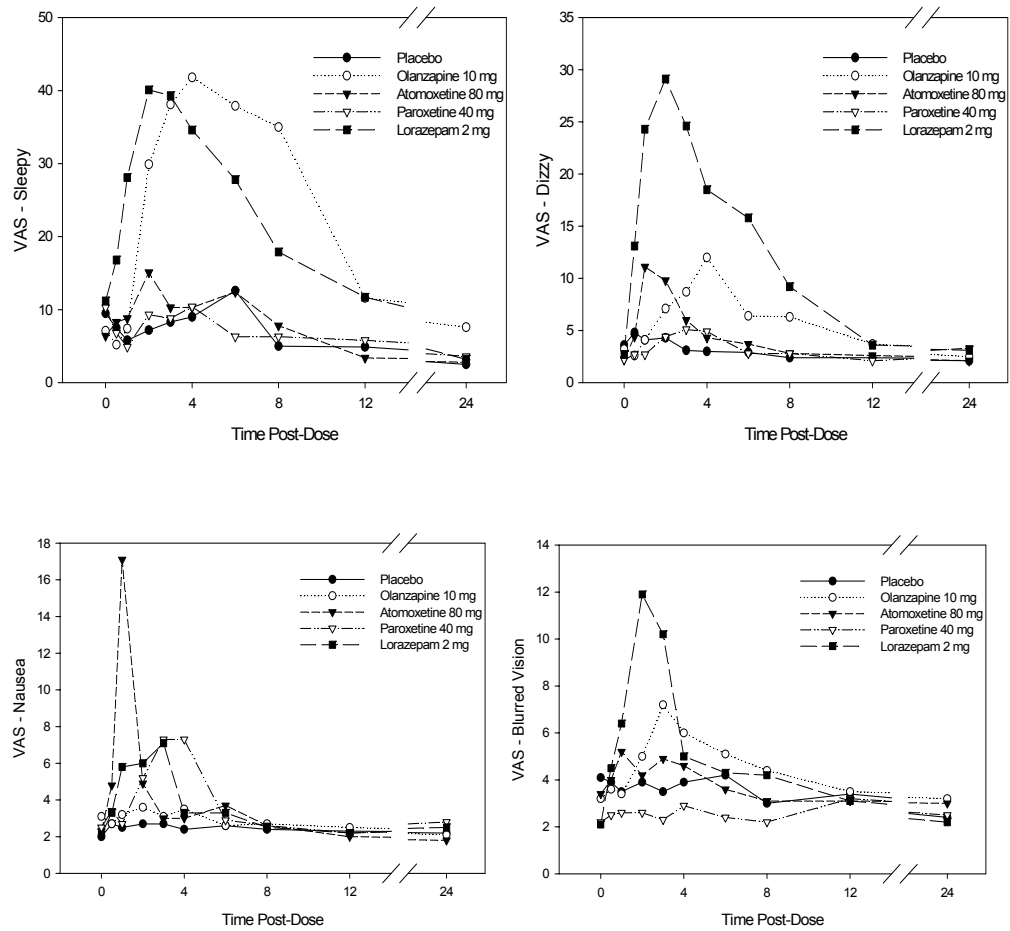


Figure 1.4. Mean VAS effect vs. time pharmacodynamic profiles of sleepiness, dizziness, nausea, and blurred vision measured in 20 healthy volunteers after administration of single oral dose of Lorazepam 2 mg, Olanzapine 10 mg, Paroxetine 20 mg, Atomoxetine 80 mg, and placebo (data on file, Pfizer report).

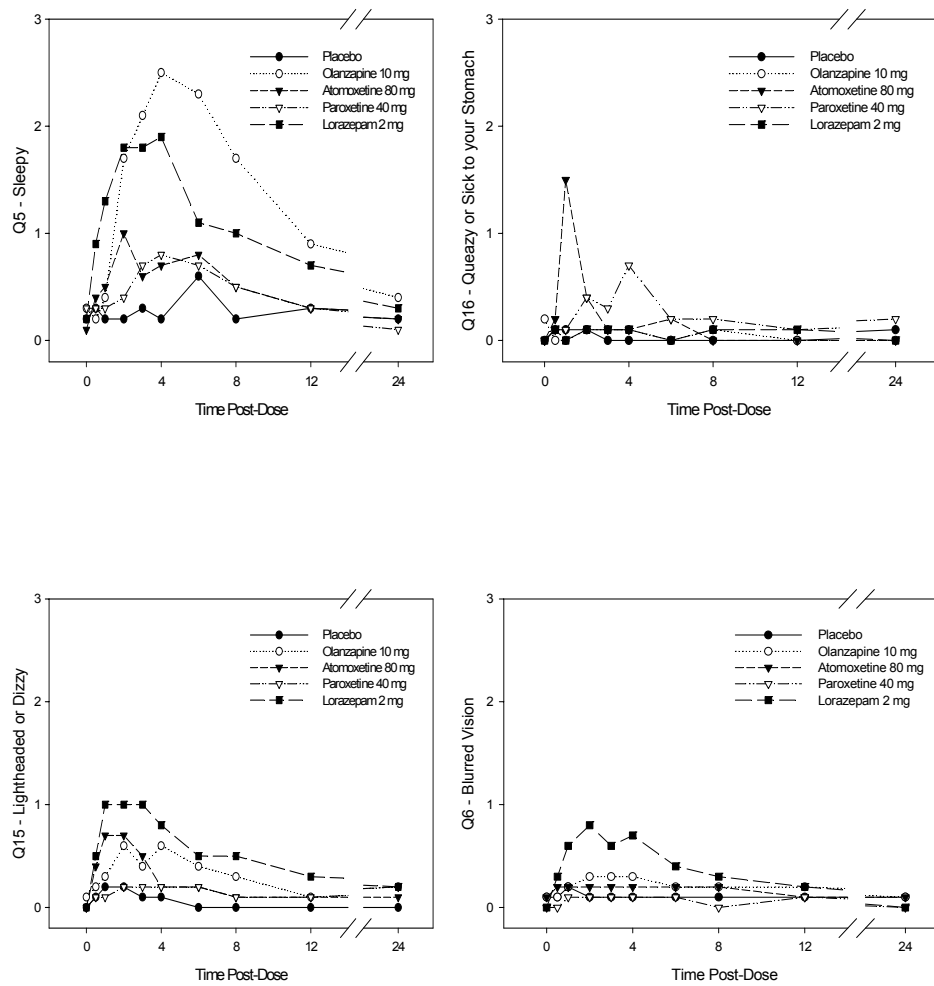


Figure 1.5. Mean ordered categorical effect vs. time pharmacodynamic profiles of sleepiness, dizziness, nausea, and blurred vision measured in 20 healthy volunteers after administration of single oral dose of Lorazepam 2 mg, Olanzapine 10 mg, Paroxetine 20 mg, Atomoxetine 80 mg, and placebo (data on file, Pfizer report).

References

- Ahles T.A. Cancer related Pain. II. Assessment with visual analogue scales. *J Psych Res.* 28: 121-124 (1984).
- Aitken R. A growing edge of measurement of feelings. *Proc Royal Soc Med.* 62: 989-996 (1969).
- Aitken R, Zealley K. measurement of Moods. *Brit J Hosp Med.* 4: 215-225 (1970).
- Beal SL, Sheiner LB, Eds. *NONMEM user's guides.* San Francisco: NONMEM Project Group, University of California (1992).
- Boer A, Van Lanschot J, Stalmeier P, Sprangers M. Is a single-item visual analogue scale as valid, reliable and responsive as multi-item scales in measuring quality of life? *Qual Life Res* 13: 311-320 (2004)
- Bunevicius R., Groudys G. *J Euro Coll Neuropsychopharm.* Cognitive state of hypothyroid patients and thyroid hormone replacement.7: S270 (1997).
- Deyo R, Diehr P, Patrick D. Reproducibility and responsiveness of health status measures. *Contr Clin Trials* 12:142S-158S (1991).
- DeLoach L, Higgins M, Caplan A, Stiff J. The visual analog scale in the intermediate postoperative period: intrasubject variability and correlation with a numeric scale. *Anesth Analg* 86:102-106 (1998)
- Ette EI, Ludden TM. Population pharmacokinetic modeling: The importance of informative graphics. *Pharmaceut Res* 12:1845-55 (1995)
- Feltner D, Kamal M, Moton A, Nyberg J, Ouellet D. Feasibility of using pharmacokinetic-pharmacodynamic modeling in healthy volunteers to create a preliminary drug effect differentiation profile. Abstracts presented in Annual ASCPT Conference (2005)
- Folstein M, Luria R. Reliability, validity, and clinical application of the visual analogue mood scale. *Psychol Med* 3: 479-486 (1973).
- Freyd M. The graphic rating scale. *J Educ Psychol.* 14 :83-102 (1923)
- Girard P. Clinical Trial Simulation: A tool for understanding study failures and preventing them. *Bas & Clin Pharmacol & Toxicol.* 96: 228-234 (2005).
- Grandmont P, Feine J, Tache R, Donohue W, Tanguay R, Lund J. Within-subject comparisons of implant-supported mandibular prostheses: psychometric evaluation, *J Dent Res* 73: 1096-1104 (1994).
- Gupta SK, Sathyan G, Lindemulder E, Ho P, Sheiner L. Quantitative characterization of therapeutic index: Application of mixed-effects modeling to evaluate oxybutynin dose-efficacy and dose-side effect relationships. *Clin Pharmacol Ther.* 65: 672-684 (1999)
- Guyatt G, Deyo R, Charlson M, Levine M, Michell A. Responsiveness and validity in health status measurement: a clarification. *J Clin Epidemiol.* 42: 403-408 (1989)
- Hayes M, Peterson D. Experimental development of the graphic rating method. *Psychol Bull.* 18: 98-99 (1921).

- Heine P, Weyer G, Breuel P, Muck W, Schmage N, Kuhlmann J. Lack of interaction between diazepam and nimodipine during chronic oral administration to healthy elderly subjects. *Br J clin Pharmacy*. 38: 39-43 (1994).
- Jaeschke R, Singer J, Guyatt G. A comparison of a seven-point and Visual Analogue Scales. Data from a randomized trial. *Control Clin Tri*.11:43-51 (1990)
- Jensen M, Karoly P, Braver S. The measurement of clinical pain intensity: a comparison of six methods. *Pain*. 27:117-126 (1986)
- Joyce C, Zutshi D, Mason R. Comparison of fixed interval and visual analogue scales for rating chronic pain. *Europ J Clin Pharmacol*. 8: 415-420 (1975)
- Kremer E, Atkinson J. Measurement of Pain: patient preference does not confound pain measurement. *Pain* 10: 241-248 (1981).
- Lashner B, Hanauer S, Silverstein M. Testing nicotine gum for ulcerative colitis patients: experience with single-patient trials, *Diges Dis & Sci*. 33:827-832 (1990).
- Little J, McPhail N. Measurement of depressive mood at monthly intervals. *Brit J Psych*. 122: 447-452 (1973).
- Lundeberg T, Lund I, Dahlin L, Borg E, Eriksson S. Reliability and responsiveness of three different pain assessments, *J Rehabil Med*. 33:279-283 (2001).
- Mandema JW, Verotta D, Sheiner LB. Building population pharmacokinetic-Pharmacodynamic models. I. Models for covariate effects. *J Pharmacokin Biopharm* 20:511-28. (1992)
- Mandema JW, Stanski DR. Population pharmacodynamic models for ketoralac analgesia. *Clin Pharmacol Ther*. 60: 619-635 (1996)
- McCormack H, Horne D, Sheather S. Clinical Applications of visual analogue scales: a critical review. *Psychol Med*. 18: 1007-1019 (1988).
- McCullagh P. Regression models for ordinal data. *J Roy Stat Soc* 42: 109-142 (1980)
- Mckelvie S. Graphic rating scales-how many categories? *Brit J Psychol*. 69:185-202 (1978)
- Merbitz C, Morris J, Grip J. Ordinal scales and foundations of misinference. *Arch Phys Med Rehabil*. 70:308-312 (1989)
- Mitsutomo U, Isawa S, Suzuki M, Murasake M. The effects of zolpidem and zopiclone on daytime sleepiness and psychomotor performance. *Jpn J. Neuropsychopharmacol*. 20:123-130 (2000)
- Ohnhaus E, Alder R. Methodological problems in the measurement of pain: A comparison between the verbal rating scale and the visual analogue scale. *Pain* 1: 379-384. (1975).
- Rampling D, William R. Evaluation of group processes using visual analogue scales. *Aust & New Zeal J Psych*. 11: 189-191 (1977)
- Robinson R, McHugh P, Folstein M. Measurement of appetite disturbances in psychiatric disorders. *J Psych Res*. 12: 59-68 (1975).
- Scott J. & Huskisson E. Graphic representation of Pain. *Pain* 2: 175-184 (1976).
- Seymour R. The use of pain scales in assessing the efficacy of analgesics in post-operative dental pain. *Eur J Clin pharmacol*. 23: 441-444 (1982)
- Sheiner LB, Stanski DR, Vozeh S, Miller RD, and Ham J. Simultaneous modeling of pharmacokinetics and pharmacodynamics: Application to *d*-tubocurarine. *Clin Pharmacol Ther*. 25:358-71. (1979)

Sheiner LB. A new approach to the analysis of analgesic drug trials, illustrated with bromfenac data. *Clin Pharmacol Ther.* 56: 309-322 (1994)

Smith R, Kkroboth P, Vanderlugt J, Philips J, Juhl R. Pharmacokinetics and pharmacodynamics of alprazolam after oral and IV administration. *Psychopharmacol.*84:452-456 (1984)

Stevens S. On the theory of scales measurement. *Science.* 103: 677-680 (1946).

Svensson E. Ordinal invariant measures for individual and group changes in ordered categorical data. *Statis. Med.* 17: 2923-2936 (1998)

Svensson E. Comparison of the quality of assessments using continuous and discrete ordinal rating scales. *Biomet J* 42:417-434 (2000).

Vickers A. Comparison of an ordinal and a continuous outcome measure of muscle soreness. *Int J Tech Assess Health Care.* 15: 709-716 (1999)

Volkow N, Wang J, Hitzemann R, Wolf A. Depression of thalamic metabolism by lorazepam is associated with sleepiness. *Neuropsychopharmacol.* 1995; 12:123-132.

CHAPTER 2

UTILITY OF AN ORDERED CATEGORICAL PHARMACODYNAMIC SCALE TO EVALUATE LORAZEPAM SLEEPINESS AND DIZZINESS

Abstract

Pharmacokinetic/pharmacodynamic (PK/PD) modeling of ordered categorical scales may provide insight into drug response by utilizing relatively small samples of subjects. Two lorazepam adverse events (AEs), sleepiness and dizziness, were modeled to identify differences in PD parameters and differences compared to relative incidence rates in the drug label (15.7% and 6.9%, respectively). Healthy volunteers (n=20) received single oral doses of 2 mg lorazepam or placebo in a randomized, double-blind, cross-over fashion. A 7 point categorical scale measuring the intensity of AEs was serially administered over 24 hr. PK samples were obtained over 72 hr. The Maximum Score (MaxS), and Area Under the Effect Curve (AUEC) were determined by noncompartmental methods and compared using a paired t-test. Individual scores were modeled using a logistic function. AUEC and MaxS for sleepiness were significantly higher than dizziness (20.35 vs. 9.76, $p < 0.01$) and (2.35 vs. 1.45, $P < 0.01$). Model slope estimates were similar for sleepiness and dizziness (0.21 vs. 0.19 logits*ml/ng), but baseline logits were significantly higher for sleepiness (-2.81 vs. -4.34 logits). Therefore, the higher intensity of sleepiness may be directly related to baseline (no drug present) while the increase in intensity due to drug was relatively similar for both AEs.

Introduction

Ordered categorical scales have been used in a variety of clinical settings to measure subjective effects and feelings which are clinically relevant but yet difficult to measure using objective tests. A good example is pain where several analgesic trials used various categorical scales (Jensen et al, 1986; Lundeberg et al, 2001). Such scales have been reported to display high validity and reproducibility (Lundeberg et al, 2001; Svensson 2000) during repeated assessments and are usually quick and easy to administer (Jensen et al, 1986; Merbitz et al, 1989).

Pharmacokinetic-pharmacodynamic modeling of ordered categorical scales may provide insight into the PD of drug action utilizing relatively small samples of subjects. The feasibility of using different subjective scales as biomarkers of PD response was investigated in a small clinical pharmacology study with four model Central Nervous System (CNS) drugs (Moton et al, 2005). The rationale was that these responses may be used to compare potency and tolerability of new drugs relative to marketed drugs and thus be used as biomarkers of adverse event rates in the development of new CNS agents. In that study, seven-point ordered categorical scales measuring different types of subjective response (e.g. sleepiness, dizziness, etc) were administered serially after single dose administration to measure intensity of drug effects over 24 hours. Inspection of the effect-time profiles of the more common drug effects showed differential profiles for the different CNS agents, the onset and offset of response as well as the relationship to plasma concentrations.

The current analysis focuses on the categorical measures of two adverse effects (AEs) of one of the representative CNS drugs studied (Moton et al, 2005), namely lorazepam sleepiness and dizziness, with an aim to identify differences in relevant pharmacodynamic parameters using a PK/PD modeling approach. To date, no pharmacodynamic data, whether being categorical or continuous, have been published contrasting lorazepam induced sleepiness and dizziness in the context of population modeling. Their incidence rates in the drug label offer a unique benchmark for comparison. Thus, any differences found in PD measures between sleepiness and dizziness in the current analysis will be compared to differences in incidence rates in the drug label (Ativan Drug Insert). This pharmacometric approach is novel and may have significant utility in early clinical development particularly in constructing pharmacodynamic and adverse event differentiation profiles (Moton et al, 2005) for drug candidates under development and marketed comparators.

Moreover, from the spectrum of CNS effects measured in the larger study (Moton et al, 2005), lorazepam sleepiness and dizziness were selected as the endpoints of interest because: 1) these effects showed a relatively high scale signal amplitude and highest statistical significance in the time- averaged- change- from -baseline differences with placebo , 2) sleepiness is a more common AE of lorazepam than dizziness according to incidence rates in the label, and 3) their pharmacology is thought to be conferred by benzodiazepine receptor activity in distinctly different areas of the brain (Volkow et al, 1995; Schreckenberger et al, 2004) - sleepiness from GABA inhibition of the thalamus and sensory cortex and dizziness from the cerebellum.

It must be noted that modeling categorical data can not be performed using conventional nonlinear regression because it has a polynomial distribution which violates the assumption of homogeneity of variance (Hastie et al, 1989). In shifting from one effect category to another, the direction of change is known but not the magnitude, and the categories cannot be assumed to be equidistant (Merbitz et al, 1989). However, if the probabilities of reporting the effect categories as a function of time are modeled, a special type of regression known as logistic regression can be used. The current study employs a logistic function (Sheiner, 2004; Mandema and Stanski, 1996) to model sleepiness and dizziness categorical scores and assesses model performance using previously published pharmacometric methodology (Ette et al, 2003; Mandema et al, 2005, Yano et al, 2001) .

Methods

Data Collection

Twenty healthy volunteers were randomized in a double blind, single dose, 5-way crossover design (Moton et al, 2005). All subjects gave written informed consent to participate in the study. The study was conducted at the Clinical Pharmacology Unit of Pfizer (Ann Arbor, MI) in accordance with the principles of the Declaration of Helsinki. The study protocol was approved and performed in compliance with the Institutional Review Board/Independent Ethics Committee (IRB/IEC) and International Committee on Harmonization (ICH) Good Clinical Practice guidelines. Each subject received an oral dose of either lorazepam 2 mg, as one of four CNS drugs, or placebo. All study drugs were commonly used marketed compounds within their respective therapeutic indications

and were selected to produce different AE profiles which could potentially be measurable after single dose administration. Each regimen was separated by a one week washout period for a total trial period of five consecutive weeks. Blood samples were drawn before dosing and at 0.5, 1, 2, 3, 4, 6, 8, 10, 12, 24, 48, and 72 hr after the morning dose.

Prior to each blood collection during the first 24 hr, a 69 item questionnaire was administered. Items on the questionnaire covered various complaints, symptoms, or feelings the subject experienced. For each statement the subject was to answer how strongly he or she felt the complaint, symptom, or feeling on a seven-point ordered categorical scale. The seven effect categories were 0=none, 1=minimum, 2=mild, 3=moderate, 4=significant, 5=severe, 6=extreme.

Analytical Assay

Plasma levels of lorazepam were determined using liquid chromatography tandem mass spectrometry (LC/MS/MS). Briefly, 0.1 mL of human plasma containing sodium heparin was extracted by a liquid-liquid extraction using methyl t-butyl ether. The organic extract was dried and reconstituted in 0.2 mL of formic acid/methanol/5 mM ammonium formate (0.1:50:50, v/v/v), and an aliquot was injected into the LC/MS/MS system. The compounds were separated by reverse phase on a C₁₈ column (2.0 mm x 50 mm, 5 μm) by gradient elution using a binary mobile phase consisting of formic acid/methanol/water (0.1:10:90, v/v/v) and 0.1% formic acid in methanol (v/v). The analytes were ionized in the mass spectrometer in a Turbo IonSpray source with positive ion atmospheric pressure electrospray ionization and detected with multiple-reaction monitoring modes. The nominal ion transitions monitored were $m/z = 321 > 275$ for lorazepam and $m/z 327 > 281$ for the internal standard (lorazepam-d₄). These transition

ions were selected based on predominant fragmentation pathways of lorazepam and internal standard and their intensity, as observed in their product ion mass spectra. The lorazepam standard was linear over the range of 0.5 to 50 ng/mL when 0.1 mL plasma was used for the analysis ($r^2 > 0.998$). The intra- and inter-assay variations were less than 15% for the spiked standard curve and quality control samples. The variations for the long-term study quality control samples were <12%.

Data Analyses

Pharmacokinetics

A non-compartmental analysis (Benet et al, 1979) was performed using WINNONLIN on lorazepam plasma concentration-time profiles to determine maximal concentration (C_{max}), time to maximal concentration (t_{max}), Area Under the Curve from time zero to infinity ($AUC_{0-\infty}$) and the terminal half-life ($t_{1/2}$). Compartmental population analyses were conducted in NONMEM (Beal and Sheiner, 1992) using the first order conditional estimation method with interaction. The general model building strategy is based on modification of different approaches discussed by Beal and Sheiner (1992), Mandema et al, (1992) and Ette and Ludden (1995). During model building, the goodness of fit of different models to the data was evaluated using the following criteria: change in the minimum objective function (MOF), visual inspection of concordance and residual plots, precision of the parameter estimates, and decreases in both inter-individual and residual variability. A decrease in the MOF of at least 3.8 upon addition of a parameter was considered statistically significant. This corresponds to a nominal p value of <0.05

and one degree of freedom in the chi square distribution of the difference of MOF between hierarchical models.

The initial PK model was a one-compartment model defined in terms of the following structural parameters: oral clearance (CL/F), volume of distribution (V1/F), and first-order rate of absorption (ka). Other models tested include a term for lag time in absorption (tlag) and/or 2-compartments. Inter-subject variability on mean PK parameters was modeled using an exponential error term and was estimated sequentially on structural parameters such as oral clearance (CL/F), volume of distribution in the central and peripheral compartments (V1/F, V2/F), and on the first order absorption rate constant (ka). Various models of residual variability were tested including additive, proportional and combined additive/proportional error models. During model building, the off-diagonal elements of the variance-covariance matrix were fixed to 0, i.e., it was assumed that there was no correlation between PK parameters. In the final step, the correlation between all parameters was estimated in NONMEM.

To explain interindividual variability in PK parameter estimates, possible covariates were tested serially by including each covariate one at a time in NONMEM and checking for statistical significance. Covariates tested included the effects of age, gender, weight, and creatinine clearance on CL/F and the effects of age, gender and weight on V1/F. Covariates were centered using the mean and modeled initially using a simple linear relationship. All covariates found to be statistically significant were included sequentially in NONMEM based on their rank order of significance and starting with the covariate that resulted in the largest decrease in MOF.

Parameter estimates of CL/F and $t_{1/2}$ were compared to the non-compartmental results to ensure that model was adequate. Confidence intervals around parameter estimates were generated using nonparametric bootstrap procedure (n=500 runs) as described by Ette et al (2003).

Pharmacodynamics

In order to produce a typical value versus time curve for sleepiness and dizziness categorical scores, the expected value at each time point was calculated. The expected value or average score of the categorical measure of sleepiness and dizziness at time t can be defined by the following equation:

$$E(X) = \sum_{x=0}^m x_i \cdot P(x)$$

Equation 1

where X is the discrete random variable denoting the categorical measure of sleepiness or dizziness, x_i is the categorical sleepiness or dizziness score at time t with a set of possible categorical values m ranging from 0-6 and P(x) is the probability (obtained as a frequency) of reporting a categorical score x at time t. This equation is equivalent to taking the sum of all categorical scores at each time t and dividing by n (the total number of scores). The former definition is preferred due to the categorical nature of the data (Merbitz et al, 1989).

To examine whether or not there were differences in sleepiness and dizziness intensities, a noncompartmental analysis of the time course of average sleepiness and dizziness scores was conducted. Effect intensity endpoints determined were maximum score (MaxS) and area under the effect curve (AUEC) over the entire dosing interval (24

hr). A paired t-test was used to determine whether differences in MaxS and AUEC between sleepiness and dizziness were statistically significant.

Population modeling of the time course of sleepiness and dizziness scores was implemented in NONMEM using a logistic function (Sheiner, 1994; Mandema and Stanski, 1996) with the second order Laplacian method of estimation (Beal and Sheiner, 1992). Since the intensity of pharmacodynamic effect was self-rated on the 7-point categorical scale (0-6), the logistic function was used to model the probability (P) of observing scores $P \geq m$ ($m = 0$ to 6) as a function of baseline effect, drug concentrations, and placebo effect. The logistic function used was:

$$g\{P(Y_t \geq m_\eta)\} = \sum_{i=1}^m \beta_m + drug + placebo + \eta \quad \text{Equation 2}$$

where $g\{P(Y_t \geq m_\eta)\}$ is the function describing the probability of being greater than or equal to a particular effect category, m ; $\sum \beta_m$ is the sum of baseline parameters ($\beta_1, \beta_2, \beta_3, \dots, \beta_m$) describing the baseline probability of experiencing a particular effect category; ‘drug’ and ‘placebo’ are model components describing drug and placebo effects; and η is a subject specific random effect parameter quantifying inter-individual variability in response assumed to be normally distributed with a mean of 0 and variance ω^2 . The logit transform function was used to convert the function $g\{P(Y_t \geq m_\eta)\}$, which is in logits, into a probability.

$$P(Y_t \geq m) = \frac{e^{\eta}}{1 + e^{\eta}} \quad \text{Equation 3}$$

Initial inspection of sleepiness data showed the highest reported effect category as 5 (severe). As such, the probabilities modeled over time were ($P \geq 1$, $P \geq 2$, $P \geq 3$, $P \geq 4$, $P \geq 5$). By definition, $P \geq 0 = 1$, and this is not modeled. For the dizziness data, the highest reported category was three, and the probabilities modeled over time were ($P \geq 1$, $P \geq 2$, $P \geq 3$). Model building was conducted by adding the model components in Equation 2 sequentially and observing the change in the MOF.

First, baseline probabilities for each effect category were modeled as constants as described by Sheiner (1994). From Equation 2, β_1 is the Y intercept (in logits) describing the baseline for reporting an effect category of at least minimum intensity (1 or more), β_2 is the intercept added to β_1 to determine the baseline logit contribution for reporting an effect category of at least mild (2 or more), and so forth. The drug component was added by beginning with a simple linear slope function as described below:

$$E = S * C \quad \text{Equation 4}$$

where E is the drug effect, S is the slope describing the relationship between drug effect in the logistic domain and drug concentrations C. Originally C was tested as concentration in the central compartment determined by posthoc individual PK parameter estimates. Addition of an effect compartment (Sheiner et al, 1979), where C in Equation 4 now represents concentration in the effect compartment, was tested to account for any delay in effect with respect to peak plasma concentrations. This required addition of an extra parameter ke_0 , the first order rate constant describing lag in effect in the biophase (Sheiner et al, 1979) compared to central compartment concentrations. A hill function without and with a sigmoidicity constant were also tested. Change in the MOF and

inspection of the correlation matrix of estimates to ensure model stability was used to select final models.

For the placebo component of Equation 2, several models were tested including a constant modeled as a parameter in logits and a Bateman-like function. Incorporation of the placebo component in this manner resulted in the covariance step being aborted. However, inspection of the individual placebo profiles revealed some subjects as non-responders and others as mild to moderate responders with a Bateman-like response. As such a mixture model (Frame et al, 2003) on placebo response was tested. A mixture model assumes the population is composed of two or more subpopulations, each having a distinct population mean and random effects. Therefore, if the subject belonged to subpopulation 1 of non-responders, the placebo response was set to zero. If the subject belonged to subpopulation 2, the placebo response was modeled using a Bateman-like function with a theta parameter in logits describing the amplitude of placebo effect, and first order rate constants describing the onset and offset of placebo effect.

Assessment of PK/PD Model Performance

Nonparametric bootstrapping (Ette et al, 2003) and simulation based on bootstrap estimates were performed using SPLUS VI software (Insightful Corporation, Seattle, Washington). Five-hundred bootstrap runs were conducted to determine confidence intervals of parameter estimates. This analysis was repeated using successful bootstrap runs only. Simulations were then performed using each set of bootstrap estimates to generate five hundred sets of data as described by Ette et al (2003). Using this simulated data, cumulative probability plots of reporting at least an effect intensity m ($P \geq m$) as a function of time were constructed to show the performance of the model across effect

categories. Ninety percent prediction intervals (Mandema et al, 2005) of the time course of categorical scores were also constructed to visually depict the degree of uncertainty in the models due to random effects and parameter estimate uncertainty. In addition, posterior distributions of relevant PD endpoints were constructed and overlaid on the observed mean values as described by Yano et al (2001). The PD endpoints selected were those determined in the PD noncompartmental analysis -MaxS and AUEC.

Comparison of PD Parameters and Label Incidence

The relative ratio of label incidence of lorazepam sleepiness and dizziness was compared to the relative ratio of various data-derived PD parameters including MaxS, AUEC, and the maximum probability of reporting at least a particular effect category m ($P \geq 1$, $P \geq 2$, $P \geq 3$). The relative ratio of model-derived PD parameters such as slope was also related to the ratio of label incidence of sleepiness and dizziness.

Results

Pharmacokinetics

Table I shows the demographic information of the twenty study subjects. The time course of observed mean \pm SD, mean predicted, and individual plasma concentrations after single oral dose administration of lorazepam 2 mg are shown in Figure 2.1. A noncompartmental analysis yielded mean (CV%) estimates for C_{max} of 26.8 ng/ml (22.9), t_{max} of 1.7 hr (40.8), $t_{1/2}$ of 16.8 hrs (21.3) and a total systemic exposure or $AUC_{0-\infty}$ of 551 ng*hr/ml (31.0). Significant decreases in the MOF, residual and inter-individual variability, and inspection of concordance and residual plots

indicated that a two-compartment model with first order absorption adequately described the time course of plasma concentrations of 2 mg oral lorazepam.

Table 2.2 shows the final pharmacokinetic population parameter estimates. Significant covariates were determined to be creatinine clearance on CL/F and weight on V1/F. The population mean parameter estimates were in good agreement with parameters derived using non-compartmental analysis for both CL/F (3.63 vs. 4.02 L/hr) and the derived half-life (16.7 vs. 16.8 hrs). Results of the non-parametric bootstrap analysis are included in Table 2.2. The model was robust with 87% of the runs minimizing successfully. The parameter estimates and confidence intervals obtained from the bootstrap procedure which included all runs (even those which failed) were generally comparable to the estimates derived from NONMEM. Similar bootstrap estimates and confidence intervals were obtained using only successful runs.

Pharmacodynamics

Noncompartmental analyses conducted on the effect-time profiles of sleepiness and dizziness scores showed significant differences between these AEs in the maximum score (MaxS) and area under the effect curve (AUEC) endpoints. The MaxS of lorazepam sleepiness (\pm SE) was significantly higher than dizziness (2.35 ± 0.26 vs. 1.45 ± 0.22 , $p < 0.01$), as was the AUEC (20.35 ± 3.58 vs. 9.76 ± 2.45 , $p < 0.01$). The time to reach MaxS for lorazepam sleepiness scores was delayed (3.98 hr, Figure 2.3) compared to time of maximal lorazepam concentrations (1.71 hr, Figure 2.1). This observation justified addition of the effect compartment (Sheiner et al, 1979) to describe drug effect in

the lorazepam sleepiness model. In contrast, the dizziness effect peaked (2.55 hr, Figure 2.3) at time similar to that observed for peak plasma drug concentrations.

Population PD model-building was initialized by addition of baseline logit intercepts for each effect category. As indicated in Equation 2, these are added sequentially from $i=1$ to m in order to quantify the probability of experiencing a score category m or more in the absence of drug or placebo. Table III shows the final PD model estimates. As shown, β_1 (which represents the probability in logits of reporting a score of 1 or more at baseline) was significantly higher for sleepiness (-2.81) than dizziness (-4.34) as indicated by the 95% confidence intervals, whereas the baseline intercept parameters β_2 and β_3 were not significantly different across these AEs β_4 and β_5 were included in the sleepiness model as they resulted in significant decreases in the MOF. Addition of the drug component of the model as a slope as described in Equation 4 resulted in a decrease in point reduction in the MOF of 216 and 174 for sleepiness and dizziness models, respectively, indicating a significant drug effect. As shown in Table III, slope estimates of sleepiness (0.21 logits/ml*ng) and dizziness (0.19) were not significantly different on inspection of the 95% confidence intervals. Addition of an effect compartment as described in Equation 5 was significant for sleepiness (MOF reduction was 3.9) but not dizziness, and the final estimate of ke_0 , the first order rate constant describing lag in effect in the biophase compared to central compartment concentrations, was 2.44 hr^{-1} .

Placebo effect was modeled as a mixture of non-responders and responders in the final model, where the responder component was described using a Bateman-like function. Modeling the placebo effect as a mixture, remedied the initial problem

encountered with abortion of the covariance step and resulted in stabilization of the final model as indicated by the correlation matrix of estimates being devoid of high correlations (>0.8) among parameters. PLAC describes the amplitude of response and, as indicated in Table III, was similar for sleepiness (3.6 logits) and dizziness (4.3 logits) as was k_1 , the first order rate constant describing onset of placebo effect. When k_2 , the first order rate constant describing offset of placebo effect, was modeled for sleepiness placebo, it resulted in over-parameterization as determined by inspection of the correlation matrix of estimates. However, given that the individual responder profiles showed a Bateman pattern of effect and not exponential decay, k_2 was modeled as a fraction of k_1 and the constant used to determine this fraction was determined using a sensitivity analysis. The majority of subjects were non-responders to placebo effect as indicated by $P(1)$, the subpopulation proportion that was non-responder to placebo, and this estimate was similar between sleepiness (63%) and dizziness (71%). The inter-individual random effects parameter Ω_1 was significantly higher for sleepiness effect (3.31 logits) compared to dizziness (0.32 logits).

As shown in Table 2.3, mean population parameter estimates obtained from the bootstrap procedure were generally comparable to the estimates from the final model with the exception of the estimate of β_5 of the sleepiness model. The bootstrap CI of this parameter showed a smaller lower bound (-21.3 logits) compared to the NONMEM lower bound. The success rate of bootstrap runs was 80% for the lorazepam sleepiness model and 83% for the dizziness model.

Figure 2.2 shows the observed and simulated cumulative probabilities of reporting a sleepiness and dizziness effect greater than or equal to a particular effect category over

time ($P \geq m$). The simulations describe the data adequately. As shown, the cumulative probabilities decrease with increasing effect category (m). Moreover, peak probabilities of reporting at least an effect category m at time of maximal effect are higher for lorazepam sleepiness ($P_{\geq 1}=1$, $P_{\geq 2}=0.45$, $P_{\geq 3}=0.25$, $P_{\geq 4}=0.1$, $P_{\geq 5}=0.05$) than for lorazepam dizziness ($P_{\geq 1}=0.7$, $P_{\geq 2}=0.3$, $P_{\geq 3}=0.15$) as shown in Figure 2.

Figure 2.3, shows the observed (points) and overlaid mean simulated scores (lines) and 90% shaded prediction intervals (PIs) obtained from five hundred sets of bootstrap parameter estimates. The mean simulations adequately describe the time course of sleepiness and dizziness scores with the prediction intervals (shaded region) capturing the data and mean simulations. The one exception, however, is a data point of placebo sleepiness (at 6 hr) which is not captured by the model and lies slightly outside of the shaded interval. The shaded PI for lorazepam sleepiness is wider than that of lorazepam dizziness indicating the greater model uncertainty of sleepiness.

Figure 2.4 shows histograms of the simulated distribution of MaxS and AUEC obtained from 500 sets of bootstrap parameter estimates, overlaid on the observed mean of these PD endpoints (represented by the vertical black bar). The panels indicate that that proposed models simulate posterior distributions of these parameters which are centered close to the observed means.

Finally, Table 2.4 relates the various data-derived PD parameters, and the model-derived PD parameter, slope, to the incidence rates of the adverse events in the more general patient populations, as reported in the drug label. The ratio of the sleepiness/dizziness endpoints was calculated across these parameters. As shown by the

relative ratios, $\text{Max}(P \geq 2)$, $\text{Max}(P \geq 3)$ and AUEC, show the greatest concordance to label incidence, followed by MaxS and $\text{Max}(P \geq 1)$. However, the ratio of sleepiness to dizziness slope parameters was very close to 1 indicating that drug effect may not explain the differences between sleepiness and dizziness across these PD parameters.

Discussion

The current PK/PD analyses of an ordered categorical scale utilized as a biomarker of drug effect was used to gain insight into pharmacodynamics using a relatively small sample of subjects. Using the representative CNS agent lorazepam, this was illustrated by comparing the time course, self-rated on the scale by twenty healthy volunteers, of two of the most common AEs of the anxiolytic, sleepiness and dizziness. The 2 mg dose of drug selected in this study represents the daily recommended dose of lorazepam for maintenance treatment of generalized anxiety disorder.

PK estimates obtained from the noncompartmental and compartmental analysis of the concentration-time profiles are consistent with previous reports (Greenblatt DJ, 1981) and showed that lorazepam is rapidly absorbed ($K_a = 1.04 \text{ h}^{-1}$), has peak plasma concentrations occurring at about 2 hours post dose and that it has relatively moderate steady state volume of distribution (90 L), low systemic clearance (4 L/h), and moderate terminal half-life (16.7 hr).

The noncompartmental analysis of the effect-time profiles of sleepiness and dizziness scores indicated that the MaxS of sleepiness was significantly higher than dizziness (2.35 vs. 1.45, $p < 0.01$) as was the AUEC (20.35 vs. 9.76, $p < 0.01$). As shown in Table 2.4, The ratios of sleepiness/dizziness of these PD parameters are in concordance

to the ratio of label incidence, with AUEC showing stronger concordance. It must be noted that while these parameters are related to label incidence, they reflect effect intensity rather than effect frequency.

Differences in reporting various effect intensities between these AEs are seen in the cumulative effect probability plots in Figure 2.2. Maximum probabilities of reporting at least a minimal effect ($P \geq 1$) are higher for lorazepam sleepiness ($P=1$) than dizziness ($P=0.7$). Likewise, the peak cumulative effect probabilities of at least mild and moderate intensity are higher for lorazepam induced sleepiness ($P \geq 2=0.45$, $P \geq 3=0.25$) than for dizziness ($P \geq 2=0.3$, $P \geq 3=0.15$). Since these parameters may be determined by taking the cumulative frequency of categorical scores at a time t , they are data-derived PD parameters reflecting the probability of reporting a cumulative, categorical effect intensity in a conceptual population. As shown in Table IV, the sleepiness/dizziness ratio across these PD parameters are also in concordance to the ratio of label incidence with Max ($P \geq 2$) and Max ($P \geq 3$) showing the highest concordance followed by Max ($P \geq 1$). Since these represent the cumulative probabilities (which is a frequency) of reporting an effect of given intensity in a conceptual population, their relationship to label incidence is more direct than MaxS and AUEC.

The lack of significant difference between the slope estimate of sleepiness (0.21) and dizziness (0.19) at the 95% confidence level suggests that lorazepam confers similar intensity of sleepiness and dizziness effects and that drug does not contribute to the observed differences in the PD of these effects. Nevertheless, the proposed population PK/PD model gives possible insight into the differences in PD endpoints between these AEs. To understand certain PD model estimates reported in logit units in Table 2.3, it

may be helpful to refer to Figure 2.5, which shows the relationship between the logistic domain (which is rather abstract) and the probability domain (which is more familiar). On inspection of the population CIs of PD parameter estimates in Table 2.3, the only parameter that is significantly different between these effects at 95% confidence level is β_1 , the baseline intercept parameter of effect category 1 (likelihood of having a response of at least minimum intensity). The difference between this estimate for sleepiness and dizziness effects is 1.5 logits. As shown in Figure 2.5, the majority of the probability domain ($0.1 \leq y \leq 0.9$) occurs in the logit range $-3 \leq x \leq 3$, and 0 logits corresponds to the inflection point at $y=0.5$. In this range, 1.5 logits corresponds to a probability of 0.82. Since 0 logits corresponds to $P=0.5$ the difference $P=0.82-0.5=0.32$ corresponds to the greater likelihood of reporting sleepiness then dizziness due to the baseline difference. From Figure 2.2, the difference in observed cumulative effect ($P \geq 1$) at t_{max} between sleepiness and dizziness is $1-0.7=0.3$ equivalent to the value determined above. Since ($P \geq 1$) is the cumulative effect across all effect categories, differences in this endpoint between sleepiness and dizziness at t_{max} closely resembles differences in Max Score. It is unclear from a physiological standpoint why the difference in baseline effect exists between sleepiness and dizziness, but one possible explanation may be the time of day in which the data was collected. Given that the scale was first applied in the morning, some subjects may have experienced a residual sleepiness in the morning that was reported at baseline.

Another explanation may be that subjects may have a greater tendency to report a sleepiness effect than dizziness even in the absence of any drug. However, no placebo response rates of these effects are reported in the lorazepam label to confirm this. Placebo

data in the current study as shown in Figure 2.3, show a slightly greater sleepiness response at earlier time points (at 0.5 hrs post dose administration), suggesting that differences in reporting sleepiness and dizziness in the absence of drug may be related to time of day.

As mentioned, addition of an effect compartment was significant in the PD model of sleepiness (decrease in 3.9 of MOF). From Table 2.3, the ke_0 estimate was 2.44 h^{-1} and the half-life in the biophase is determined as $\ln(2) / 2.44 = 0.28 \text{ h}$. Approximately five half-lives in the biophase (1.5 hr) is equivalent to the slight delay in sleepiness effect with respect to peak plasma concentrations of lorazepam confirmed by results of the non-compartmental PD analysis (2.2 hr). Slight delays in psychomotor and cognitive PD measures with respect to peak plasma concentrations after single dose administration of lorazepam 2mg have been reported previously (Ellinwood et al, 1985; Bin et al, 1999). On the other hand, dizziness showed no such significant delay in effect and the time to Max Score was close to the t_{max} of lorazepam concentrations. While this contrast is unclear, one plausible pharmacologic explanation may be the distinct anatomical location in the brain from which these CNS effects originate. It is known that lorazepam induced sleepiness is the result of binding to and inhibition of benzodiazepine receptors of GABA complexes in the thalamus and sensory cortex of the brain (Volkow et al, 1995; Schreckenberger et al, 2004). The receptor binding causes downstream inhibition of glucose metabolism (Volkow et al, 1995; Schreckenberger et al, 2004), which might account for the delayed sensation of sleepiness recorded by the scale. On the other hand, lorazepam induced dizziness is conferred by benzodiazepine action in receptors of the cerebellum (responsible for maintenance of balance) and these receptors may have a

different subunit composition (Lunddens et al, 1995), altering rates of downstream signaling.

The performance of the final population models was assessed by a number of diagnostics including the simulations in Figure 2.2 which capture the observed cumulative probabilities, and the mean simulations in Figure 2.3 which adequately capture the time course of drug and placebo scores. As a further check, the invalidity of these models was refuted by results of the posterior predictive check (Yano et al, 2001) which showed that the simulated distributions of MaxS and AUEC were centered close to the observed mean. These PD parameters were selected based on them being clinically relevant, data-derived parameters which could be determined using the profile of an individual subject (Yano et al, 2001). The 90% PI in Figure 2.3 show the model uncertainty conferred by both random effects and uncertainty in estimating the parameter estimates. Typically, the 90% as opposed to 95% PI is assessed, because some confidence to detect a type I error is compromised to compensate for the increased uncertainty incurred by random effects. As shown in Figure 2.3, the PI of lorazepam sleepiness is wider than dizziness indicating greater model uncertainty. This may be the result of the greater random effects as shown in Table 2.3 (Ω is higher for sleepiness). Since overlaying PIs of these effects shows separation beyond 2 hours, one can make the conclusion that, given uncertainty in the model estimates and random effects, the models can detect a difference between the time course (at t_{max} and beyond) of these effects at the 90% confidence level.

A particular feature of the logistic function that underscores its quantitative power is the ability to quantify a population incidence of a cumulative or specific effect category

at a particular time post dose administration using population model estimates, as illustrated in the following example. To determine the probability $P \geq 3$ of reporting a drug induced sleepiness of at least moderate effect intensity at C_{max} in the biophase (26 ng/ml), Equation 2 and final model estimates from Table 2.3 can be used to determine the total logits as $(\beta_1 + \beta_2 + \beta_3) + (\text{Slope} * C_{max}) = (-2.81 - 2.57 - 1.79) + (0.21 * 26) = -1.71$ logits. Referring to Figure 2.5, or by using the logit transform (Equation 3), this logit corresponds to a probability of 0.15. Likewise the probability $P \geq 3$ of reporting lorazepam dizziness effect at t_{max} is 0.03. Therefore, the model predicts that at time of peak lorazepam effect, 15% of the population will experience a sleepiness effect of at least moderate intensity while 3% will experience a dizziness effect of at least moderate intensity.

While sleepiness and dizziness are the most commonly reported AEs of lorazepam according to the drug label and endpoints obtained in the study (Moton et al, 2005), the effects show minimal to moderate amplitude on the categorical scale as shown in Figure 3. This observation speaks to the power of the approach described, underscoring the sensitivity of the categorical scale in discerning small differences between relatively mild to moderate PD effects over time, and the ability to model such data from a relatively small sample of subjects using the logistic function. Currently, tolerability is described in drug labels as AE incidence rates, rates of dropouts associated with particular AEs, or label warnings. The high variability in AE rates in labels due to the varying methods of collecting AEs, varying populations, and varying doses used in clinical trials make them inadequate for assessing relative tolerability between compounds unless the sample size is large and there is a within study comparison of

drugs. The 7 point categorical scale described in this study can therefore have important utility as a biomarker of AE rates in smaller pharmacology studies, and the logistic function can be used to model the time course of AEs to provide more insight into the PD of AEs.

A question that arises, however, is whether less frequent or less intense AEs could be quantified using the pharmacometric approach, trial design, and sample size described. Clinical trial simulation (Girard, 2005) studies will therefore be needed to apply sensitivity analysis (Girard, 2005) to the proposed model parameters, such as slope, to determine the minimum intensity signal that can be quantified using the current clinical trial design. It must also be pointed out that a slope model was used in this study rather than an Emax model since only one dose which represents the maximum daily recommended dose for maintenance treatment was studied, however an Emax model may be used in future clinical studies where dose escalation may be performed on a candidate drug until the maximum effect is reached.

Another question that arises is which of the PD parameters shown in Table 2.4 is most adequate to relate to label incidence. As mentioned, AUEC and MaxS are data-derived PD parameters which reflect effect intensity rather than effect frequency. Moreover, AUEC may not always relate directly to label incidence, since the AUEC of an effect which has a large intensity but short duration may be similar to that of an effect with low intensity and longer duration yet these effects may have different incidence rates. Therefore, AUEC may not be adequate to use when comparing the AE rates of drugs of vastly different PK profiles. In such situations AUEC normalized to time may be better related to incidence. Max ($P \geq 1$), Max ($P \geq 2$) and Max ($P \geq 3$) are also data-derived

PD parameters which reflect frequency of reporting a cumulative categorical effect intensity in a conceptual population. The stronger concordance of Max ($P \geq 2$) and Max ($P \geq 3$) to label incidence seems to suggest that the frequency of reporting categorical effects of higher intensity may be better related to population incidence. The Slope parameter, which is model-derived, is very important since it shows whether the difference in incidence is drug related or not. If the differences in incidence were entirely drug related, in this scenario, a 2 fold greater slope of sleepiness would be expected to that of dizziness. More studies using this scale with different AE endpoints, and implementing the pharmacometric approach described in this paper will ultimately confirm and clarify the PD parameter in Table 2.4 showing the strongest concordance to label incidence consistently across studies.

Lastly, in emphasizing other potential utilities of this ordered categorical scale in early clinical development, the approach described in this paper may not be limited to comparing effects of the same drug as done in the current study, but can be applied to other scenarios as well. If the comparison was conducted between the dizziness AE of an anxiolytic under development and lorazepam for example, the relative ratio PD parameters in Table 2.4, e.g. Max ($P \geq 3$), and the lorazepam label incidence of dizziness may be used to extrapolate an estimate of dizziness incidence for the candidate under development. This would assist in developing a PD differentiation profile of the candidate which would show advantages and disadvantages of the candidate compared to marketed comparators early on in development. The scale may not only have utility as biomarker of AEs but of Pharmacodynamic effect in general. For example, in another scenario, if the comparison was conducted on sleepiness scores between two different

hypnotic drug candidates under development, prediction intervals as those shown in Figure 2.3 may be used to determine at which level of confidence a difference in sleepiness effect (which is now therapeutic rather than AE) between these drugs is seen given the uncertainty in model estimates and random effects. Such an analysis would, again, show a competitive advantage/disadvantage of a particular candidate and assist in go/no go decision making during early drug development. Other scenarios include PD comparisons of different formulations of the same compound, or between different study populations (e.g. geriatric vs. non-geriatric), or in assessing PD drug-drug interactions.

In conclusion, this study has shown that use of an ordered categorical scale as a measurement of drug effect, coupled to PK/PD modeling, may be applied successfully in a small study setting to gain valuable insight into the pharmacodynamics of drug action. This was illustrated by characterizing the exposure-response relationship of two common effects (sleepiness and dizziness) of the representative CNS agent lorazepam, and showing that differences in the PD endpoints described may be due to differences in baseline parameters. Differences between data-derived PD measures of sleepiness and dizziness were consistent with differences in incidence rates reported in the label, suggesting the utility of this scale as a biomarker of adverse event rates in early clinical development.

Table 2.1. Subject Demographics (n=20).

| Parameter | Mean (SD) |
|------------------------------|------------------|
| Gender, n | |
| Male | 5 |
| Female | 15 |
| Race, n | |
| White | 17 |
| Black | 3 |
| Age, y | 43 (11) |
| Weight, kg | 72 (12) |
| Creatinine clearance, ml/min | 103 (22) |

Table 2.2. Pharmacokinetic Parameters in Healthy Volunteers after a 2 mg Oral Dose of Lorazepam (n=20).

| Parameter | NONMEM Estimate | NONMEM 95% CI | Bootstrap Estimate | Bootstrap 95% CI |
|-------------------------------------|------------------------|----------------------|---------------------------|-------------------------|
| CL/F (L/h) | 4.02 | 3.58 - 4.46 | 4.02 | 3.57- 4.47 |
| V1/F (L) | 53.6 | 48.1-59.1 | 53.4 | 45.5-59.0 |
| V2/F (L) | 37.6 | 33.3-41.9 | 38.0 | 33.3-44.7 |
| Ka (h ⁻¹) | 1.04 | 0.82-1.26 | 1.03 | 0.79-1.27 |
| Q (L/h) | 10.9 | 9.00-12.8 | 11.0 | 9.13-13.9 |
| TVCL = CL/F+ θ_1 *(CLCR-103) | $\theta_1=0.03$ | 0.01 - 0.05 | 0.03 | 0.01-0.05 |
| TVV = V1/F+ θ_2 *(WGT-72) | $\theta_2=1.11$ | 0.87 -1.36 | 1.13 | 0.83-1.39 |
| Ω -CL/F | 25.4% | 12.1- 38.7 | 24.0% | 16.6-30.6 |
| Ω -V1/F | 9.24% | 2.08- 16.4 | 8.60% | 0.70-14.4 |
| Ω -V2/F | 13.1% | 3.98-19.1 | 12.5% | 1.08-19.1 |
| Ω -Ka | 35.9% | 16.4-55.5 | 34.8% | 20.9-45.0 |
| Residual Proportional Error | 8.34% | 5.54 - 11.1 | 8.09% | 5.79-10.9 |

CL is systemic clearance, F is bioavailability, V1 is central compartment volume, V2 is peripheral compartment volume, Ka is the first order rate of absorption, Q is intercompartmental clearance, TVCL and TVV are typical population value of clearance and volume, θ_1 and θ_2 are covariate parameters on CLCR (creatinine clearance) and WGT (weight), and Ω is a random effects parameter estimating inter-subject variability.

Table 2.3. Pharmacodynamic Parameters in Healthy Volunteers after a 2mg Oral Dose of Lorazepam or Placebo (n=20).

| Model Parameter | Lorazepam Sleepiness | | | | Lorazepam Dizziness | | | |
|---------------------------------|----------------------|----------------|--------------------|-----------------|---------------------|----------------|--------------------|-----------------|
| | Nonmem Estimate | Nonmem CI | Bootstrap Estimate | Bootstrap CI | Normem Estimate | Nonmem CI | Bootstrap Estimate | Bootstrap CI |
| <i>Baseline Effect</i> | | | | | | | | |
| β_1 (logits) | -2.81 | (-4.0, -1.62) | -2.78 | (-4.02, -1.82) | -4.34 | (-5.18, -3.5) | -4.50 | (-5.90, -3.68) |
| β_2 (logits) | -2.57 | (-3.27, -1.87) | -2.60 | (-3.24, -2.08) | -3.17 | (-4.51, -1.83) | -3.34 | (-5.26, -2.21) |
| β_3 (logits) | -1.79 | (-2.37, -1.21) | -1.84 | (-2.34, -1.41) | -1.08 | (-1.68, -0.48) | -1.09 | (-2.19, -0.59) |
| β_4 (logits) | -2.81 | (-4.02, -1.59) | -2.87 | (-3.78, -2.15) | NA | NA | NA | NA |
| β_5 (logits) | -1.55 | (-3.44, 0.34) | -1.31 | (-21.3, 5.7E-9) | NA | NA | NA | NA |
| <i>Drug Effect</i> | | | | | | | | |
| SLOPE (logits*ml/ng) | 0.208 | (0.17, 0.25) | 0.208 | (0.18, 0.26) | 0.190 | (0.15, 0.23) | 0.192 | (0.16, 0.25) |
| k_{∞} (h ⁻¹) | 2.44 | (0.4, 4.48) | 2.46 | (1.28, 7.76) | NA | NA | NA | NA |
| <i>Placebo Effect</i> | | | | | | | | |
| PLAC (logits) | 3.60 | (1.74, 5.46) | 4.17 | (2.31, 7.54) | 4.30 | (1.65, 6.95) | 5.34 | (2.70, 13.01) |
| k_1 (h ⁻¹) | 0.188 | (0.02, 0.36) | 0.189 | (0.11, 0.38) | 0.11 | (0.07, 0.29) | 0.15 | (0.03, 1.02) |
| k_2 (h ⁻¹) | NA | NA | NA | NA | 2.13 | (0.17, 4.09) | 2.02 | (0.37, 3.68) |
| P(1) | 62.80% | (20, 96) | 65.61% | (17, 94.5) | 71.00% | (41, 89) | 65.21% | (50, 86.29) |
| <i>Random Effects</i> | | | | | | | | |
| Ω_1 | 3.31 | (0.33, 6.29) | 3.45 | (1.85, 5.97) | 0.316 | (-0.62, 1.25) | 0.29 | (1.98E-9, 1.57) |

β_1 - β_5 are intercept logistic parameters describing the baseline, PLAC is amplitude of placebo effect, k_1 and k_2 are the first order rates of onset and offset of placebo response, P(1) is percentage of non-responders to placebo, SLOPE describes the relationship between drug effect and concentrations, k_{∞} is the first order rate constant describing lag in the effect compartment compared to lorazepam concentrations in the central compartment, Ω_1 is a random effects parameter describing inter-subject variability.

Table 2.4. Relationship of Data-Derived and Model-Derived PD Parameters to the Label Incidence of Sleepiness and Dizziness in Healthy Volunteers after Administration of a 2 mg Oral Dose of Lorazepam.

| Endpoint/ Parameter | Label Incidence | AUEC | MaxS | Max(P≥1) | Max(P≥2) | Max(P≥3) | Slope |
|------------------------------|------------------------|-------------|-------------|-----------------|-----------------|-----------------|--------------|
| Sleepiness | 15.7 | 20.35 | 2.34 | 1 | 0.57 | 0.35 | 0.21 |
| Dizziness | 6.9 | 9.76 | 1.45 | 0.7 | 0.25 | 0.15 | 0.19 |
| Ratio (Sleepiness/Dizziness) | 2.3 | 2.1 | 1.6 | 1.5 | 2.3 | 2.3 | 1.1 |

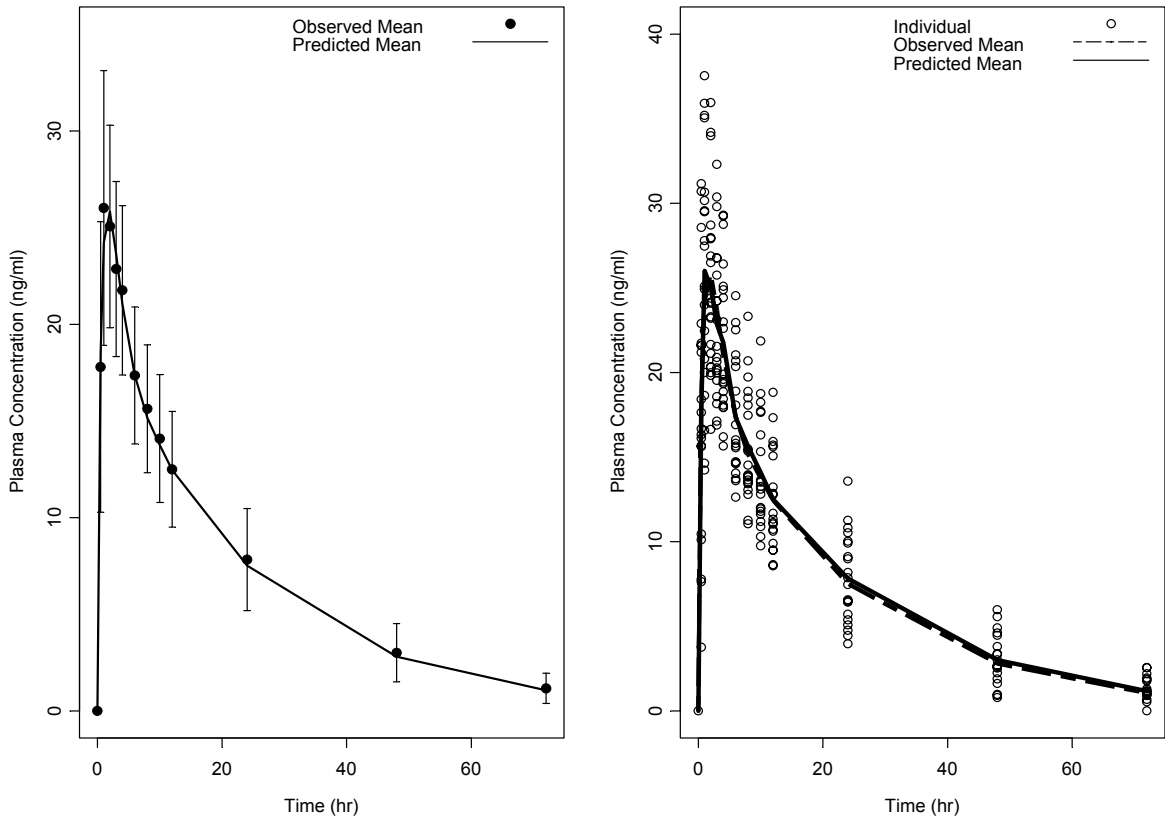


Figure 2.1. Left Panel: Observed mean \pm SD and predicted mean plasma concentrations versus time after a 2mg oral dose of lorazepam in healthy volunteers (n=20). Right Panel: Observed Individual, mean, and predicted mean plasam concentrations versus time.

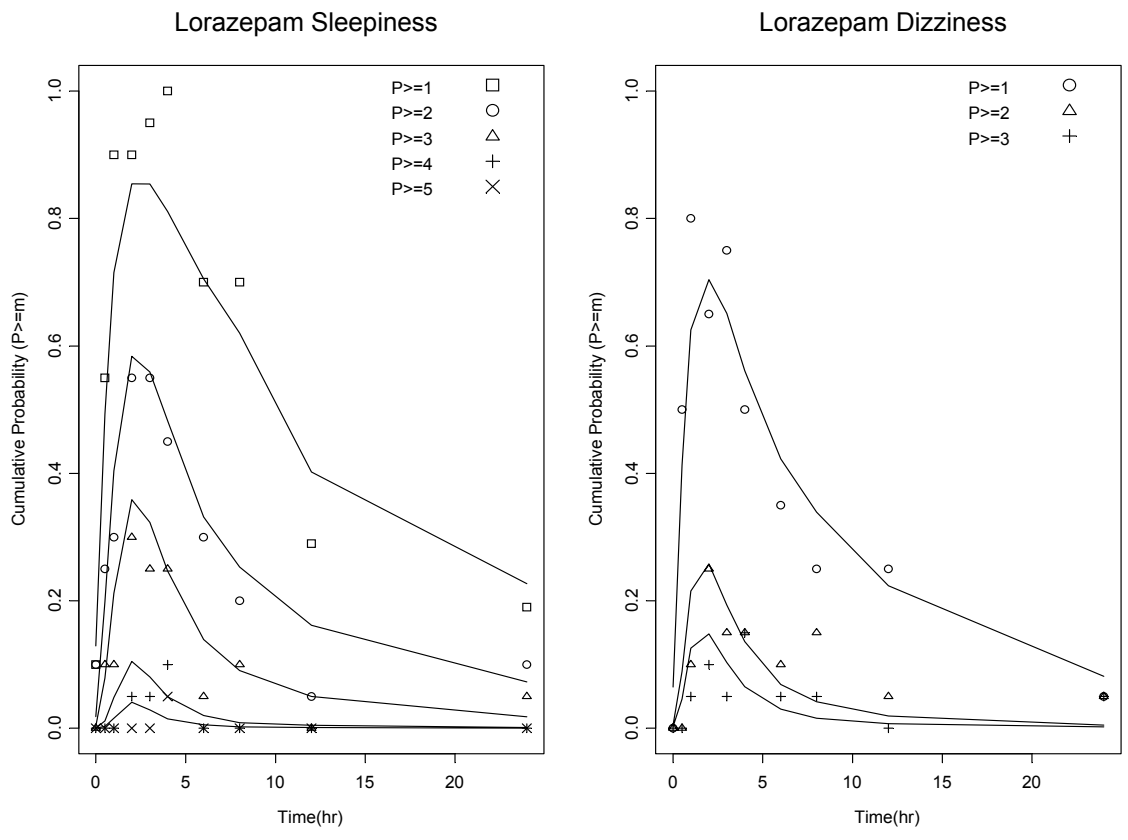
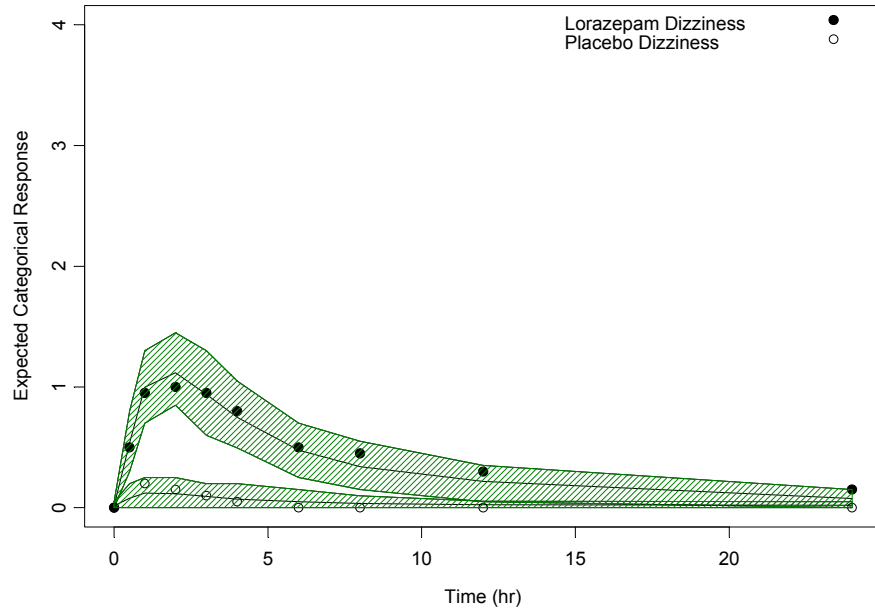
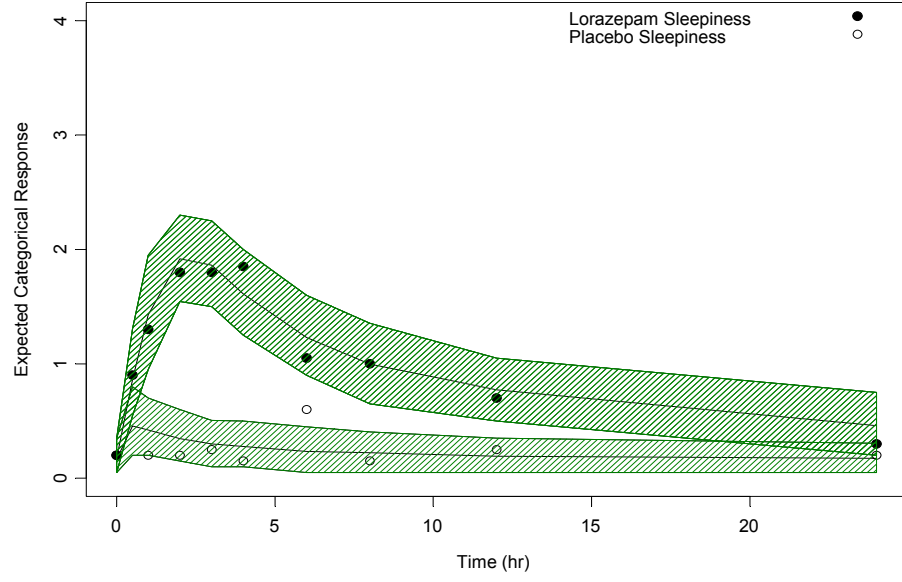


Figure 2.2. Cumulative probability plots of reporting sleepiness and dizziness. $P \geq 1-5$ is the cumulative probability of reporting an effect of at least minimum, mild, moderate, significant, and severe intensity on the categorical scale.



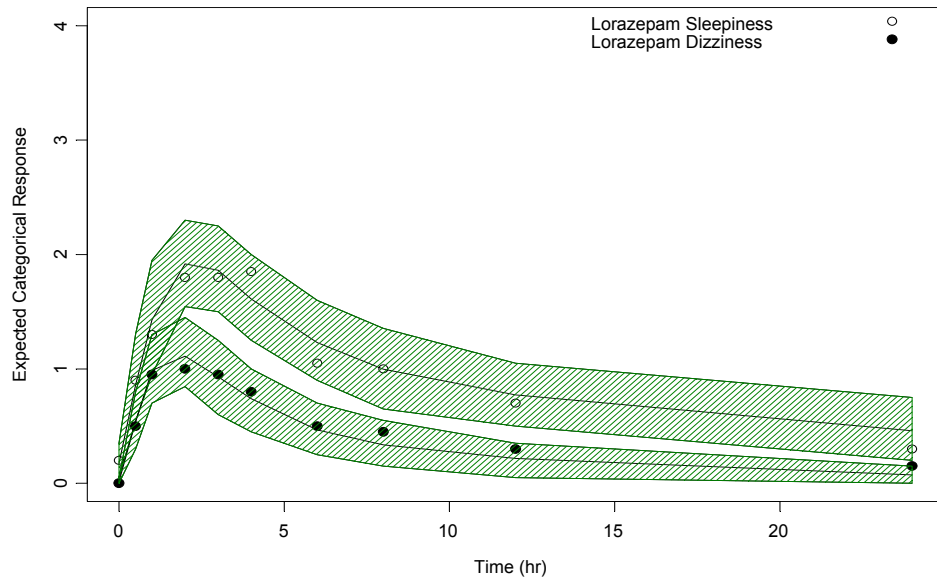


Figure 2.3. Ninety percent prediction intervals of sleepiness and dizziness scores in healthy volunteers as a function of time (n=20). Panel one shows lorazepam and placebo sleepiness, panel two lorazepam and placebo dizziness, and panel three lorazepam sleepiness and dizziness. Symbols indicate observed data, middle line indicates simulated data, and lower and upper lines indicate lower and upper prediction interval bounds.

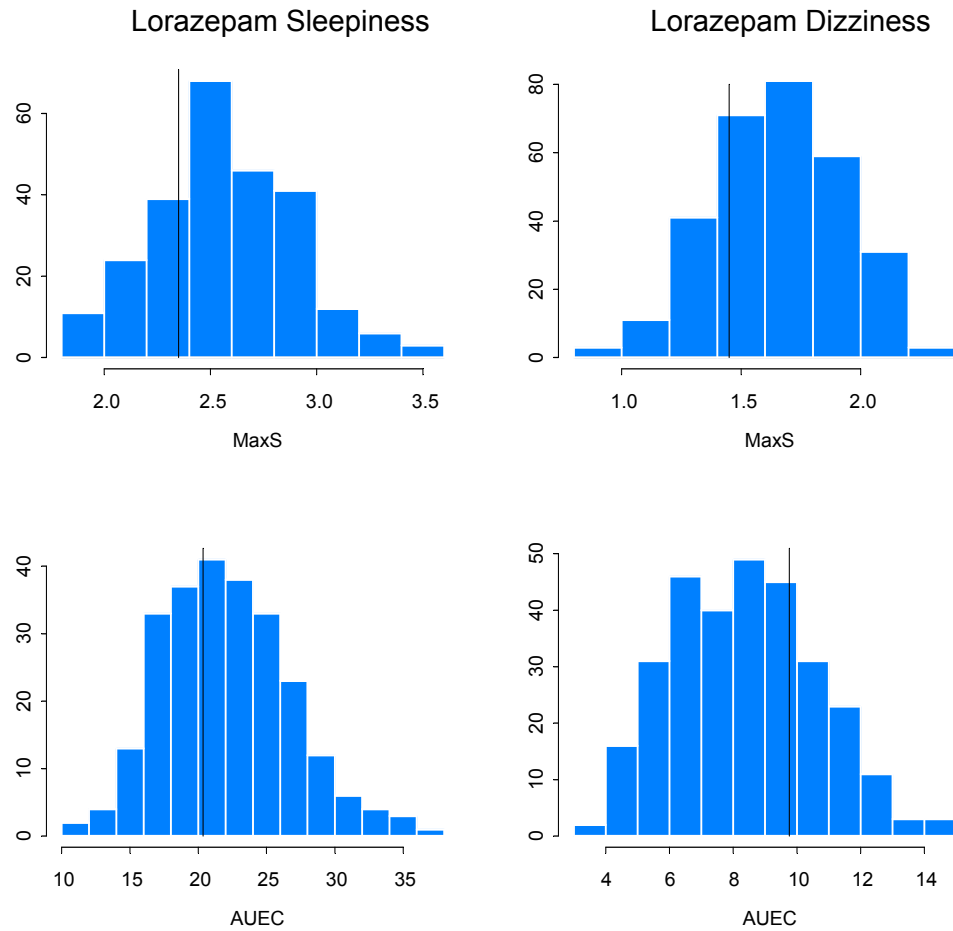


Figure 2.4. Posterior distributions of MaxS and AUEC for lorazepam sleepiness and dizziness in healthy volunteers after a 2 mg oral dose of lorazepam(n=20). Line indicates mean observed value. MaxS is the maximum reported categorical score, AUEC is the area under the effect curve from 0h-24h.

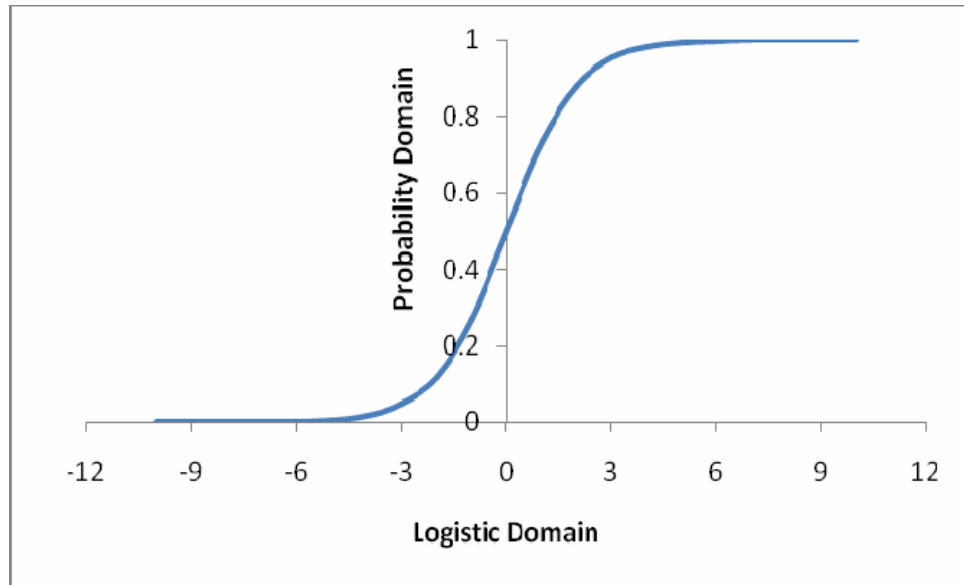


Figure 2.5. Relationship between the probability and logistic domains.

References

- Ativan (lorazepam) tablet package insert. Biovail Pharmaceuticals, Inc.
- Beal SL, Sheiner LB, Eds. NONMEM user's guides. San Francisco: NONMEM Project Group, University of California (1992).
- Benet LZ, Galeazzi RL. Non-compartmental determination of the steady-state volume of distribution. *J. Pharm Sci.* 68:1071-1073 (1979).
- Blin O, Jacquet A, Durrand A, Bruguerolle B, Pisano P. Pharmacokinetic-pharmacodynamic analysis of mnesic effects of lorazepam in healthy volunteers. *Brit J Clin Pharmacol.* 48:510-512 (1999).
- Ellinwood E, Heatherly D, Nikiado A, Bjornsson T, Kilts C. Comparative pharmacokinetics and pharmacodynamics of lorazepam, alprazolam, and diazepam. *Psychopharmacol.* 86:392-399 (1985).
- Ette EI, Ludden TM. Population pharmacokinetic modeling: The importance of informative graphics. *Pharmaceut Res.* 12:1845-55 (1995).
- Ette EI, Williams PJ, Kim YH, Lane JR, Liu MJ, Capparelli EV. Model appropriateness and population pharmacokinetics modeling. *J Clin Pharmacol.* 43:610-623 (2003).
- Frame B, Miller R, Lalonde R.L. Evaluation of mixture modeling with count data using NONMEM. *J Pharmacokinet & Pharmacodynam.* 30:167-183 (2003).
- Girard P. Clinical Trial Simulation: A tool for understanding study failures and preventing them. *Bas & Clin Pharmacol & Toxicol.* 96: 228-234 (2005).
- Greenblatt, D.J. Clinical Pharmacokinetics of oxazepam and lorazepam. *Clin. Pharmacokinet.* 6:89-105 (1981).
- Hastie TJ, Botha JL, Schintzler CM. Regression with an ordered categorical response. *Stat Med.* 8:785-94 (1989)
- Jensen M, Karoly P, Braver S. The measurement of clinical pain intensity: a comparison of six methods. *Pain.* 27: 117-126 (1986)
- Lüddens H, Korpi ER, Seeburg PH. GABA_A/benzodiazepine receptor heterogeneity: Neurophysiological implications. *Neuropharmacol.* 34: 245-254 (1995).
- responsiveness of three different pain assessments, *J Rehabil Med.* 33:279-283 (2001).
- Lundeborg T, Lund I, Dahlin L, Borg E, Eriksson S. Reliability and
- Mandema JW, Stanski DR. Population pharmacodynamic models for ketoralac analgesia. *Clin Pharmacol Ther.* 60: 619-635 (1996).
- Mandema J, Hermann D, Wang W, Sheiner T, Milad M, Bakker R, Hartman D. Model-based development of Gemcabene, a new lipid-altering agent. *AAPS Journal.* 7(3):513-522 (2005).
- Mandema JW, Verotta D, Sheiner LB. Building population pharmacokinetic-Pharmacodynamic models. I. Models for covariate effects. *J Pharmacokin Biopharm.* 20:511-28 (1992).
- Merbitz C, Morris J, Grip J. Ordinal scales and foundations of misinference. *Arch Phys Med Rehab.* 70:308-312 (1989).

Moton A, Ouellet D, Morlock R, Nyberg J, Feltner D. Feasibility of assessing differential pharmacodynamic (PD)/adverse events(AE) profiles on CNS agents. *Clin Pharm & Therap.* 77:2 (2005).

Schreckenberger M, Bartensteina P, Grunderb G. The thalamus as the generator and modulator of EEG alpha rhythm: a combined PET/EEG study with lorazepam challenge in humans. *Neuroimage.* 22:637-644 (2004).

Sheiner LB, Stanski DR, Vozeh S, Miller RD, Ham J: Simultaneous modeling of pharmacokinetics and pharmacodynamics: application to d-tubocurarine. *Clin.Pharmacol.Ther.* 25: 358-371(1979)

Svensson E. Comparison of the quality of assessments using continuous and discrete ordinal rating scales. *Biometric J.* 42:417-434 (2000)

Sheiner LB. A new approach to the analysis of analgesic drug trials, illustrated with bromfenac data. *Clin Pharmacol Ther.* 56: 309-322 (1994).

Volkow N, Wang J, Hitzemann R, Wolf A. Depression of thalamic metabolism by lorazepam is associated with sleepiness. *Neurosyndromopharmacol.* 12:123-132 (1995) .

Yano Y, Beal SL, Sheiner LB. Evaluating pharmacokinetic/ pharmacodynamic models using the posterior predictive check. *J Pharmacokinetic & Pharmacodynamic.* 28:171-192 (2001).

CHAPTER 3

PHARMACOMETRIC ANALYSES OF A CONTINUOUS VISUAL-ANALOG MEASURE OF LORAZEPAM SLEEPINESS

Abstract

A continuous measure of drug effect may have potential advantages over a categorical counterpart in pharmacometrics. This study investigates the feasibility of modeling a pharmacodynamic measure of the Visual Analog Scale (VAS) using a population mixed effects approach. Healthy volunteers (n=20) received single oral doses of 2 mg lorazepam or placebo in a randomized, double-blind, cross-over fashion. The VAS was serially administered over 24 hr to measure the intensity of several effects including sleepiness. Lorazepam C_{max} (26 ng/ml) occurred at 1.7 hrs while maximal VAS sleepiness (MaxS=50.6 mm) was delayed occurring at 3.3 hrs. Lorazepam-induced sleepiness was modeled using a linear slope model with an effect compartment implemented in NONMEM. High unexplained interindividual and residual variability, poor concordance plots and Montecarlo simulations were observed. Inspection of the histograms of VAS scores at various time points showed a right-skewed distribution, Logistic transformation of the VAS scores produced distributions closer to normal, greatly improving concordance plots, residual plots, and simulations. In conclusion, the logistic transformation well handles the skewness and boundedness aspects of the VAS, making such data suitable for non-linear mixed effects analyses in NONMEM.

Introduction

Continuous and ordered categorical subjective scales have been used to measure effects which are clinically relevant yet have no alternative objective measure. The Visual Analog Scale (VAS) is an example of a continuous subjective scale which has been used in clinical studies to measure relevant effects such as pain (Deloach et al, 1998; Lundeberg et al, 2001; McCormack et al, 1998), mood (Aitken et al, 1970; Folstein and Luria, 1973; McCormack et al, 1998), and anxiety (McCormack et al, 1998). It consists of a 10 cm line anchored at both ends with words descriptive of the maximal and minimal extremes of the dimension being measured. Figure 3.1 shows an illustration of the modified VAS drawn to scale.

The feasibility of using different subjective scales as biomarkers of pharmacodynamic (PD) response was investigated in a small clinical pharmacology study with four model Central Nervous System (CNS) drugs (Moton et al, 2005). The rationale was that these scales may be used as biomarkers of efficacy and tolerability to create preliminary pharmacodynamic differentiation profiles in the development of new CNS agents. In that Phase I study (Moton et al, 2005), the VAS and a seven point ordered categorical scale measuring different types of subjective response (e.g. sleepiness, dizziness, etc) were administered serially after single dose administration to measure intensity of drug effects over 24 hours. Inspection of the effect-time profiles of the more common drug effects showed differential profiles for the different CNS agents, the onset and offset of response as well as the relationship to plasma concentrations.

The criteria for selecting the most ideal subjective scale for pharmacometric

utility in a small study setting are unclear. From a clinical outcomes perspective, the controversy in the literature over the superiority of categorical versus VAS scales stresses the need to closely investigate the suitability of a subjective scale for a particular clinical study design. We have previously shown that 7-point ordered categorical measures of lorazepam sleepiness and dizziness reported by twenty healthy volunteers were modeled successfully using a logistic function, and demonstrated the potential utility of this scale as a biomarker of adverse events. (chapter 2). However, a continuous measure of drug effect may have potential, inherent advantages over a categorical counterpart in pharmacometrics. Aitken and Zealley (1970) popularized use of the VAS arguing such scales can quantify sensitively what subjects wish to convey, however words may fail to describe the ‘exactness of the subjective experience’ while categorical scales impose artificial categories on the continuous phenomena of feelings. Moreover, with a continuous scale such as the VAS, the change in effect can be quantified, i.e., in going from 10 mm to 20 mm the change may assumed to be the same as going from 30 to 40 mm, however the effect categories in a categorical scale cannot be assumed to be equidistant (Merbitz et al, 1989). The VAS also has the potential to be more sensitive than a categorical scale in detecting small changes in clinical effect over time (Scott and Hiskinsson, 1976). Since a continuous scale provides scores which are amenable to parametric analysis using non-linear regression (Robinson et al, 1975), such data may also potentially offer a better characterization of interindividual variability compared to a categorical scale.

From the spectrum of CNS effects measured in the phase I study (Moton et al, 2005), the endpoint of lorazepam-induced sleepiness was selected for analysis because

this measure: 1) showed the largest signal on both VAS and categorical scales, 2) showed the highest statistical significance in time-averaged change from baseline differences with placebo ($p < 0.001$), and 3) was analyzed previously using the categorical measure (Chapter 2). The current study investigates the exposure/response relationship of VAS-measured- lorazepam-sleepiness and explores the feasibility of modeling this VAS measure using a population mixed effects approach.

Methods

Data Collection

Twenty healthy volunteers were randomized in a double blind, single dose, 5-way crossover design (Moton et al, 2005). All subjects gave written informed consent to participate in the study. The study was conducted at the Clinical Pharmacology Unit of Pfizer (Ann Arbor, MI) in accordance with the principles of the Declaration of Helsinki. The study protocol was approved and performed in compliance with the Institutional Review Board/Independent Ethics Committee (IRB/IEC) and International Committee on Harmonization (ICH) Good Clinical Practice guidelines. Each subject received an oral dose of either lorazepam 2 mg, as one of four CNS drugs, or placebo. All study drugs were commonly used marketed compounds within their respective therapeutic indications and were selected to produce different AE profiles which could potentially be measurable after single dose administration. Each regimen was separated by a one week washout period for a total trial period of five consecutive weeks. Blood samples were drawn before dosing and at 0.5, 1, 2, 3, 4, 6, 8, 10, 12, 24, 48, and 72 hr after the morning dose and were assayed for lorazepam concentrations as previously described (Chapter 2).

Prior to each blood collection during the first 24 hr, the VAS, as shown in Figure 3.1, was administered along with the 7 point ordered categorical scale previously reported (Kamal et al, in press). Subjects were asked to indicate how they felt at the moment for 9 separate VAS scales measuring sleepiness, dizziness, nausea, forgetfulness, confusion, weakness, stiffness, and blurred vision. The scales consisted of 100 mm line anchored at both ends by “Not at all” and “Extremely” as shown in Figure 3.1. Subjects were instructed to draw a slash across the line between these anchor points and the effect was quantified by measuring the distance of the slash from the minimal extreme, “Not at all”, and was recorded to the nearest millimeter.

Data Analysis

Logistic Transformation

Distribution of the lorazepam sleepiness VAS scores at various time points was skewed to the right as shown in Figure 3.3A. VAS scores were transformed using the following logistic transformation as described by Senn (2002).

$$Y = \text{Log} \left(\frac{\text{VAS Score}}{100 - \text{VAS Score}} \right) \quad \text{Equation 1}$$

Where Y denotes the transformed score in logits. For this transformation to be applied, 1 mm was added to zero data and 1 mm was subtracted from 100 mm data (if any). The following reverse logit transform was used to reconvert transformed scores in logits to VAS millimeters.

$$\text{VAS score} = 100 * \left[\frac{e^Y}{1 + e^Y} \right] \quad \text{Equation 2}$$

Where Y denotes the transformed variable obtained by Equation 1.

Structural PK/PD Model

PK/PD modeling of the time course of lorazepam concentrations and transformed VAS sleepiness scores were conducted in NONMEM (Beal and Sheiner, 1992) using the first order conditional estimation method with interaction (FOCE INTERACTION). The general model building strategy is based on modification of different approaches discussed by Beal and Sheiner (1992), Mandema et al (1992), and Ette and Ludden (1995). During model building, the goodness of fit of different models to the data was evaluated using the following criteria: change in the minimum objective function (MOF), visual inspection of concordance and residual plots, precision of the parameter estimates, the distribution of interindividual variability, and decreases in both inter-individual and residual variability. A decrease in the MOF of at least 10.83 upon addition of a parameter was considered statistically significant. This corresponds to a nominal p value of <0.001 and one degree of freedom in the chi square distribution of the difference of MOF between hierarchical models.

The previously reported two-compartment model with first order absorption employed in the categorical analysis was used to describe the time course of plasma concentrations of 2 mg oral lorazepam (Kamal et al, in press). VAS sleepiness scores were modeled as a function of baseline effect, placebo effect, and lorazepam drug concentrations. The general model describing VAS sleepiness scores was:

$$\text{VAS Score} = \text{BSL} + \text{PLAC} + \text{DRUG}$$

Equation 3

Where BSL a constant describing baseline sleepiness effect, PLAC is a structural model describing placebo sleepiness effect and DRUG is a structural model component describing lorazepam sleepiness effect. Exploratory analyses of each component was done separately by modeling baseline initially and then adding drug and placebo model components sequentially while observing the decrease in MOF.

Several models of drug effect were tested including: linear slope models using actual concentrations, post hoc PK estimates, and effect compartment concentrations. Hill functions with a fixed ($E_{max} = 100$) and non-fixed E_{max} with and without a sigmoidicity factor were also tested. Examination of the PK- and PD-time profiles showed a lag between concentrations and effect and as such used an effect compartment model was proposed. In the final model, the effect of lorazepam (DRUG) is linearly related to lorazepam concentrations in the effect compartment and was written as:

$$\text{Drug} = \text{SLOPE} * \text{CE} \quad \text{Equation 4}$$

Where SLOPE is the slope of the relationship between the increase in VAS response and CE, the concentrations of lorazepam in the hypothetical effect compartment, as described by Sheiner et al (1979). Concentrations in this effect site are linked to the central compartment with a first order rate process and assume negligible mass transfer of drug to that compartment. Thus, the equilibration between the central and effect compartment is driven by a first order rate constant (K_{e0}) which describes the delay between appearance of concentrations in plasma and onset of PD effect. Concentrations in the central compartment were predicted from the posthoc Bayesian estimates from the final PK model (chapter 2).

Many models were tested for placebo response including a simple constant response, exponential decay and a Bateman function. Although the Bateman function showed the lowest MOF, when k_2 , the first order rate constant describing offset of placebo effect, was modeled for sleepiness placebo, it resulted in over-parameterization as determined by inspection of the correlation matrix of estimates. The approach taken was to use a single first order rate constant k using the Equation 5 below:

$$\text{PLAC} = \alpha * k * t * \exp(-k * t). \quad \text{Equation 5}$$

Where PLAC is placebo response, α is a parameter describing amplitude of placebo response and k is a first order rate constant. This resulted in stabilization of the final placebo model and the lowest MOF.

Intersubject and Residual Variability

Intersubject variability was estimated on the mean pharmacodynamic parameter θ using an exponential error term. This was tested sequentially on all structural parameters and those parameters that were significant were retained during model building. Residual variability was described using an additive error model as this model showed the greatest decrease in the MOF.

Assessment of PK/PD Model Performance

In addition to concordance and residual plots, Monte-Carlo simulations were performed to assess the final model performance and these simulations were visually compared to those of the model applied to the untransformed VAS scores.

Results

Table 3.1 shows the demographic information of the twenty study subjects. The time course of observed mean \pm SD, after single oral dose administration of lorazepam 2 mg are shown in Figure 3.2. A noncompartmental analysis yielded mean (CV%) estimates for C_{max} of 26.8 ng/ml (22.9), t_{max} of 1.7 hr (40.8), $t_{1/2}$ of 16.8 hrs (21.3) and a total systemic exposure or $AUC_{0-\infty}$ of 551 ng*hr/ml (31.0). Peak lorazepam sleepiness score (MaxS) recorded on the VAS was 50.6 mm. The time to reach MaxS for lorazepam sleepiness scores was delayed (3.3 hr, Figure 3.2, B) compared to time of maximal lorazepam concentrations ($t_{max}=1.71$ hr, Figure 3.2, A). This temporal delay in relation to plasma concentrations was shown as a counter-clockwise hysteresis in the effect/concentration plot (Fig 3.2, C) and justified addition of the effect compartment to describe drug effect in the lorazepam sleepiness model.

Figure 3.3A shows the right skewed distribution of lorazepam sleepiness VAS scores at baseline and various time points. Figure 3.3B shows how applying the logistic transform shown in Equation 1 remedies the skewness, making the distributions look near normal.

Population PD model-building was initialized by addition of baseline parameter (BSL) Addition of the drug component of the model as a slope as described in Equation 4 resulted in a decrease in point reduction in the MOF > 300 indicating a significant drug effect. Table 3.2 shows the final PD parameter estimates. Addition of an effect compartment as described in Equation 5 was significant for sleepiness (MOF reduction was 22 points) and the final estimate of ke_0 , the first order rate constant describing lag in effect in the biophase compared to central compartment concentrations, was 5.17 hr^{-1} .

Addition of the k_1 parameter as shown in Equation 5 stabilized the model and significantly reduced the MOF (by >20 points).

Improvement in the diagnostics of the model after logistic transformation is seen in Figure 3.4. The PRED vs. Observed plots (panel A, Figure 3.4) showed an improvement after transformation as well as the IPRED vs. Observed concordance plot (panel B, Figure 3.4). The residual plot of WRES vs. PRED also showed great improvement with outliers (defined as points lying outside the range -5 to 5) seen in the upper panel of C, Figure 3.4, but absent in the lower panel.

The monte-carlo simulations of the model applied to untransformed and transformed VAS scores is shown in Figure 3.5. As shown, a significant improvement in the fit is seen after the scores are transformed.

Discussion

Although the VAS has been used in several clinical studies to measure subjective effects such as pain and mood, its pharmacometric utility in measuring drug effects in relation to drug exposure particularly in smaller studies is not well established. The current analysis investigates the pharmacokinetic/pharmacodynamic relationship of a VAS measure of sleepiness after single oral dose administration of lorazepam 2 mg reported by 20 healthy volunteers using a mixed effects population approach. The 2 mg dose of lorazepam represents the maintenance dose used in the treatment of generalized anxiety disorder.

Noncompartmental PK estimates of the plasma concentration/time plot shown in Figure 3.2, showed oral lorazepam 2 mg displayed rapid absorption kinetics with a t_{max}

of 1.71 hr, C_{max} of 26.8 ng/ml, and biological half life (t_{1/2}) of 16.8 hr. The PK model which was previously described (Chapter 2) was a 2 compartmental model with first order absorption which adequately characterized the time course of lorazepam plasma concentrations.

Mean peak Lorazepam sleepiness score (MaxS) recorded on the VAS was 50.6 mm at 3.3 hrs. This delay in effect in relation to plasma concentrations was shown as a counter-clockwise hysteresis in the effect/concentration plot (C, Fig 3.2). This temporal delay in lorazepam sleepiness observed with the categorical scale (chapter 2)..Peak lorazepam dizziness effect measured on the VAS showed no such delay (closed hysteresis loop, data not shown) and this temporal relationship was also in agreement with the categorical measure of dizziness (chapter 2), suggesting PK/PD temporal consistency between the VAS and the 7 point categorical scale. The temporal difference between lorazepam sleepiness and dizziness may be explained the presence of the Blood-Brain-Barrier (BBB). Subjects may be experiencing vertigo which is reported as dizziness. Such an effect occurs due to action of the benzodiazepine at GABA receptors in the vestibular nuclei of the inner ear and this does not require traversing the blood brain barrier. On the other hand, sleepiness may occur due to GABA receptor activity in the thalamus and sensory cortex in the brain (Volkow et al) and this requires traversing the BBB, which causes the temporal delay recorded on both VAS and categorical (chapter 2) scales.

Although the current VAS analysis uses non linear regression as opposed to the categorical analysis which uses logistic regression, the VAS pharmacodynamic model described in the current analysis contained similar structural features to the categorical

pharmacodynamic model, i.e. constant baseline, linear slope model with an effect compartment to characterize drug effect, and a Bateman-like placebo response.

The right skewed distribution of VAS scores at various time points at baseline and post lorazepam administration is shown in Figure 3.3A. This skewness phenomenon is the product of applying a bound scale, and as such there is a need to transform the data to make it normal or near normal. Typically, a Log transformation is applied in such situations (Senn, 2002), however while the log transformation may address the skewness, the transformed scores remained bound on a finite interval. Moreover, since zero data exists, there is a need to bias such data using a constant (c) and there is the problem of model predictions lying outside the interval $\text{Log}(c) \leq Y \leq \text{Log}(100)$. A transformation that addresses both the skewness and boundedness of the VAS is the logistic transform shown in Equation 1. As shown in Figure 3.3B, the distribution of VAS scores after logistic transformation approaches normality. The function also accommodates the scale limits at 0 and 100 mm by unsqueezing the values on both ends of the scale, converting the finite interval to the unbound logistic domain. To employ the transformation in the current analysis, there was a need to bias the extreme data by adding 1 mm to the minimal extreme (0 mm) and subtracting 1mm from the maximal extreme (100 mm) to accommodate the minimum and maximum asymptotes of the logistic function.. Since the subjects were not instructed to avoid marking anchor points in the current study protocol, there is a need in future studies to instruct subjects not to mark the anchor points of the VAS so as to avoid the need to induce this bias by the pharmacometrician. This may also necessitate modifying the scale, for example, changing the minimum anchor phrase in Figure 3.1 from “Not at all” to “ minimally” to assist the subject in following this

directive during a clinical trial. As shown in Figure 3.4, the concordance of the population predictions (PRED) and individual model predictions (IPRED) to observed VAS sleepiness scores improved greatly after transforming the data to the logistic domain. This is also reflected in the improvement in Montecarlo simulations in Figure 3.5 when re-converting transformed scores to the original scale using Equation 2. Both the lorazepam treatment and placebo response simulations adequately capture the observed mean VAS responses.

Conclusion

Similar to the categorical measure, the VAS measure of lorazepam sleepiness was recorded with a delay compared to peak plasma concentrations. The logistic transformation remedied the skewness and boundedness of VAS scores and greatly improved pharmacodynamic model diagnostics.

Table 3.1 Subject Demographics

| Parameter | Mean (SD) |
|------------------------------|------------------|
| Gender, n | |
| Male | 5 |
| Female | 15 |
| Race, n | |
| White | 17 |
| Black | 3 |
| Age, y | 43 (11) |
| Weight, kg | 72 (12) |
| Creatinine clearance, ml/min | 103 (22) |

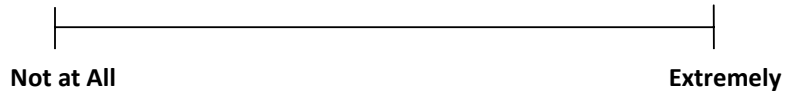
Table 3.2. Pharmacodynamic Parameters in Healthy Volunteers after a 2mg Oral Dose of Lorazepam or Placebo (n=20).

| Parameter | NONMEM Estimate | 95% CI |
|-------------------------|------------------------|---------------|
| BSL (logit) | -3.53 | -3.93 , -3.13 |
| SLOPE (logit*ml/ng) | 0.07 | 0.04, 0.1 |
| Keo (h ⁻¹) | 5.17 | 1.3, 9.1 |
| alpha (logit) | 2.03 | 1.12, 2.94 |
| k (h ⁻¹) | 0.36 | 0.27 , 0.45 |
| IIV-BSL | 22.25 | 9.96, 34.53 |
| IIV-Slope | 68.48 | 22.32, 114.6 |
| IIV-keo | 148.32 | 40.76, 255.75 |
| IIV-alpha | 60.17 | 21.31 , 99.03 |
| Residual Additive Error | 0.9 | 0.26, 1.54 |

BSL describes the baseline, SLOPE describes the relationship between drug effect and concentrations, ke0 is the first order rate constant describing lag in the effect compartment compared to lorazepam concentrations in the central compartment, alpha, describes the amplitude of placebo effect, k is a second order rate constant , IIV represents the percent inter-subject variability.

Place a slash (/) across the line in the position that best describes your response.

How sleepy do you feel right now?



| | | |
|--|--|--|
| | | |
|--|--|--|

Score in mm
(investigator's use only)

Figure 3.1. A modified Visual Analog Scale used to measure sleepiness.

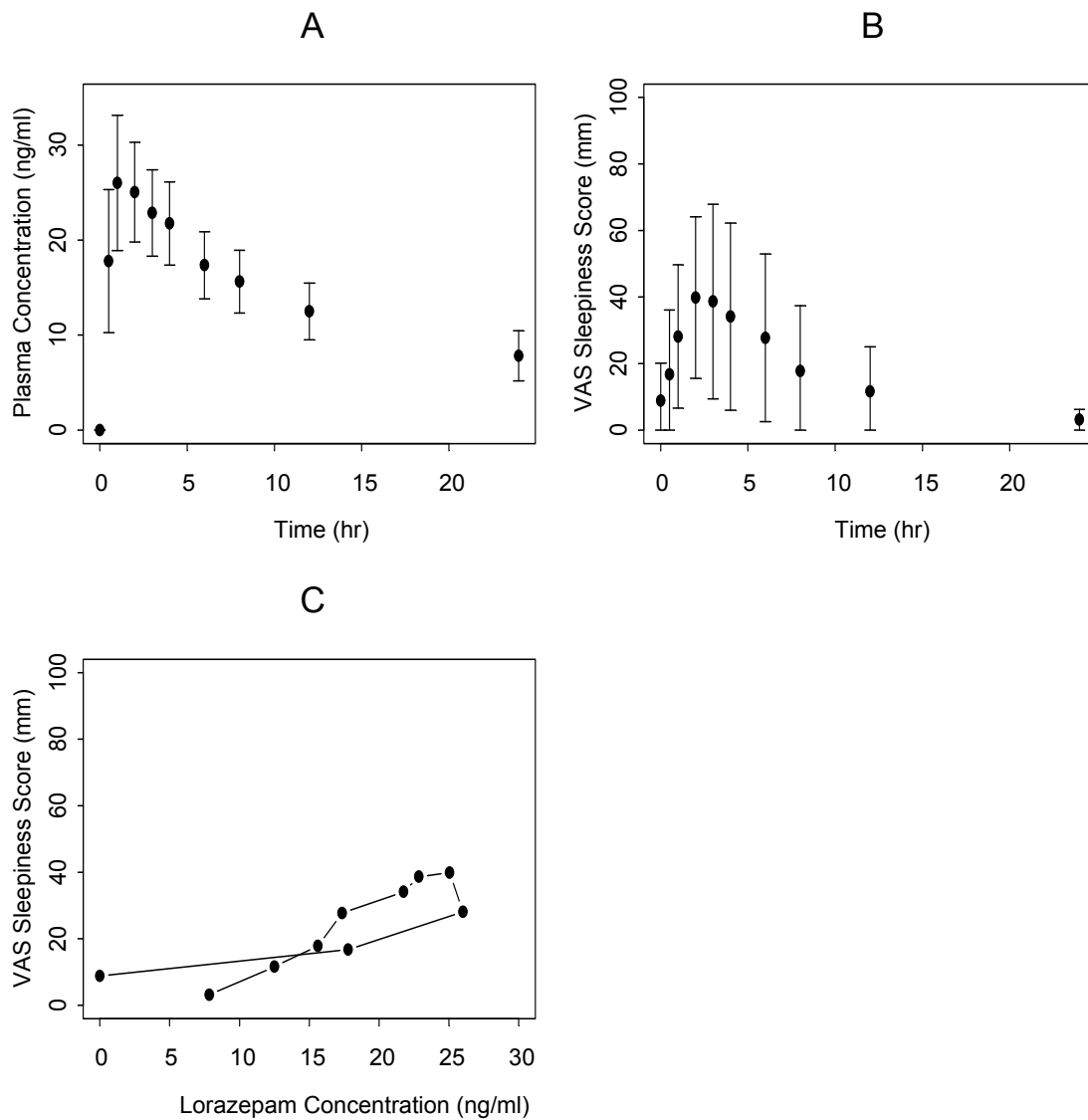


Figure 3.2. **A:** The time course of Lorazepam plasma concentrations after oral administration of a 2 mg dose in twenty healthy volunteers. **B:** Time course of Sleepiness measured on the VAS after administration of 2 mg Lorazepam. **C:** Counter-Clockwise Hysteresis on the Effect-Concentration plot denoting the lag in Sleepiness effect compared to plasma lorazepam concentrations.

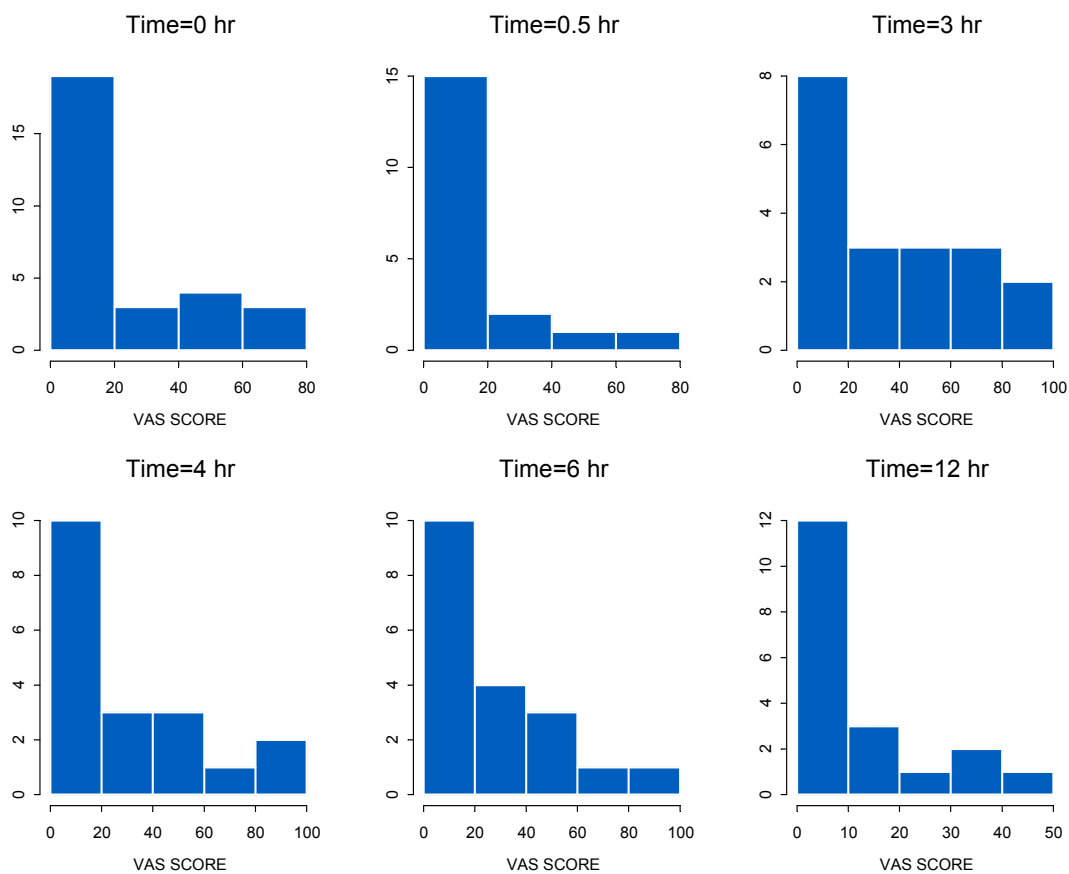


Figure 3.3A Histograms showing the right skewed distribution of VAS sleepiness scores reported by 20 healthy subjects after oral administration of a 2 mg dose at various time points (Time = 0, 0.5, 3, 4, 6, 12 hr).

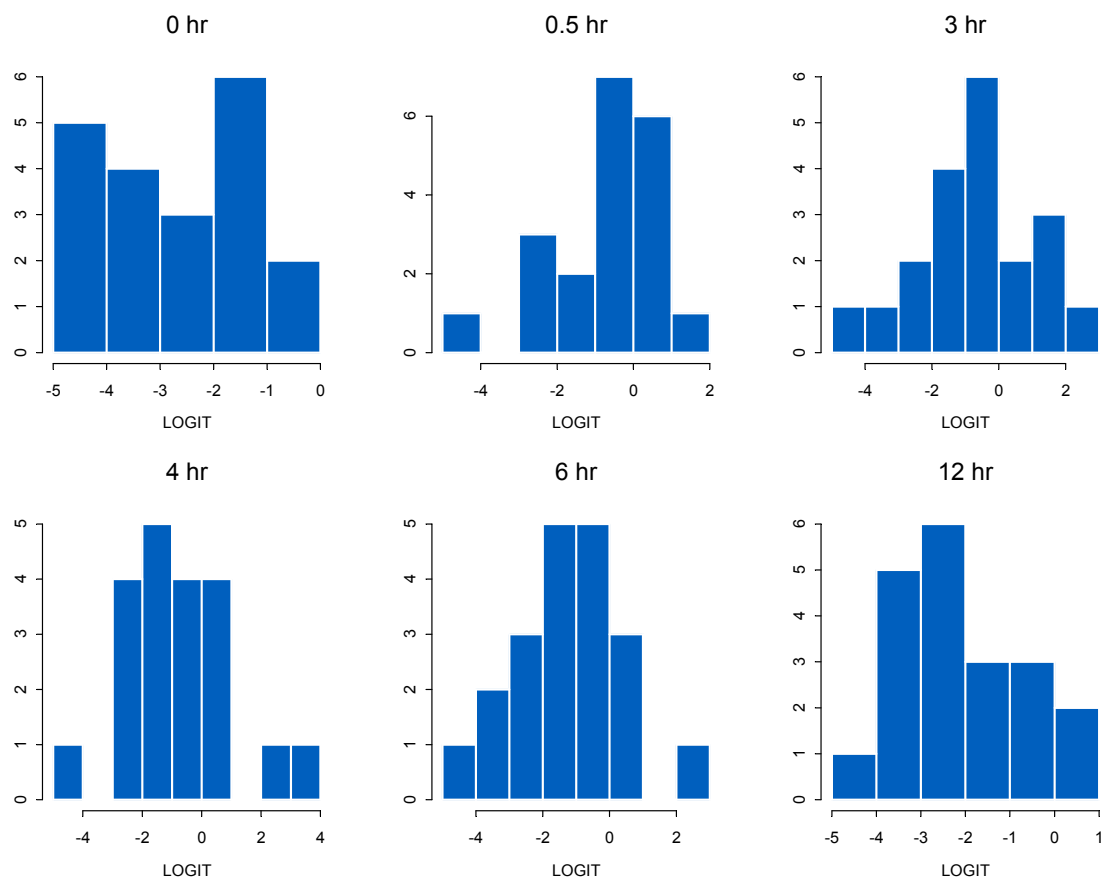


Figure 3.3B Histograms showing the distribution of Logit transformed VAS scores reported by 20 healthy subjects after oral administration of a 2 mg dose at various time points (Time = 0, 0.5, 3, 4, 6, 12 hr).

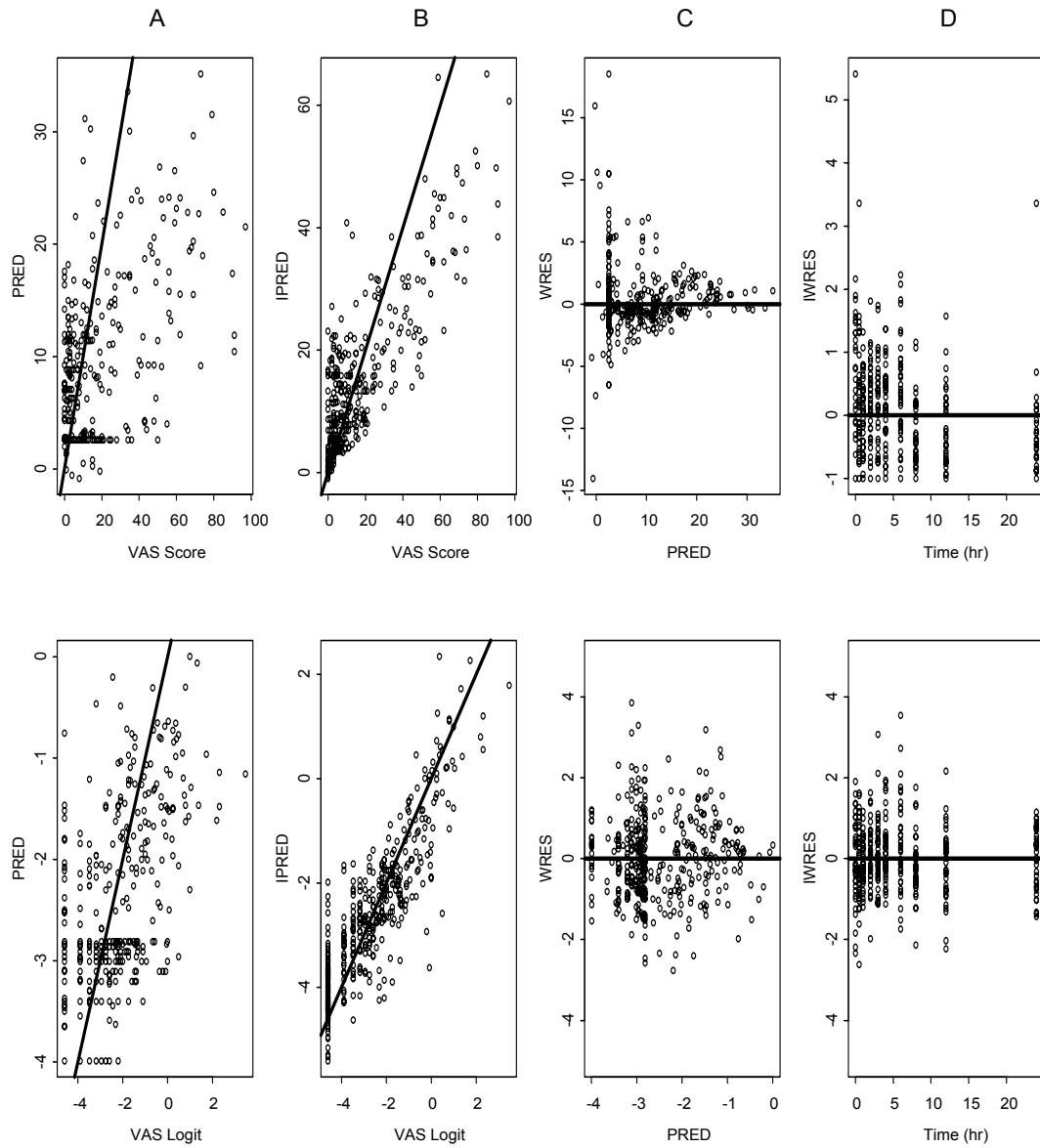


Figure 3.4. Concordance Plots. (Top panel: Model applied to VAS Scores in the Untransformed Domain. Bottom Panel: Model applied to Transformed VAS scores in the Logistic Domain). **A** Predicted (PRED) VAS scores versus Observed (OBS). **B** Individual Predicted VAS Scores (IPRED) versus Observed (OBS). **C**: Weighted Residuals (WRES) versus time. **D** Individual Weighted residuals versus Time.

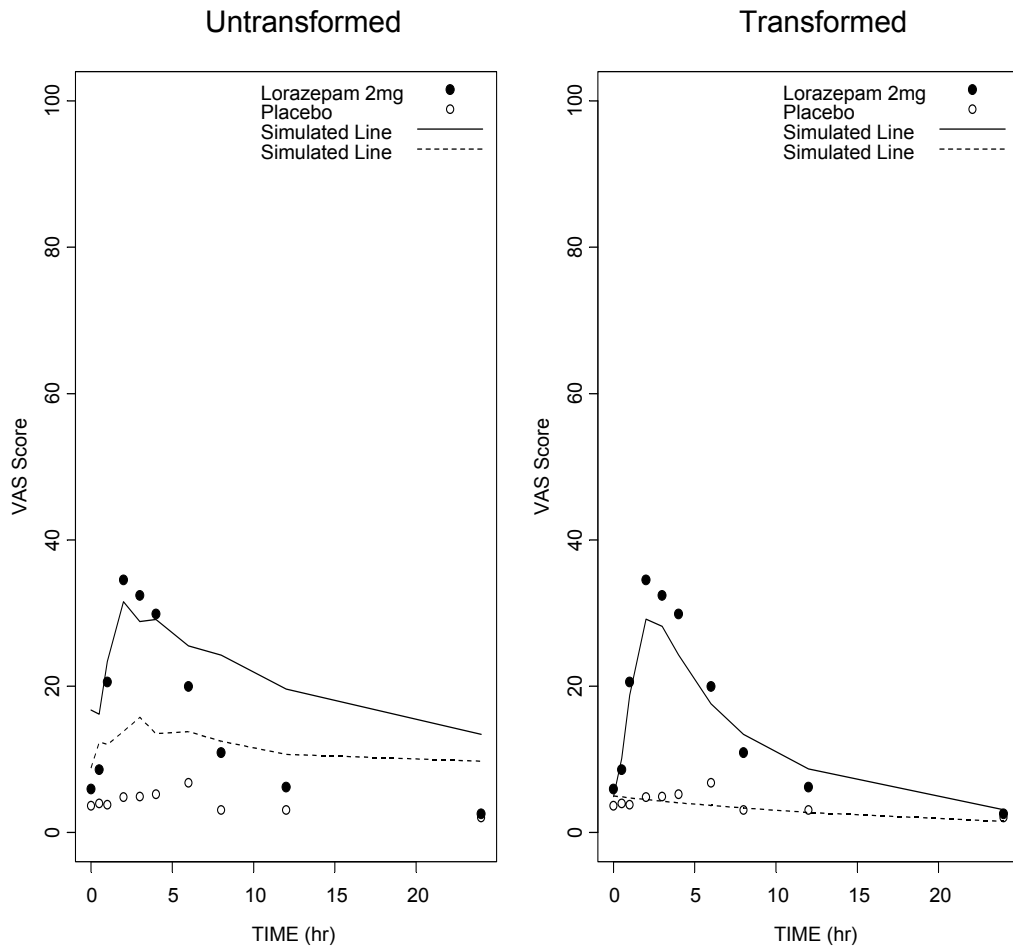


Figure 3.5. Monte-Carlo simulations of the VAS untransformed scores and transformed scores converted to the original scale.

References

- Aitken R. A growing edge of measurement of feelings. *Proc Royal Soc Med.* 62: 989-996 (1969).
- Aitken R, Zealley K. measurement of Moods. *Brit J Hosp Med.* 4: 215-225 (1970).
- Beal SL, Sheiner LB, Eds. NONMEM user's guides. San Francisco: NONMEM Project Group, University of California (1992).
- Carlsson, A. M. Assessment of chronic pain. I. Aspects of the reliability and validity of the visual analogue scale. *Pain, 16*, 87–101. (1983).
- DeLoach L, Higgins M, Caplan A, Stiff J. The visual analog scale in the intermediate postoperative period: intrasubject variability and correlation with a numeric scale. *Anesth Analg* 86:102-106 (1998)
- Ette EI, Ludden TM. Population pharmacokinetic modeling: The importance of informative graphics. *Pharmaceut Res.* 12:1845-55.(1995)
- Ferraz MB, Quaresma MR, Aquino LR, Atra E, Tugwell P, Goldsmith CH. Reliability of pain scales in the assessment of literate and illiterate patients with rheumatoid arthritis. *J Rheumatol.* 18:1269-70. (1991)
- Folstein M, Luria R. Reliability, validity, and clinical application of the visual analogue mood scale. *Psychol Med* 3: 479-486 (1973).
- Frueh BC, Johnson D, Smith DW, Williams MA. A potential problem with the response format of the dissociative experiences scale: A significant correlation with intelligence among combat veterans with PTSD. *J Trauma Stress.* 9:651-656 (1996).
- Hornblow, A. R., & Kidson, M. A. The Visual Analogue Scale for Anxiety: A validation study. *Aus & New Zeal J Psych, 10*, 339–341 (1976).
- Jaeschke R, Singer J, Guyatt G. A comparison of a seven-point and Visual Analogue Scales. Data from a randomized trial. *Control Clin Tri.* 11:43-51 (1990)
- Little J, McPhail N. Measurement of depressive mood at monthly intervals. *Brit J Psych.* 122: 447-452 (1973).
- Lundeberg T, Lund I, Dahlin L, Borg E, Eriksson S. Reliability and responsiveness of three different pain assessments, *J Rehabil Med.* 33:279-283 (2001).
- Mandema JW, Verotta D, Sheiner LB. Building population pharmacokinetic-Pharmacodynamic models. I. Models for covariate effects. *J Pharmacokin Biopharm.;* 20:511-28 (1992)
- McCormack H, Horne D, Sheather S. Clinical Applications of visual analogue scales: a critical review. *Psychol Med.* 18: 1007-1019 (1988).
- Merbitz C, Morris J, Grip J. Ordinal scales and foundations of misinference. *Arch Phys Med Rehab.* 70:308-312. (1989)
- Moton A, Ouellet D, Morlock R, Nyberg J, Feltner D. Feasibility of assessing differential pharmacodynamic (PD)/adverse events(AE) profiles on CNS agents. *Clin Pharm & Therap.* 77(2).(2005)
- Senn S. Cross-over trials in clinical research. 2nd Edition, pg 93-96.(2002)
- Sheiner LB, Stanski DR, Vozeh S, Miller RD, Ham J: Simultaneous modeling of pharmacokinetics and pharmacodynamics: application to d-tubocurarine. *Clin.Pharmacol.Ther.* 25: 358-371.(1979)

Svensson E. Comparison of the quality of assessments using continuous and discrete ordinal rating scales. *Biomet J* 42:417-434. (2000).

Vickers A. Comparison of an ordinal and a continuous outcome measure of muscle soreness. *Int J Tech Assess Health Care*. 15:709-716. (1999)

CHAPTER 4

CONCLUSION TO PART I

Major Findings

The pharmacometric analyses have shown that the ordered categorical measures of lorazepam sleepiness and dizziness were successfully modeled using a logistic function. The performance of the models were shown to be appropriate and verified by simulation and various posterior predictive checks. Logistic transformation of the VAS lorazepam sleepiness scores normalized the right skewed distribution of VAS scores, greatly improved model diagnostics and simulations compared to those of the model applied to untransformed scores.. Although results of these pharmacometric analyses are promising, certain limitations of the current study preclude any definite conclusion of standard pharmacometric utility of the categorical scale or the VAS in small clinical studies and warrant further investigation. The major limitations of the analyses include the inclusion of one study drug only (lorazepam) with the exclusion of the other three drugs studied (olanzapine, atomoxetine, and paroxetine). Atomoxetine and paroxetine both showed very weak PD signals on both scales whereas olanzapine showed a strong sleepiness signal on both scales, however, was excluded because sleepiness incidence data in the label was based on schizophrenic patients and not healthy volunteers. Another limitation of the study was that the order of tests (i.e. categorical vs. VAS) was not randomized at each time they were administered which may induce a bias, further complicating any direct comparison of these scales.

Proposed Future Studies

Future studies should investigate the following:

- 1) Modeling the VAS measure of lorazepam dizziness. Such an analyses would allow determination of whether the potency (i.e. slope) ratio between sleepiness and dizziness are constant across both categorical and VAS measures.
- 2) The measurement of PD differentiation profiles of adverse events in patients as opposed to healthy volunteers. To what degree are tolerability and efficacy PD profiles similar between actual patients and healthy volunteers?
- 3) Since most PD signals recorded on these scales were of fairly low amplitude, further investigation into what constitutes the minimum quantifiable signal using the current power and study design is justified. The proposed population models may serve as a platform for clinical trial simulation studies to conduct sensitivity analysis on effect intensity parameters such as slope. Moreover, other factors need to be investigated such as the added power of current 5-way cross-over study designs and what power would be needed when using other study designs. Since a mixture of responder and non-responder sleepiness and dizziness was observed in the placebo group, simulation studies should also aim to determine what power is necessary to model responder data for a given ratio of responders.
- 4) The approach described of relating model-derived PD parameters to label incidence in creating preliminary PD differentiation profiles should be explored with other drugs and adverse event endpoints to determine the extent to which the approach is applicable in early small clinical studies.

5) Investigation of the interaction of certain factors such as age and drug effects altering mental alertness (e.g. sleepiness) on the ability of the subject to use categorical and VAS instruments during the course of a clinical trial are warranted, especially to identify those factors which contribute to potential respondent error.

PART II
**ROLE OF PEPT2 SYSTEM IN NEUROPEPTIDE DISPOSITION,
DYNAMICS, AND TOXICITY**
CHAPTER 5

INTRODUCTION to PART II

Proton-Coupled Oligopeptide Transporters (POTs)

Four peptide transporters - PEPT1, PEPT2, PHT1 and PHT2- have been identified in mammals and are part of the proton-coupled oligopeptide transporter (POT) superfamily. These transporters are responsible for translocating small peptide fragments (di- and tripeptides) across biological membranes. What is unique about these peptide transporters are their driving force and substrate specificity. An inwardly-directed proton gradient and negative membrane potential is used as the driving force rather than ATP hydrolysis or Na^+ concentration gradient for the transporters. PEPT1 was the first mammalian oligopeptide transporter cloned, using expression-cloning strategies from a rabbit intestinal cDNA library (Fei et al., 1994). PEPT2 was the next peptide transporter identified, which was cloned from a human kidney cDNA library (Liu et al., 1995). Recently, two oligopeptide transporters, PHT1 (Yamashita, et al., 1997) and PHT2 (Sakata, et al., 2001), were cloned from a rat brain cDNA library. The transporters are unique from PEPT1 and PEPT2 in that they were shown to transport the amino acid, L-histidine, as well as di- and tri-peptides in the same proton gradient-dependent manner

The primary physiological function of POTs has long been recognized as the main

route for absorbing dietary nitrogen in the intestine and reabsorbing filtered peptide-bound nitrogen in the kidney. The fact that the absorption of protein digestion products in the small intestine occurs primarily in the form of small peptides (Matthews, 1975), and that up to 50% of circulating plasma amino acids is peptide bound (Seal et al, 1991; Schlagheck et al., 1984), further exemplifies the nutritional importance of peptide transporters. However, the wide expression of transporters in various tissues, especially PEPT2, implies the transporters might be involved in transporting peptides into cells for cellular metabolism and controlling overall amino acid homeostasis in the body. In particular, PEPT2 transcripts (Berger et al., 1999), protein (Novotny et al., 2000; Shu et al., 2002) and functional activity (Teuscher et al., 2000; 2001) have been reported in choroid plexus and this transporter is believed to play a role in neuropeptide homeostasis and the efflux of peptides/mimetics from cerebrospinal fluid.

The peptide transporters also have important pharmacological relevance because of their ability to transport numerous peptidemimetic drugs including amino β -lactam antibiotics of the cephalosporin and penicillin classes, angiotensin-converting enzyme inhibitors, aminopeptidase inhibitors (e.g., bestatin), renin inhibitors, photosensitizing agents (e.g., 5-aminolevulinic acid) and even non-peptidic compound (e.g., valacyclovir, valganciclovir). The oral absorption of these substrates is peptide transporter dependent, suggesting that their efficacy is at least partially attributable to the peptide transporters. Once the drugs are circulating in the plasma, they are filtered through the glomerulus then reabsorbed in the kidney via peptide transporters. This reabsorption lowers the renal clearance of drug, thereby increasing its half-life in the circulation. The transporters also affect the drug distribution and disposition in the other organs such as the brain, lung and

eye. Hence, the peptide transporters play a critical role in the pharmacokinetic profile and, ultimately, the therapeutic effect of various peptidomimetic drugs.

POT Tissue and Cellular Localization

PEPT1 protein is localized on the brush border membrane of the absorptive epithelia cells of the small intestine (Ogihara et al., 1996) and the kidney (Shen et al., 1999; Terada et al., 1997). More specifically, intestinal PEPT1 is confined to duodenum, jejunum and ileum of intestine, and S1 segments of the proximal tubule in the kidney (Shen et al., 1999). These segments are shown in Figure 5.2. PEPT1 is thought to be the predominant POT located on the brush border membrane of the small intestine, and is primarily responsible for the absorption of small peptide fragments from the digestion of dietary proteins (Fei et al., 1994). PEPT1 mRNA is mainly expressed in the small intestine and at low levels in the kidney, liver and pancreas (Fei et al., 1994; Gonzalez et al., 1998). PEPT1 however, is unable to be detected either as mRNA in rabbit, human or rat brain (Fei et al., 1994; Saito et al., 1995; Liang et al., 1995; Doring et al., 1998; and Fujita et al., 1999) or as protein in rat brain (Shen et al., 2004).

PEPT2 exhibits different expression patterns in the kidney when compared to that of PEPT1 (Liu et al., 1995; Boll et al., 1996). More specifically, it is confined to the S2 and S3 segments of the proximal tubule (Shen et al., 1999) shown in Figure 5.2, and is especially enriched in the brush border membrane of the renal villi. PEPT2 is believed to play a more dominant role than that of PEPT1 with respect to conservation of peptide-bound amino acids in the kidney (Shu et al., 2001; Shen et al., 1999). PEPT2 mRNA expression is not only found in the kidney but also exhibits strong levels of expression in

the brain, lung and mammary gland, with weaker signals detected in the pancreas, skeletal muscle, heart, liver, spleen and colon (Doring et al., 1998). In regard to PEPT2 brain distribution, PEPT2 mRNA has been specifically localized to astrocytes, subependymal cells, ependymal cells and epithelial cells of the choroid plexus (Berger et al., 1999). Recently, PEPT2 protein was demonstrated in choroid plexus by Western blot analysis (Novotny et al., 2000; Shu et al., 2002) and by functional analysis (Teucher et al., 2000; 2001; Shu et al., 2002). Western blots also show that PEPT2 protein is expressed in whole brain homogenates (Novotny et al., 2000) as well as in the peripheral nervous system glial cells (Groneberg et al, 2001a). In the eye, *in situ* hybridization studies have localized PEPT2 mRNA to the retina (Berger et al., 1999). In the lung, PEPT2 protein was demonstrated to be expressed in alveolar type II pneumocytes, bronchial epithelium, and endothelium of small vessels (Groneberg et al, 2001b). As previously mentioned, the function of PEPT2 is also confirmed in mammary gland, in which it may contribute to the reuptake of short-chain peptides derived from hydrolysis of milk proteins secreted into the lumen and may reduce the burden of xenobiotics in milk (Groneberg et al, 2002).

PHT1 mRNA has been found in the brain and eye, particularly in the choroid plexus and retina (Yamashita et al., 1997). PHT2 mRNA transcripts were expressed primarily in the lymphatic system, lung, spleen and detected faintly in the brain (Sakata et al., 2001). However, the physiological role of PHT1 and PHT2 in these different organs and tissues has yet to be elucidated. In comparison to PEPT1 and PEPT2, relatively little is known about their cellular localization (i.e. plasma membrane vs. intracellular compartment).

PEPT2 Transport Models

As early as in 1983, Ganapathy discovered that the transport of peptides via the peptide transporters is driven by an inward H^+ gradient and a negative transmembrane potential difference. However, this proton motive force is generated by different mechanisms depending on the tissue and cell type where the proton-coupled oligopeptide transporter is located.

PEPT2 is assumed to be located on the apical membrane of the epithelium based on functional and immunolocalization studies in neonatal CP cells in primary culture (Shu et al., 2002). What is unclear, at present, is the mechanism generating the proton motive driving force by which peptides and mimetics are transported across apical membranes and into choroid plexus epithelial cells. Normally, the pH of bulk CSF is similar to that in plasma, but about 0.3 units lower in choroid plexus cells (Johanson, 1985). Unlike most epithelial cells, the choroid plexus distributes Na^+/K^+ -ATPase to the apical membrane and not the basolateral membrane (Ernst et al., 1986). This unique distribution is involved in the formation of CSF. Recently, a model for the transport of peptides and peptidomimetics in choroid plexus was proposed by Smith et al. (in press) and involves three primary steps: 1) Na^+/K^+ -ATPase in the apical membrane causes a sodium efflux from the cell and thus Na^+ gradient; 2) this gradient is then utilized by two Na^+/H^+ exchangers. The Na^+/H^+ exchanger located in the basolateral membrane applies this gradient for extruding protons into the blood with pumping Na^+ into the cell. The other Na^+/H^+ exchanger located in the apical membrane also exploits this gradient for exporting protons into CSF and creates an acid microenvironment at the choroidal epithelial surface between apical microvilli, such as that observed in the intestine and

kidney (Lucas, 1983); 3) the acid microenvironment or local hydrogen gradient drives uptake of peptides via the proton-coupled oligopeptide cotransport system. Figure 5.1 shows the transport model of PEPT2 in the choroid plexus epithelial cell.

While the basolateral localization of Na^+/H^+ antiporter in the CP has been confirmed (Speake et al., 2001), an apical Na^+/H^+ exchanger need further experiments to confirm its presence in CP. Figure 5.1A shows a representation of the oligopeptide transport model in the choroid plexus epithelial cell. Figure 5.1B shows a different representation of peptide/mimetic transport in the proximal tubule epithelial cell. As shown this model differs from that of the choroid plexus epithelial cell in the distribution of transporters on the apical and basolateral side.

General Substrate Structure

After an initial understanding of di- and tripeptide transport via POT, researchers began to evaluate the possibilities of transporting drug molecules using these peptide transporters. Drugs (and prodrugs) such as amino-cephalosporins and penicillins, angiotensin-converting enzyme (ACE) inhibitors, bestatin and renin inhibitors have been reported to be transported by the POT transporters. Figure 5.5 shows the structures of various substrates of PEPT2 under study in our lab.

While specific pharmacophore models have been developed for both PEPT1 and PEPT2, in general, several structural features of substrates are important for high-affinity interactions and binding by PEPT1 and PEPT2. These features include: 1) a peptide backbone of 2-3 amino acid residues, 2) both a free amino and carboxyl terminus (with free anion group in α -position), 3) the presence of hydrophobic side chains and 4)

stereoselectivity (with L-amino acids and trans-conformers being preferred). Still, the structural requirements for substrate recognition by the binding sites of oligopeptide transporters are even broader than once believed. A peptide bond is not an absolute requirement for transport, nor is the presence of a terminal amino or carboxyl group. Some significant exceptions have been demonstrated (Han et al, 1998) and, until a three dimensional crystal structure of the transporter protein is available, current pharmacophore models will continue to be refined by trial and error.

Choroid-Plexus and the Blood-CSF Barrier

The brain is an unusual tissue in that the entry of drugs from the circulating blood into the central nervous system (CNS) is restricted by presence of the blood-brain barrier (BBB) and the blood-cerebrospinal fluid barrier (BCSFB). The blood-brain-barrier, formed by the cerebral endothelial cells, is the interface of the circulating blood and the brain interstitial fluid (ISF), which surrounds the neurons and glia. The cerebral endothelial cells are characterized by presences of tight junctions which connect these cells to each other and by the paucity of fenestra or pinocytotic vesicles (Davson et al., 1989 Fenstermacher et al., 1989). The other barrier, the blood-CSF barrier, is formed by the choroid plexus and the arachnoid membrane. The tight junction between the epithelial cells, but not the endothelial cells of the choroid plexus, is involved in the functional role of this barrier (Cserr et al., 1971).

Once across these initial barriers, drug accumulation in the brain can be further restricted by a number of mechanisms including passive efflux into the bulk flow of cerebrospinal fluid (sink effect), metabolic degradation, and active efflux via transporters in the

epithelial cells of the choroids plexus and endothelial cells of the brain capillaries. In considering the therapeutic and toxic effects of drugs in the CNS, it is important to elucidate the routes and mechanisms by which these drugs that enter and leave brain. Figures 5.3 and 5.4 show sites of the barriers in the central nervous system.

Structure and Function of the Choroid Plexus

The choroid plexuses (CPs) are located in the two lateral ventricles, and the third and fourth ventricles. The CP in the fourth ventricle, like a single sheet of tissue, forms the roof of the cavity. Inside these tissues there is a complex, highly permeable, mainly venular, capillary network, which supplies the blood gases and nutrients to support the active secretion of CSF and the transport processes between blood and CSF. The epithelial cells of the CP are joined together by an occluding band of tight junctions close to the CSF side of the cell. These junctions are made up of multiple strands yet are more permeable than those of the BBB (Meller et al., 1985). The tight junctions do permit the flow of water and some salts between the cells (the paracellular pathway) yet restrict the passage of small molecules such as mannitol. The fact that the choroid plexus is the major site of CSF secretion probably entails that it be a relatively leaky barrier tissue with a greater potential for leakage of neuroactive substances from blood. To prevent the entry of such agents from blood, transporters or enzyme may be required to remove any substances that cross the epithelium. It is possible that paracellular mechanisms may be a therapeutic target to enhance drug permeability if such confounding efflux transporters and enzymes could be avoided.

The cell walls of the basolateral sides of CP cells are highly convoluted, which expands the surface area between the cytoplasm and the extracellular fluid (ECF) of CP. The cell walls on the apical or CSF side of these cells are covered with microvilli, which greatly expands the surface area at the interface between the cytoplasm and CSF. Besides containing the apical brush border and basolateral interdigitations mentioned previously, the choroid plexus epithelium is endowed with mitochondria, which is required to maintain a high rate of oxidative metabolism during secretory and transport processes. Moreover, the cells also have well-developed subcellular organelles such as Golgi complexes, endoplasmic reticulum, ribosomes and a vesicular network. These structures may be involved in peptide and protein disposition such as synthesis, transcytosis, endocytosis and degradation. Figure 5.4 shows a representation of the choroid plexus and other barriers in the CSF.

As shown in Figure 5.1A, the epithelial cell membrane of the CP displays sidedness, i.e., the basolateral side of the choroid cells or the side facing the plasma has structural and functional features strikingly different from those associated with the opposite, apical pole of the cell in contact with the CSF. The basolateral side of choroid plexus epithelial cells also has a different repertoire of ion channels and pumps compared to the apical (CSF) side. Such polarization allows the net secretion of solutes from blood to CSF concurrently with net reabsorption of other compounds in the reverse direction. This asymmetric two-way traffic of solutes across the BCSFB is finely coordinated so that there is resultant homeostasis of both choroidal cellular fluid and the generated CSF. By elucidating the physiologic nature for transepithelial fluxes of solute across the

choroidal membrane, the pharmacologist and clinician should be better able to manipulate the movement of drugs between plasma and CSF.

The main functions of the choroid plexus are to: 1) secrete CSF. 70-90% of CSF is generated by choroidal tissues located in all four ventricles; 2) provide buoyancy and protection where the floating of brain on a fluid cushion of CSF within the skull protects the brain from injuries that would otherwise result from abrupt movements such as a car crash; 3) Control and buffer extracellular fluids composition forming a physical barrier to the diffusion of molecules between blood and CSF. 4) Participate in neurohumoral signaling in transduction either as a target or a source of synthetic endocrine messenger; 5) Provide immune privilege acting as is a 'port of entry' for many pathogens into brain and contains cells of the immune system that can present antigen and stimulate the production of peripheral T helper cells to form a critical "arm" of the cellular immune system of brain (Cserr and Knopf, 1992).

Potential for Drug Delivery

The blood-CSF barrier route has been considered to have a minor role for drug delivery to CNS compared to the blood-brain barrier. The main argument has been that the surface area of the CP is three to four orders of magnitude less than the total circumferential surface area of the brain capillaries (Pardridge et al., 1981). Another fact is that all parenchymal cells are within about 50 μm of a capillary, whereas cells in deep brain structures may be substantially further away from the CSF system, especially in species with large brain, such as man. However, other blood-CSF barrier studies have revealed that the choroid plexus may play a more significant role in brain drug delivery

than previously viewed. First, as previously mentioned, the choroidal surface available for exchange between the blood and the CSF is largely increased by the basolateral infolding, and the apical microvilli of the choroidal cells. (Keep, 1990). As estimated from the choroid plexus of 1-month-old rats, which is typically 2-3 mg wet weight, the total apical surface area of the choroidal epithelium approximates 75 cm^2 , about one half that of the blood-brain barrier (155 cm^2) (Keep, 1990).

Second, drugs introduced into the ventricular CSF are quickly distributed by the flow of this fluid that circulates by different routes within and around the brain to various tissues, such as ependymal, leptomeninges, velae, outer layers of pial vessels and perivascular spaces of parenchymal vessels (Gherzi-Egea et al., 1996). Thus, CPs constitute a direct access to pharmacological targets for diseases (Alzheimer's, AIDS dementia, stroke, epilepsy, cancer and bacterial meningitis).

Moreover, the paracellular permeability of the choroidal epithelium is higher than that of the endothelium forming BBB (Davson and Segal, 1996; Meller, 1985), which implies the blood-CSF barrier is somewhat "leakier" than the blood-brain barrier. As demonstrated stavudine, a polar antiretroviral agent, can slowly diffuse into the CSF through the CPs, whereas its penetration cross the BBB is almost completely prevented (Thomas et al., 1998).

Finally, the expression of a large number of influx and efflux transport systems (e.g. PEPT2) and metabolic enzymes at the choroid plexus has been recently found. For many solutes and substances, their main, if not exclusive, route of entry into the brain is by the way of the blood-CSF barrier through specific saturable carriers. Such selectivity

in the CP affords pharmacological opportunities for manipulating fluxes of therapeutic agents into the highly protected cerebral environment. However, the blockade of efflux transporters and enzyme has been explored as an alternative approach to increasing CNS drug exposure (Wong et al., 1993).

Transporter Distribution at Choroid Plexus

The choroid epithelia, unlike the cerebral endothelia, are equipped with channels for large-capacity secretion of ions and water into the CNS (Johanson, 1988). Additionally, there are specialized carrier transport systems in CP for facilitating the movement of micronutrients. Numerous transport systems related to drug delivery at the choroid plexus have been identified. They include organic anion transporters and organic cation transporters (OATs and OCTs, SLC22 family) (Gherzi-Egea et al., 2002), organic anion transporting polypeptides (OATPs, SLC21) (Choudhuri et al., 2003), Na⁺/dicarboxylate cotransporters, monocarboxylate transporters (MCTs), metal transporters (Choudhuri, 2003), bile acid transporters (Choudhuri, 2003), peptide transporters (POT, SLC15) (Teucher et al., 2000; 2001; Shu et al., 2002; Choudhuri, 2003) and glucose transporters. Compounds such as taurine (Keep et al., 1996), amino acids, choline, antipyrine and barbital (Johanson et al., 1997), nucleosides, riboflavin, and hypoxanthine have been characterized with respect to their uptake at the blood-CSF barrier. In addition, Rao *et al.* (Rao et al., 1999) determined the expression of the drug efflux protein, P-glycoprotein (multidrug resistance, MDR, ABCB) and the multidrug resistance-associated protein (MRP, ABCC) in human and rat choroid plexus.

Role of PEPT2 in Choroid Plexus Whole Tissue: *In Vitro* Studies

While many *in vitro* studies have been performed to elucidate the role of PEPT2 in transport of peptides these studies are confounded by the overlapping substrate specificities of the various transporters located on the epithelia of the choroids plexus. Thanks to development of the knockout PEPT2 model in our lab, *in vitro* whole tissue studies performed using transgenic knockout mice have provided preliminary evidence to the unequivocal role of PEPT2 in the transport of neuropeptides and peptide/mimetics.

Many *in vitro* studies have provided preliminary evidence as to the role of PEPT2 in the uptake kinetics of neuropeptides and peptide/mimetics. The proton-stimulated (pH 6.5) uptake of the dipeptide, glycylsarcosine (GlySar), in isolated whole choroid plexus tissue obtained from PEPT2^{-/-} mice was found to be functionally absent. Only 10.9% and 3.9% of the GlySar uptake present in PEPT2^{+/+} mice was still present at 5 min and 30 min in PEPT2^{-/-} mice, thereby providing functional evidence for the successful development of the PEPT2 transgenic knockout model and the conclusion that PEPT2 is the only transporter responsible for GlySar uptake at the choroid plexus (Shen et al., 2002).

Moreover uptake of the neuropeptide carnosine in rat choroid plexus primary cell cultures and choroid plexus whole tissue from PEPT2 knockout mice was investigated (Teuscher et al, 2004). Results indicated that carnosine was preferentially taken up from the apical as opposed to basolateral membrane of monlayers, and that this uptake process was characterized by a high affinity ($K_m=34$ μ M), low capacity ($V_{max}=73$ pmol/mg protein/min) process consistent with that of PEPT2. Studies demonstrated that PEPT2

was responsible for over 90% of carnosine's uptake in choroids plexus whole tissue while the non-saturable component was small and only accounted for 3% of total uptake.

To further investigate the relative importance of PEPT2 in the transport of peptide-like drugs, as opposed to model peptides and/or neuropeptides, uptake studies were performed with radiolabeled cefadroxil in the isolated choroids plexus of wild-type and PEPT2 knockout mice. At normal pH (pH 7.4) and temperature (37 °C), the uptake of 1 μ M cefadroxil was reduced by 83% in PEPT2^{-/-} mice as compared with PEPT2^{+/+} mice ($p < 0.001$). Although a proton-stimulated uptake of cefadroxil was demonstrated in PEPT2^{+/+} mice (pH 6.5 versus pH 7.4; $p < 0.01$), no pH dependence was observed in PEPT2^{-/-} mice. Based on kinetic and inhibitor analyses, it was determined that (under linear conditions), 80 to 85% of cefadroxil's uptake in choroid plexus is mediated by PEPT2, 10 to 15% by organic anion transporter(s), and 5% by nonspecific mechanisms (Ocheltree et al., 2004a). These findings demonstrate that PEPT2 is the primary transporter responsible for cefadroxil uptake in the choroid plexus. Moreover, the data also suggest a role for PEPT2 in the clearance of peptidomimetics from cerebrospinal fluid.

Role of PEPT2 in Peptide/Mimetic Disposition: *In Vivo* Studies

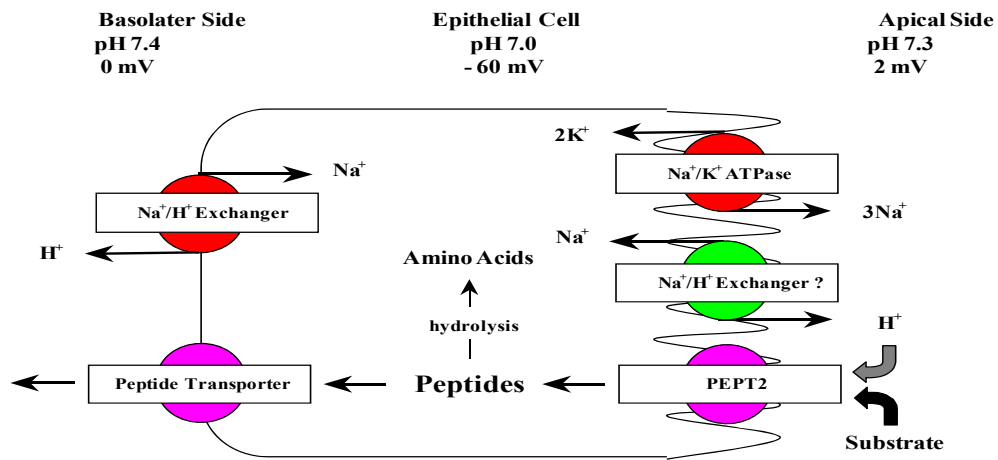
While great improvements have been made in the design of *in vitro* studies they are still limited by *in vitro* experimental designs which employ non-physiologic conditions, such as the lack of an intact blood supply. Moreover, as alluded to before the presence of multiple transport systems in a tissue or organ of interest, some of which are even unknown at time of study, makes it difficult to accurately determine the significance

of a single specific transporter relative to other transporters. Such a situation exists in the brain where multiple POT transporters are present with overlapping substrate specificities (e.g., PEPT2, PHT1 and PHT2) (Yamashita et al., 1997; Sakata et al., 2001). Thus, it is difficult to accurately define the function and significance of PEPT2 in relation to other peptide transporters.

The studies using wild type and PEPT2-deficient mice offer a unique opportunity to study the role and relevance of PEPT2 under physiological *in vivo* conditions. As both a nutrient and drug transporter, we believe that PEPT2 will play a pivotal part in affecting the pharmacodynamics, tissue distribution and systemic exposure of peptides, neuropeptides and therapeutically important peptide/mimetic drugs. This contention is supported by preliminary data from our laboratory (Ocheltree et al, 2004b) in which GlySar was administered as an iv bolus dose (0.05 $\mu\text{mol/g}$ body weight) to wild type and PEPT2 null mice. In the study, the *AUC* was lower in PEPT2^{-/-} mice than in wild-type animals, as a result of the approximately two-fold difference in total clearance values (0.46 ml/min in PEPT2^{-/-} mice vs. 0.27 ml/min in PEPT2^{+/+} mice). However, no differences were observed in the volume of the central compartment (~ 3.8 ml) or volume of distribution steady-state (~ 10 ml) between genotypes. PEPT2^{-/-} mice demonstrated a shorter half life (18 min vs. 25 min) and mean residence time (24 min vs. 34 min), and a faster central compartment elimination rate (0.12 min⁻¹ vs. 0.07 min⁻¹) as compared to PEPT2^{+/+} mice. Greater tissue concentrations of GlySar (nmol/g) were observed in the kidney (5 fold), lung (3-fold) and liver (1.5 fold) of PEPT2^{+/+} mice compared to PEPT2^{-/-} mice. In contrast, PEPT2^{-/-} mice demonstrated a 2-fold greater concentration of GlySar in cerebrospinal fluid (CSF) and 4-fold greater CSF/choroids plexus ratio. Although

Glysar is a synthetic substrate with no physiological significance, these preliminary results suggest that the pharmacokinetics of a peptide/mimetic or peptide-like drug can be significantly altered by the presence and functional activity of PEPT2 in the body, particularly the kidney and brain.

A



B

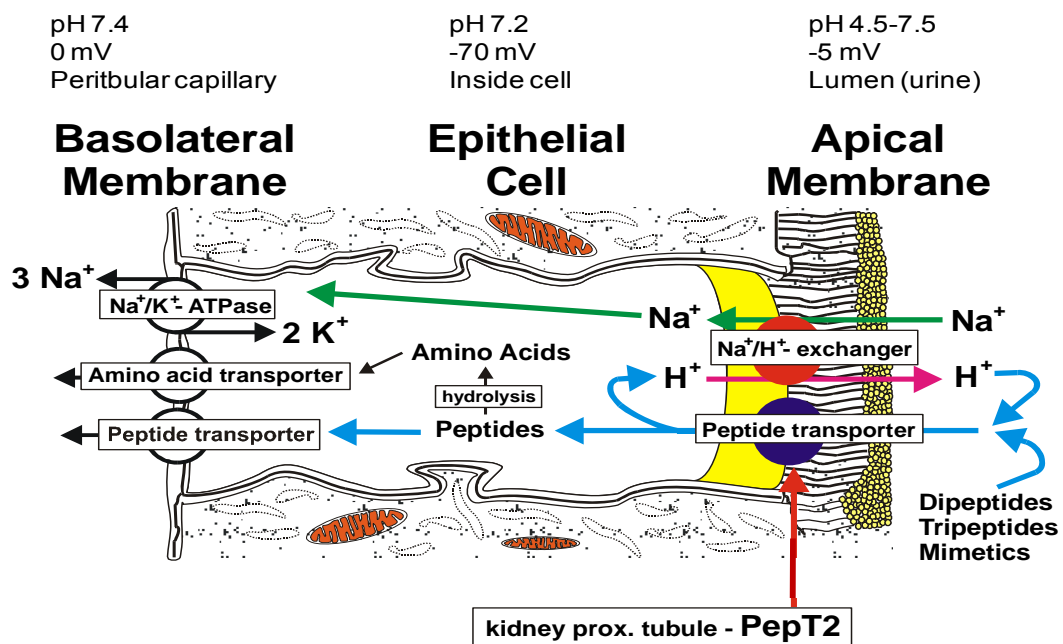
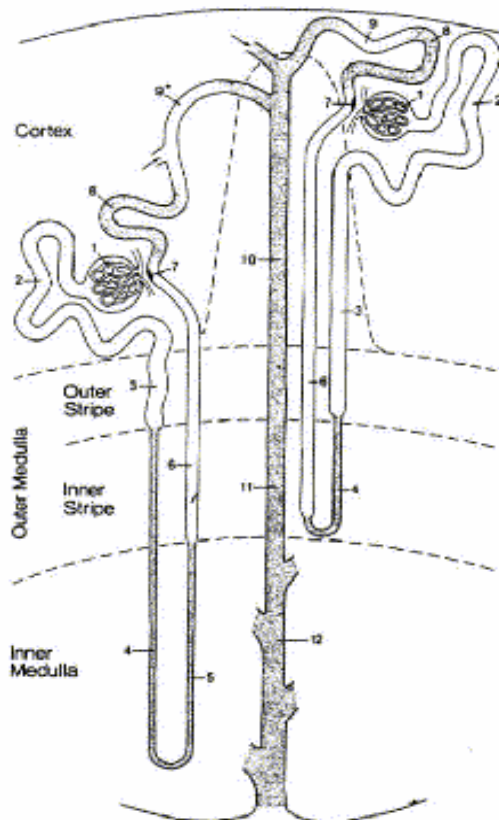
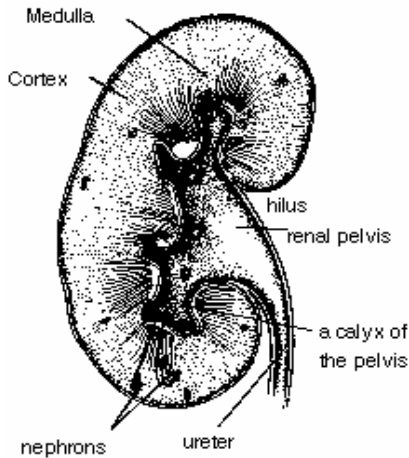


Figure 5.1. Sequential models of peptide/ mimetic transport in the choroid plexus [A] and renal proximal tubule epithelium [B] by PEPT2 showing the concerted action of apical and basolateral transporters in creating the acidic microenvironment at the apical interface.



- 1 = Renal corpuscle including Bowman's capsule and the glomerulus (glomerular tuft)
- 2 = Proximal convoluted tubule
- 3 = Proximal straight tubule
- 4 = Descending thin limb
- 5 = Ascending thin limb
- 6 = Distal straight tubule (thick ascending limb)
- 7 = Macula densa located within the final portion of the thick ascending limb
- 8 = Distal convoluted tubule
- 9 = Connecting tubule
- 9* = Connecting tubule of the juxtamedullary nephron that forms an arcade
- 10 = Cortical collecting duct
- 11 = Outer medullary collecting duct
- 12 = Inner medullary collecting duct

Fig. 1. Scheme of nephron. This scheme depicts a short-looped and a long-looped nephron together with the collecting system. Not drawn to scale. Within the cortex a medullary ray is delineated by a dashed line

Figure 5.2. Schematic of the kidney and nephron functional unit. PEPT1 is localized in the S1 segment of the cortex (convoluted proximal tubule), while PEPT2 is localized in the later segment of the proximal tubule (corresponding to the S2-S3 segments of the outer medulla). Adapted from: Kriz W, Bankir L, Bulger RE, et al. A standard nomenclature for structures of the kidney. The Renal Commission of the International Union of Physiological Sciences. *Kidney Int.* 33:1 (1998).

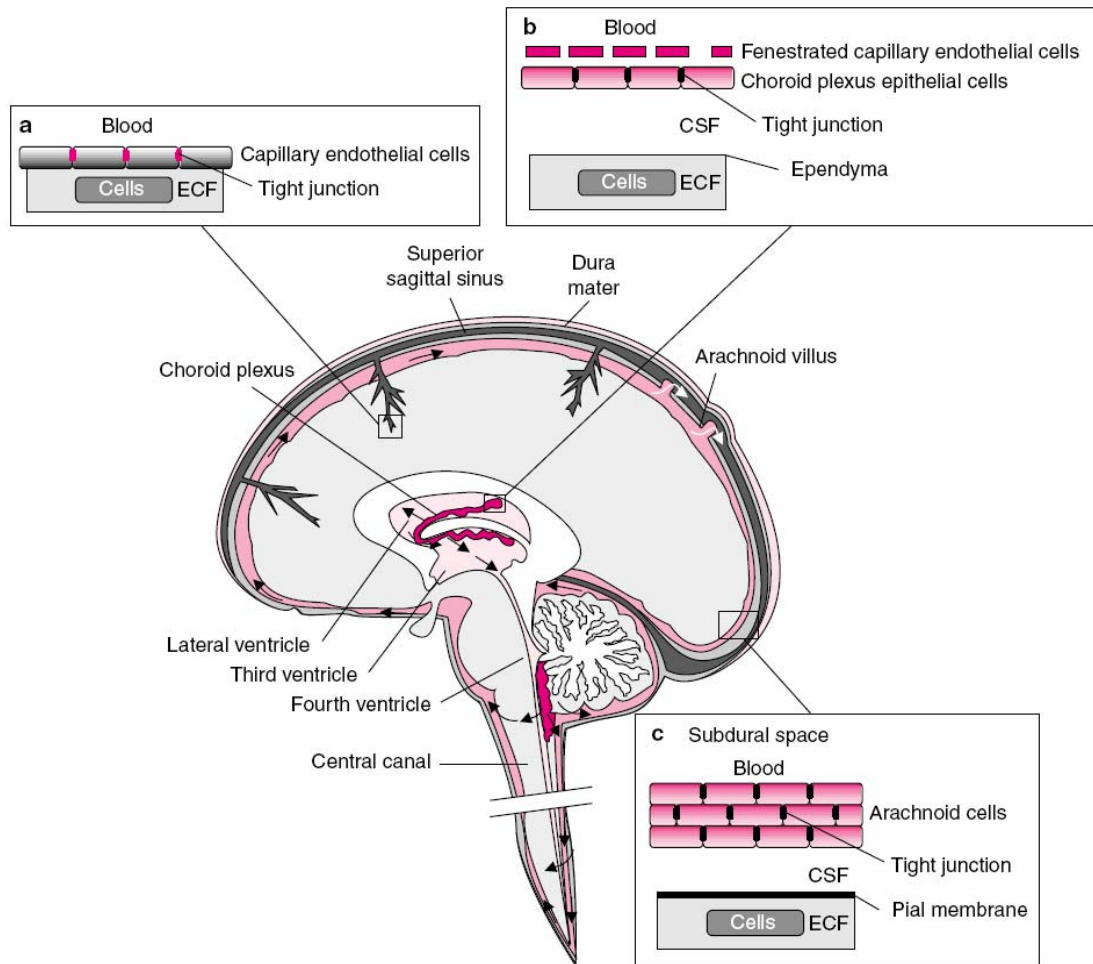


Figure 5.3. Sites of the barriers of the nervous system. Specialized endothelial cells with tight junctions form the blood-brain barrier (BBB). Tight junctions of the choroidal epithelium and the arachnoid epithelium form the blood-CSF barrier (BCSFB). ECF = extracellular fluid; CSF = cerebrospinal fluid. (Taylor, *Clin Pharmacokinet.*, **41**(2):81-92, 2002).

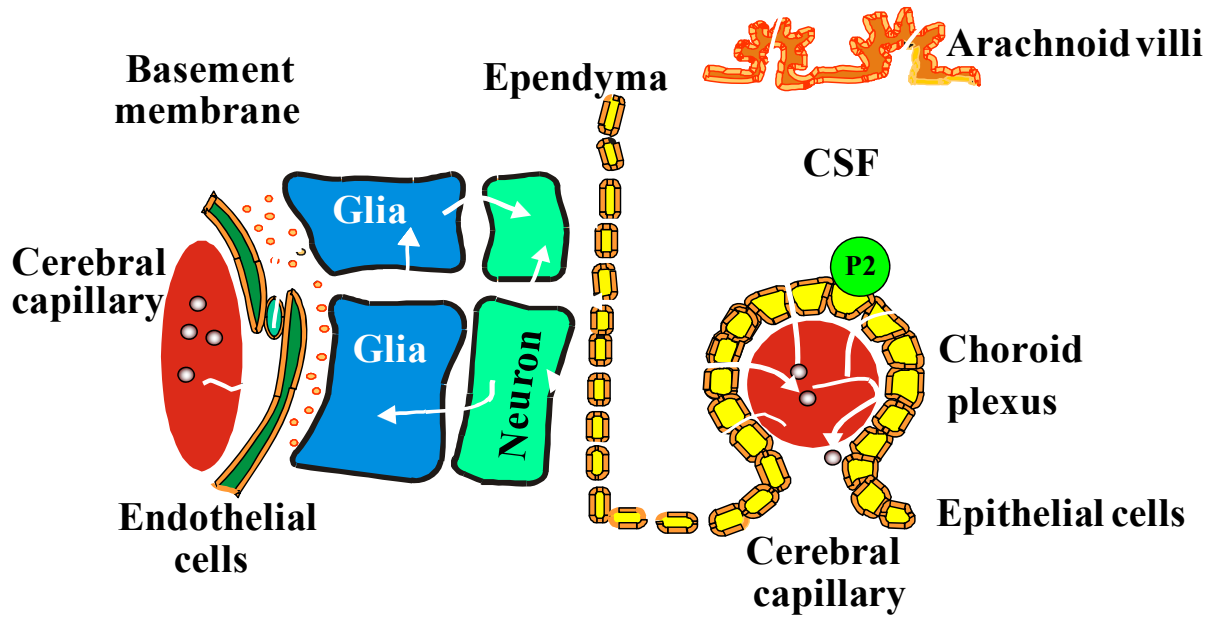
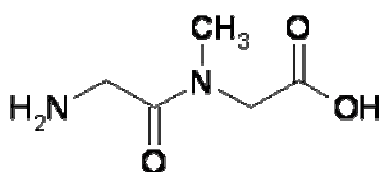
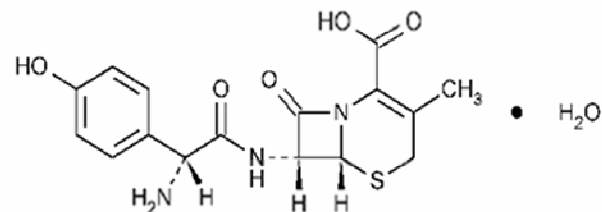


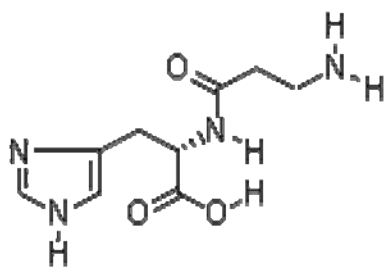
Figure 5.4. Illustration of the the Blood-Brain and Blood-CSF Barriers. The leaky ependyma separates the CSF and extracellular fluid surrounding the brain parenchymal cells. PEPT2 (shown as P2 above) is localized on the apical side of the choroid plexus epithelium and acts to remove peptides/mimetics from the CSF into the choroid plexus.



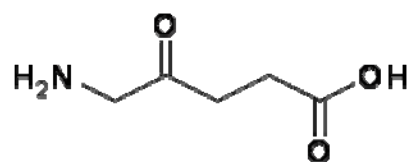
Glysar



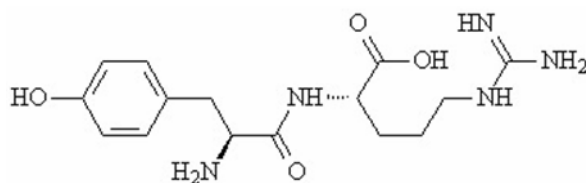
Cefadroxil



L-carnosine



5-ALA



L-Kyotorphin

Figure 5.5. Structures of various substrates of PEPT2 under study. Glysar is a synthetic dipeptide, while L-carnosine, 5-ALA, and L-Kyotorphin are physiologically relevant dipeptides. Cefadroxil is a peptide-mimetic amino-cephalosporin.

References

- Berger U, Hediger M. Distribution of peptide transporter PEPT2 mRNA in the rat nervous system. *Anat. Embryol.* 199: 439-449 (1999)
- Choudhuri S, Klaassen C. Constitutive expression of various xenobiotic and endobiotic transporter mRNAs in the choroids plexus of rats. *Drug Metab Dispos.* 31:1337-45 (2003)
- Cserr HF. Physiology of the choroid plexus. *Physiol. Rev.* 51:273-311 (1971)
- Cserr HF, Knoff P. Cervical lymphatics, the blood brain barrier and the immunoreactivity of the brain. *Immunol. Today* 13:507-512 (1992)
- Davson H. History of the blood brain barrier concept. In: E.A. Neuwelt, Editor. *Implications of the blood brain barrier and its manipulation*, New York: Plenum publishing corporation, pp27-52 (1989)
- Doring et al. Delta-aminolevulinic acid transport by intestinal and renal peptide transporters and its physiological and clinical implications. *J Clin. Invest* 101:2761-2767 (1998)
- Fei Y-J, Kanai Y, Boron WF and Heidiger MA. Expression cloning of a mammalian proton-coupled oligopeptide transporter, *Nature (Lond)* 368: 563-566 (1994)
- Fenstermacher JD. Pharmacology of the blood brain barrier. In: E.A. Neuwelt, Editor, *Implications of the blood-brain barrier and its manipulation*, Plenum, New York, pp.137-156 (1989)
- Fujita T et al. Interaction of kyotorphin and brain peptide transporter in synaptosomes prepared from rat cerebellum: implications of high affinity type H⁺/peptide transporter PEPT2 mediated transport system, *Neurosci. Lett.* 271: 117-20 (1999)
- Ganapathy V, Leibach F. Role of pH gradient and membrane potential in dipeptide transport in intestinal and renal brush-border membrane vesicles from the rabbit. Studies with L-carnosine and glycyl-L-proline. *J Biol. Chem* 258(923): 14189-92(1983)
- Gherzi-Egea J, et al. Fate of cerebrospinal fluid-borne amyloid beta-peptide: rapid clearance into blood and appreciable accumulation by cerebral arteries. *J Neurochem* 67:880-883 (1996)
- Gherzi-Egea J, et al. Choroid plexus transporters for drug and other xenobiotics. *J Drug Target* 10 (4):353-357 (2002)
- Gonzalez DE, Covitz K, Sadee W. An oligopeptide transporter is expressed at high levels in the pancreatic carcinoma cell lines AsPc-1 and Capan-2, *Cancer. Res.* 58:519-525 (1998)
- Groneberg DA, et al. Expression of PEPT2 peptide transporter mRNA and protein in glial cells of rat dorsal root ganglia. *Neurosci. Lett* 304:181-4 (2001a)
- Groneberg DA, et al. Localization of the peptide transporter PEPT2 in the lung: implications for pulmonary oligopeptide uptake, *Am. J Pathol.* 158:707-714 (2001b)
- Groneberg DA et al. Peptide transport in the mammary gland: expression and distribution of PEPT2 mRNA and protein. *Am J Physiol. Endocrinol. Metab.* 282:E1172-E1179 (2002).

- Han H, Oh D, Amidon G. Cellular uptake mechanism of amino acid ester prodrugs in Caco-2/hPEPT1 cells overexpressing a human peptide transporter, *Pharm Res.* 15(9):1382-6 (1998)
- Johanson CE, Smith QR. Cl-HCO₃ exchange in choroids plexus: analysis by the DMO method for cell pH. *Am J Physiol.* 249: F478-84 (1985)
- Keep RF, Jones HC. A morphometric study on the development of the lateral ventricle choroids plexus, choroids plexus capillaries and ventricular ependyma in the rat. *Brain Res. Dev. Brain. Res.* 56:47-53 (1990)
- Keep RF, Si X, Shakui P, Ennis SR, Betz AI. Effect of amiloride analogs on DOCA-salt-induced hypertension in rats. *Am J Physiol* 276:H2215-H2220,(1999)
- Liang R et al. Human intestinal H⁺/peptide cotransporter. Cloning functional expression, and chromosomal localization, *J. Biol. Chem.*270: 6456-6463 (1995).
- Lucas M. Determination of acid surface pH in vivo in rat proximal jejunum, *Gut* 24:734-739 (1983)
- Lui W, Liang R, Ganapathy V, Leibach FH. Molecular cloning of PEPT2, a new member of the H⁺/peptide cotransporter family from human kidney, *Biochem. Biophys. Acta* 1235:461-466 (1995).
- Matthews DM. Intestinal absorption of peptides. *Physiol. Rev.* 55(4): 537-608 (1975)
- Meller K. ultrastructural aspects of the choroids plexus epithelium as revealed by the rapid-freezing and deepetching techniques. *Cell Tiss. Res.* 239:189-201 (1985)
- Nishimura K, Kaya K, Hazato T, Ueda H, Satoh M, Takagi H. Kyotorphin like substance in human cerebrospinal fluid of patients with persistent pain. *Masui* 40: 1686-1690 (1991).
- Novotny A, Xiang J, Stummer W, Teuscher NS, Smith DE, and Keep R. Mechanisms of 5-aminolevulinic acid uptake at the choroid plexus. *J Neurochem* 75:321-328 (2000)
- Ocheltree SM, Shen H, Hu Y, Xiang J, Keep RF, Smith DE. Mechanisms of cefadroxil uptake in the choroids plexus: Studies in wild type and PEPT2 knockout mice. *J Pharmacol Exp Ther* 308:462-467 (2004a).
- Ocheltree SM, Shen H, Shu C, Xiang J, Keep RF, Smith DE. Role of PEPT2 in the choroid plexus uptake of glycylsarcosine and 5-aminolevulinic acid: Studies in wild type and null mice. *Pharm Res* 21:1680-1685 (2004b).
- Ogihara H, et al. immuno-localization of H⁺/peptide cotransporter in rat digestive tract, *Biochem. Biophys. Res. Commun.*220:848-52 (1996)
- Pardridge WM. Peptides as potential neuropharmaceuticals in disorders of the brain. In *Peptide Delivery to the Brain*. Raven Press, New York, 1991, pp. 23-51.
- Rao V et al. Choroid plexus epithelial expression of MDR1 P glycoprotein and multidrug resistance-associated protein contribute to the blood-cerebrospinal-fluid drug-permeability barrier. *Proc. Natl. Acad. Sci. USA* 96:3900-3905 (1999)
- Saito H, Mukai M, Inui K. Cloning and Characterization of a PH-sensing regulatory factor that modulates transport activity of the human H⁺/peptide cotransporter, PEPT1, *Biochem. Biophys. Res. Commun.* 237(3): 577-82(1997).
- Sakata K, Yamashita T, Maeda M, Shimada S. Cloning of a lymphatic peptide/histidine transporter, *J. Biochem.* 356:53-60 (2001)

- Schlaghech TG, Webb K. Characterization of peptides from the gastrointestinal tract of calves, *Federation. Proc.* 43:671-677 (1984)
- Seal C, Parker D. Isolation and characterization of circulating low molecular weight peptides in steer, sheep and rat portal and peripheral blood, *Comp. Biochem. Physiol. B.* 99:679-85 (1991)
- Shen H, Smith D, Yang T, Brosius F. Localization of PEPT1 and PEPT2 proton-coupled oligopeptide transporter mRNA and protein in rat kidney, *Am. J. Physiol.* 276:F658-F665 (1999)
- Shen H, Smith D, Keep R, Brosius F. immunolocalization of the proton-coupled oligopeptide transporter PEPT2 in developing rat brain, *Mol. Pharm* 1:248-256 (2004)
- Shen C, Shen H, Hopfer U and Smith D, keep R, Brosius F. Immunolocalization of the proton-coupled oligopeptide transporter PEPT2 in developing rat brain, *Mol.pharm.* 1: 248-256 (2004).
- Shu C, Shen H, Hopfer U, Smith D. mechanisms of intestinal absorption and renal reabsorption of an orally active ACE inhibitor: uptake and transport of fosinopril in cell cultures. *Drug Metab. Dispos.* 29: 1307-1315 (2001)
- Shu C, Shen H, Keep R, Smith D. Role of PEPT2 in peptide/mimetic trafficking at the blood-cerebral fluid barrier: studies in rat choroids plexus epithelial cells in primary culture, *J.Pharm.Exp.Ther* .301:820-829 (2002)
- Speake T, Whitwell C, Majid A, Brown P. Mechanisms of CSF secretion by the choroids plexus. *Microsc.Res. Tech.* 52:49-59(2001)
- Smith DE, Johanson CE, keep RF. Peptide and peptide analog transport systems as the blood-CSF barrier. *Adv Drug Deliv. Rev* (in press).
- Terada T, Saito H, Mukai M. Recognition of B-lactam antibiotics by rat peptide transporters, PEPT1 and PEPT2 in LLC-PK cells. *Am. Physiol Society F706-F711* (1997)
- Teuscher NS, Keep RF, Smith DE. PEPT2-mediated uptake of neuropeptides in rat choroid plexus. *Pharm Res* 18:807-813, (2001)
- Tuescher NS, Novotny A, keep RF, Smith DE. Functional evidence for the presence of PEPT2 in rat choroids plexus: Studies with glycylsarcosine. *J Pharmacol Exp Ther* 294: 494-499, (2000).
- Teuscher NS, Keep RF, Smith DE. PEPT2-mediated uptake of neuropeptides in rat choroids plexus. *Pharm Res* 18:807-813, (2001).
- Teuscher NS, Shen H, Hu Y, Xiang J, Keep RF, Smith DE. Carnosine uptake in rat choroids plexus primary cell cultures and choroids plexus whole tissue from PEPT2 null mice. *J Neurochem* 89:375-382, (2004).
- Thomas SA, Segal MB. The transport of an anti-HIV drug across the blood brain and blood-cerebrospinal fluid barriers. *Br. J. pharmacol.* 125:49-54 (1998)
- Wong S et al. Distributional transport kinetics of zidovudine between plasma and brain extracellular fluid/cerebrospinal fluid in the rabbit: investigation of the inhibitory effect of probenecid utilizing microdialysis. *J. Pharmacol. Exp. Ther.* 264:899-909 (1993).
- Yamashita T, Shimada S, Tagaki T, Tohyama M. Cloning and functional expression of a brain peptide/histidine transporter. *J Biol. Chem.* 272:10205-10211, (1997)

CHAPTER 6

A PHYSIOLOGICAL PERSPECTIVE OF PEPT2: THE DISPOSITION OF CARNOSINE IN WILD-TYPE AND PEPT2 KNOCKOUT MICE

Abstract

Carnosine (β -alanyl-L-histidine), an endogenous dipeptide substrate of the proton-coupled oligopeptide transporter PEPT2, plays an important role in many physiological processes. This study investigated the *in vivo* relevance of PEPT2 on the systemic exposure, tissue distribution, and renal handling of [3 H]carnosine (1 nmol/g intravenous dose) in wild-type and *Pept2* null mice. A marked increase in the systemic clearance of carnosine was observed in *Pept2* null versus wild-type animals (0.50 vs. 0.29 ml/min; $p < 0.001$), resulting in the decreased systemic exposure of dipeptide (AUC=43.7 vs. 73.0 min \cdot μ M; $p < 0.001$). Carnosine uptake was substantially reduced in the kidney of *Pept2* null mice and renal clearance increased 17-fold in this genotype (206 vs. 11.5 μ l/min; $p < 0.001$). Fractional reabsorption of carnosine in *Pept2* null mice was only one-fifth of the fraction reabsorbed in wild-type animals (0.20 vs. 0.94; $p < 0.001$). This finding reflected the ability of PEPT2 to mediate 83% of carnosine's total reabsorption from tubular fluid, while PEPT1 mediated 17% of the reabsorption process. PEPT2 also had a substantial impact in brain where the cerebrospinal fluid/plasma concentration ratio of carnosine was 8-fold greater in *Pept2*-deficient versus *Pept2*-competent mice (0.70 vs. 0.08; $p < 0.001$). The results demonstrate that PEPT2 is the predominant peptide

transporter in the physiological handling of carnosine in kidney, and that this protein significantly limits carnosine exposure in cerebrospinal fluid. These findings suggest that *Pept2* may act as a gene modifier for a variety of pathophysiological conditions in the kidney and brain, and that the gene product may serve as a potential target for pharmacological interventions.

Introduction

Carnosine (β -alanyl-L-histidine), an endogenous dipeptide, is abundantly expressed in the skeletal muscle and central nervous system (Flancbaum et al, Teuscher et al). Carnosine has many physiological roles including its action as a cytosolic buffer (Quinn et al), neurotransmitter/neuromodulator (Biffo et al), and metabolic reservoir of histidine which is converted to histamine during physiological stress in mammals (Flancbaum et al). The dipeptide also possesses strong antioxidant and free radical scavenging activities (Hartman et al, Quinn et al), and has been shown to be neuroprotective when administered intraperitoneally in rodent models of global and focal cerebral ischemia (Rejanikant et al, Stvolinsky et al). More recently, protective effects of carnosine have been demonstrated in ischemia/reperfusion-induced acute renal failure (Fujii et al, Kurata et al) and diabetic nephropathy (Janssen et al). Having favorable structural attributes, such as a β -amino group and L-conformation, the dipeptide is a substrate of PEPT2 (Terada et al) which is a member of the proton-coupled oligopeptide transporter family SLC15A.

PEPT2 is primarily localized in the apical membrane of kidney epithelial cells, with immunolocalization studies specifically identifying the transporter in S2 and S3 segments

of the proximal tubule (Shen et al, 1999). In brain, PEPT2 is expressed at the apical side of choroid plexus epithelial cells of the blood-cerebrospinal fluid (CSF) barrier (Berger and Hediger), and in astrocytes (newborns) and neuronal cells (newborn and adults) of brain parenchyma (Shen et al, 2003). PEPT2 protein has also been identified in the alveolar lining of lung tissue, mammary glands, as well as retina and spleen (Doring et al). The primary physiological roles of PEPT2 include: 1) the reabsorption of peptides from glomerular filtrate in renal proximal tubules, 2) the maintenance of brain homeostasis by controlling peptide trafficking in brain interstitial fluid and peptide removal from CSF, and 3) the facilitation of peptide uptake for action by intracellular peptidases. However, the significance and interplay of these physiological roles *in vivo* are not entirely clear.

A previous study has demonstrated that carnosine is taken up into choroid plexus primary cell cultures and choroid plexus whole tissue by PEPT2 (Teuscher et al). However, the *in vivo* significance of PEPT2 in mediating this dipeptide's disposition has not been investigated. It is hypothesized that PEPT2 ablation will have a profound impact on the systemic pharmacokinetics of carnosine, as well as on the regional exposure of carnosine in kidney and brain. Differences in PEPT2-mediated disposition may also alter the physiological and pharmacological benefits of carnosine, including its renal (Fujii et al., Kurata et al) and neuroprotective (Rejanikant et al, Stvolinsky et al) effects after ischemic insult.

The current study aims to demonstrate the physiological relevance of PEPT2 by contrasting the systemic exposure, tissue distribution, metabolic stability, and renal

handling of carnosine in wild-type and *Pept2* knockout mice after an intravenous bolus dose of the dipeptide.

Materials and Methods

Chemicals. [³H]Carnosine (sp act: 7.0 Ci/mmol), [³H]histidine (sp act: 44 Ci/mmol), and [¹⁴C]dextran-MW 70,000 (sp act: 79 mCi/mmol) were purchased from Moravek Radiopharmaceuticals (Brea, CA). Unlabeled carnosine was obtained from Sigma-Aldrich (St Louis, MO). Cytoscint scintillation fluid and hyamine hydroxide were obtained from ICN (Irvine, CA). All other chemicals were obtained from standard sources.

Animals. Gender- and weight-matched wild-type (*Pept2*^{+/+}) and null (*Pept2*^{-/-}) mice (>99% C57BL/6 genetic background), 8 to 10 weeks of age, were generated in-house (Shen et al, 2003) and used for all study designs. Animals were housed in a temperature-controlled environment with a 12-hour light, 12-hour dark cycle and given *ad libitum* access to food and water. All experiments with mice were performed in accordance with the guidelines from the National Institutes of Health for the care and use of animals, and were approved by the Institutional Animal Care and Use Committee.

Systemic Pharmacokinetic and Tissue Distribution Studies. Wild-type and *Pept2* null mice were anesthetized with sodium pentobarbital (65 mg/kg ip). [³H]Carnosine was injected into the tail vein of mice as a single bolus injection (1 nmol/g body weight; 5 µl/g in normal saline). Serial blood samples (~20 µl, via tail clipping) were collected at 0, 0.25, 1, 2, 5, 10, 20, and 30 min, placed in 0.2 ml thin-wall PCR tubes (United Laboratory Plastics; St. Louis, MO) containing 1 µl of 7.5% potassium EDTA, and

centrifuged at 3,000 g for 3 min at room temperature. A 5- μ l aliquot of plasma supernatant was collected for each sample, mixed with 6 ml of scintillation fluid, vortex-mixed for 5 sec, and then allowed to stand for 24 hr at ambient temperature. Radioactivity (measured in dpm/ml) for each plasma sample was measured by a dual-channel liquid scintillation counter (Beckman LS 3801; Beckman Coulter, Fullerton, CA).

An intravenous bolus of [14 C]dextran-MW 70,000 (1 μ Ci/mouse) was administered 2 min prior to harvesting the 30-min tissue samples in order to correct for the vascular space (Shen et al, 2007). A skin incision was made in the dorsal neck region to allow insertion of a 30-gauge needle into the cisterna magna for CSF sampling (~5-10 μ l). The mouse was immediately decapitated and a 10- μ l blood sample was obtained. Various organs/tissues were harvested at this time including the cerebral cortex, olfactory bulb, combined lateral and fourth ventricle choroid plexuses, kidney, liver, eye, lung, spleen, small and large intestines, and skeletal muscle. The tissue samples were blotted dry and weighed, solubilized in 1 M hyamine hydroxide, and then incubated for 48 hr at 37°C. Solubilized tissue samples (and CSF) were mixed with 6 ml of scintillation fluid and left to stand for 24 hours at room temperature. Radioactivity (measured in dpm/ml) in the blood, CSF, and tissue samples was measured by a dual-channel liquid scintillation counter.

Renal Clearance Studies. Following sodium pentobarbital anesthesia (65 mg/kg ip), *Pept2*^{+/+} and *Pept2*^{-/-} mice were administered [3 H]carnosine (1 nmol/g body weight; 5 μ l/g in normal saline) by tail vein injection. Blood samples (~20 μ l, via tail clipping) were collected serially over 30 min and the plasma harvested. The total urine of each

animal was aspirated directly from the bladder with a 28G1/2 U-100 insulin syringe at 30 min. Radioactivity in the plasma and urine was determined by dual-channel liquid scintillation counting.

Plasma Protein Binding Studies. The protein binding of carnosine was determined by an ultrafiltration method (Ocheltree et al), with minor modification. Blank plasma from each genotype was spiked with unlabeled and radiolabeled carnosine (0.1 $\mu\text{Ci/ml}$) to produce concentrations of 0.1, 1, and 10 μM , values that represent the plasma concentration range observed after a 1 nmol/g intravenous dose of carnosine. A 0.5-ml aliquot of each standard was added to a disposable Microcon YMT-30 centrifugal filter device (Millipore Corporation, Billerica, MA) using an anisotropic hydrophilic membrane that excluded molecules greater than 30 kDa. The device was capped, equilibrated for 15 min at 37°C in a 35° fixed angle rotator, and centrifuged at 1,800 g for 25 min at 37°C. The protein free ultrafiltrate was then collected for each sample. The unbound fraction in plasma was calculated as the ratio of carnosine concentration in the ultrafiltrate to that in the original plasma standard. Liquid scintillation counting was used to determine radioactive counts in the samples.

Stability Studies. [^3H]Carnosine and [^3H]histidine peaks were detected using a high-performance liquid chromatography (HPLC) system consisting of a pump (model 616 with 600S controller; Waters, Milford, MA), a Rheodyne injector port (Rohnert Park, CA) with 20 μl sample loop, a reversed-phase column stationary phase (Supelco C-18, 5 μm , 25 cm x 4.6 mm), and a radiochemical detector (FLO-ONE 515TR Series Flow Scintillation Analyzer; Perkin Elmer Life and Analytical Sciences, Boston, MA). The mobile phase was comprised of 0.10 M NaH_2PO_4 buffer (pH=3.2) and 0.10%

heptafluorobutyric acid, pumped isocratically at 1.0 ml/min under ambient conditions. Peaks were identified by injecting known standards of radiolabeled carnosine and histidine.

The metabolic stability of [³H]carnosine was determined in plasma, kidney, and urine samples following an intravenous dose (1 nmol/g body weight) in wild-type and *Pept2* null mice. Blood samples (100 µl) were collected by cardiac puncture at 2, 5, 10, 20 and 30 min, and the plasma harvested. Kidney samples (200 mg) were obtained at 30 min and homogenized in 1 ml of water (4°C). A 0.2-ml volume of trichloroacetic acid (10% w/v) was added to one volume of plasma or kidney homogenate, vortex-mixed for 1 min, and then centrifuged at 15,000 g for 10 min at room temperature. Urine samples were also centrifuged at 15,000 g for 10 min (ambient conditions) to remove any particulates. Resultant supernatants were injected into the HPLC, and stability was evaluated by the ratio of carnosine area to the total area of carnosine and histidine (x100 for percent). The physicochemical integrity of [³H]carnosine stock solution (1 µCi/ml) was also determined at 25°C and 37°C following 0.5 and 24 hr incubations.

Data Analysis of Carnosine Systemic Pharmacokinetics. The plasma concentration-time profiles of carnosine displayed biexponential pharmacokinetics and were best described by a 2-compartment open model with first order elimination and uniform weighting (WinNonLin v 5.1; Pharsight Inc., Mountain View, CA). The model goodness of fit was determined by evaluating the coefficient of determination (r^2), the coefficient of variation of parameter estimates, and by visual inspection of the residuals. Pharmacokinetic parameters included AUC, area under the plasma concentration time curve; CL, total systemic clearance; V₁, volume of the central compartment; V_{dss},

volume of distribution steady state; $t_{1/2}$, terminal half-life; and MRT, mean residence time.

Data Analysis of Carnosine Renal Pharmacokinetics. The renal clearance (CL_R) of carnosine was calculated as: $CL_R = Ae^{30}/AUC^{30}$ where Ae^{30} is the amount of carnosine excreted unchanged in the urine over 30 min and AUC^{30} is the area under the carnosine plasma concentration-time curve from 0-30 min (determined noncompartmentally by partial areas using WinNonLin). In the absence of tubular secretion (of which there is no evidence for this dipeptide), the renal clearance of carnosine can be expressed as (14): $CL_R = fu \cdot GFR \cdot (1-F)$ where fu is the fraction of carnosine unbound in plasma, GFR is the glomerular filtration rate (a measure of functional nephron mass) and F is the fraction of available dipeptide that is reabsorbed from tubular fluid. The excretion ratio (ER) and fraction reabsorbed (F) was determined according to the following: $ER = CL_R / (fu \cdot GFR) = 1-F$. Based on the sequential expression of PEPT1 and PEPT2 in the proximal tubule of the nephron (Shen et al, 2003), the renal clearance equation can be transformed to (Shen et al, 2000): $CL_R = fu \cdot GFR \cdot (1-F1) \cdot (1-F2)$ where $F1$ is the available fraction of carnosine reabsorbed by PEPT1 and $F2$ is the available fraction reabsorbed by PEPT2. Since $F2=0$ in PEPT2^{-/-} mice, an estimate of $F1$ can be made in these mice. An estimate of $F2$ can then be made in PEPT2^{+/+} mice with the assumption that $F1$ is unchanged in wild-type animals. The relative contribution of each transporter to the reabsorption of carnosine can then be calculated as % PEPT1 = $100 \cdot (F1/F)$ and % PEPT2 = $100 \cdot [F2 \cdot (1-F1)/F]$.

Statistics. The data are reported as mean±SE. Statistical comparisons between the two genotypes were performed using an unpaired t-test (GraphPad Prism v4.0; GraphPad Software, Inc., San Diego, CA).

Results

Systemic Pharmacokinetics and Tissue Distribution of Carnosine. As shown in Figure 6.1, the plasma concentrations of carnosine were significantly lower in *Pept2*^{-/-} mice as compared to *Pept2*^{+/+} animals. The altered plasma profiles are reflected in the pharmacokinetic parameters shown in Table 6.1. The systemic clearance (CL) of null animals is 2-fold higher compared to wild-type animals (p<0.001), resulting in a 2-fold lower systemic exposure (AUC) (p<0.01). PEPT2 had no effect on volume of distribution in the central compartment (V₁), however, the steady-state volume (V_{dss}) was somewhat higher in null mice (p<0.05). In contrast, no significant differences were observed in the terminal half-life (t_{1/2}) and mean residence time (MRT) of carnosine. These last two parameters are not statistically different since they reflect changes in both distribution and elimination (which increase in *Pept2*^{-/-}). Figure 6.2 shows the tissue concentrations of carnosine, normalized for plasma concentrations, 30 min following an intravenous bolus dose of dipeptide. PEPT2 ablation had a significant effect on the ability of many tissues to accumulate carnosine. Most notably, lower tissue/plasma concentration ratios of carnosine were observed in the kidney (5-fold), choroid plexus (8-fold), spleen (12-fold), eye (3-fold), lung (3-fold), cerebral cortex (3-fold), olfactory bulb (3-fold) and muscle (2-fold) of *Pept2* knockout mice. In contrast to these results, PEPT2^{-/-} mice had an 8-fold higher CSF/plasma concentration ratio (p<0.001).

Renal Clearance of Carnosine. An analysis of the renal tubular handling of carnosine is shown in Table 6.2 and Figure 6.3. The renal clearance of carnosine (CL_R) was approximately 17-fold higher in the *Pept2* null mice as compared to wild-type mice ($p < 0.001$), resulting in a significantly higher fraction of dipeptide being excreted unchanged in the urine at 30 min (f_e^{30}) ($p < 0.001$). Ultrafiltration studies showed no protein binding of carnosine across the relevant plasma concentrations of 0.1-10 μ M and, as such, the fraction unbound (f_u) for carnosine in plasma was unity. GFR was fixed at 250 μ l/min based on the consistent values between genotypes in two previous studies by our group in gender-matched mice of similar age and weight (Ocheltree et al; Shen et al, 2007). Since the excretion ratio (ER) of carnosine represents its renal clearance, corrected for filtration clearance ($f_u \bullet GFR$), the significantly higher ER in null mice reflects the reduced reabsorption of carnosine in *Pept2*-deficient mice (i.e., $F = 0.94$ vs. 0.19 for wild-type and null mice, respectively). Moreover, of the two oligopeptide transporters expressed in kidney, PEPT2 was responsible for the great majority of dipeptide reabsorption. In this regard, PEPT1 accounted for only 17% of carnosine's reabsorption from tubular fluid while PEPT2 accounted for 83% of dipeptide reabsorption in the kidney.

Stability of Carnosine. Analysis of the HPLC chromatograms showed [3 H]histidine eluting at 5.5 min and [3 H]carnosine eluting at 9.1 min. The physicochemical integrity of [3 H]carnosine stock solutions was maintained during 0.5 and 24 hr incubations, at ambient temperature and 37°C (data not shown). While the 30-min urine collections of both genotypes were stable (<5% degradation), about 12% of carnosine was degraded in the 30-min kidney samples of wild-type, but not *Pept2* null, mice (Figure. 6.4).

Likewise, serial plasma samples from *Pept2*^{-/-} mice were stable over 30 min (<3% degradation), as were the 2-, 5- and 10-min plasma samples from *Pept2*^{+/+} mice (<10% degradation). However, the 20 and 30 min plasma samples showed about 15 and 20% degradation, respectively, in wild-type mice. As a result, the plasma concentrations of carnosine in *Pept2*^{+/+} mice were corrected for the degradation observed at these times (Figure 6.1 and Table 6.1).

Discussion

Studies using wild-type and knockout mice offer a unique opportunity to study the role and relevance of a particular protein under physiological *in vivo* conditions. By challenging *Pept2*-competent and *Pept2*-deficient mice following an intravenous dose of carnosine, the significance of gene disruption can be revealed in regard to dipeptide disposition. In our studies, we found: 1) that PEPT2 was the major oligopeptide transporter responsible for dipeptide reabsorption in the kidney, 2) that the regional effects of PEPT2 in several organs, including the brain (e.g., choroid plexus and CSF), were greater than the systemic effects on dipeptide exposure, and 3) that transport-metabolic coupling of dipeptide occurs to retain amino nitrogen. These findings may have important physiological, pharmacological and pathophysiological implications including those related to nutrition, drug delivery and targeting, and ischemia.

Most notably, the results show that PEPT2 had a predominant role in the renal tubular reabsorption of carnosine. Specifically, the fraction of dipeptide reabsorbed in *Pept2* null mice was only one-fifth of that reabsorbed in wild-type animals. This finding reflected the ability of PEPT2 to mediate 83% of carnosine's total reabsorption from

tubular fluid. In addition to differences in renal handling, PEPT2 ablation led to substantially decreased levels of carnosine in tissues where the peptide transporter is predominantly localized (e.g., cerebral cortex, olfactory bulb, choroid plexus and CSF, kidney, eye, lung, spleen and skeletal muscle). The differences observed in olfactory bulb and skeletal muscle were particularly interesting since these tissues concentrate endogenous carnosine in abundance (Flancbaum et al, Teuscher et al). As a result, PEPT2 may play an important role in regulating the neurotransmitter/neuromodulator action of carnosine in the olfactory pathway (Biffo et al) and in modulating the cytosolic buffering capabilities of carnosine during muscle fatigue (Quinn et al). Given the predominance of PEPT2 on dipeptide transport in kidney, this oligopeptide transporter may also influence the renoprotective effects of carnosine during ischemic acute renal failure (Fujii et al, Kurata et al) and diabetic nephropathy (Janssen et al).

PEPT2 ablation had a significant influence on the influx of carnosine from CSF into choroid plexus as demonstrated by the 8-fold greater CSF/plasma concentration ratios of dipeptide in *Pept2* null versus wild-type mice. The greater CSF ratios of carnosine in *Pept2*^{-/-} animals reflect the directionality of PEPT2 transport from the apical, CSF-facing, side of choroid plexus epithelial cells. These differences were even more dramatic for carnosine than that observed in similarly-designed experiments for the synthetic dipeptide glycylsarcosine (Ocheltree et al) or the aminocephalosporin cefadroxil (Shen et al, 2007). Moreover, the results with carnosine, along with previous studies from our group (Ocheltree et al; Shen et al, 2007), point to the fact that PEPT2-induced changes in the regional disposition of peptides/mimetics in CSF are more dramatic than the PEPT2-induced effects on systemic exposure. While the PEPT2-induced renal accumulation of

carnosine might facilitate the renoprotective effects of dipeptide in renal failure, the limiting effect of PEPT2 on CSF exposure might diminish its reported neuroprotective effects (Rejanikant et al, Stvolinsky et al). It is unclear whether or not the PEPT2-mediated changes in regional carnosine disposition will translate into significant changes in the dipeptide's neuroprotective effects after focal and global brain ischemia. However, we have shown that PEPT2 expression in brain does protect against 5-aminolevulinic acid neurotoxicity (Hu et al, 2007).

Finally, results from the metabolic stability studies point to another physiological role of PEPT2 in facilitating the exposure of peptide substrates to tissue and serum dipeptidases. Carnosine is hydrolyzed to its constituent amino acids by carnosinase (Harding et al, Margolis et al), a non-specific dipeptidase with high enzymatic activity in the cytosol of proximal tubule renal epithelia (Margolis et al). Although C57BL/6 mice express low levels of carnosinase in their kidneys (Margolis and Grillo), some instability of carnosine was still observed in our mice. In particular, after only 30 min, about 20% and 12% of the plasma and kidney samples of wild-type mice, respectively, were in the form of carnosine hydrolysis products. However, in *Pept2* null mice, these same samples displayed little instability (<6% degradation) as did the urine samples for both genotypes (<5% degradation). These results can be explained by the greater PEPT2-mediated uptake, and subsequent renal hydrolysis, of carnosine in wild-type animals. Although other tissues may contribute to carnosine hydrolysis, this outcome is less likely given the kidney's unique combination of high PEPT2 (Ocheltree et al; Shen et al, 2007) and carnosinase activity (Harding et al). Amino acid transporters on the basolateral membrane of the renal epithelia (Broer) can then reabsorb the degradation products (i.e.,

β -alanine and/or L-histidine) back into plasma. Amino acid transporters on the apical membrane of renal epithelia (Broer) can efficiently reabsorb the degradation products of carnosine in renal filtrate and, thereby, minimize the extent of hydrolysis products found in the urine of both wild-type and *Pept2* null mice. The concerted transport-metabolic coupling of carnosine by PEPT2 and peptidases has been depicted for dipeptides previously in kidney (Daniel and Rubio-Aliaga) and demonstrated previously for glycylglutamine in choroid plexus epithelial cells (Hu et al, 2005).

Conclusion and Perspective. Using a *Pept2* knockout model in mice, we demonstrated for the first time that PEPT2 can substantially impact the *in vivo* tissue distribution, systemic and regional exposure, and renal disposition of an endogenous dipeptide. Specifically, our results are definitive in showing that PEPT2 is responsible for the great majority of carnosine reabsorption in renal tubular epithelial cells, and in substantially reducing the exposure of dipeptide in the CSF compartment. Moreover, PEPT2 functions to increase the exposure of carnosine to intracellular carnosinase, thereby affecting the metabolic profile of dipeptide and constituent amino acids. These findings suggest that *Pept2* may act as a modifier gene for a variety of pathophysiological conditions in the kidney and brain, and that the gene product may serve as a potential target for pharmacologic interventions.

Table 6.1. Systemic pharmacokinetics of carnosine in Pept2^{+/+} and Pept2^{-/-} mice after a 1 nmol/g intravenous bolus dose of drug

| Parameter | Pept2^{+/+} | Pept2^{-/-} |
|------------------------|----------------------------|----------------------------|
| AUC (min*uM) | 73.0 ± 7.4 | 43.7 ± 5.0** |
| CL (ml/min) | 0.29 ± 0.03 | 0.50 ± 0.05*** |
| V ₁ (ml) | 1.4 ± 0.2 | 1.3 ± 0.2 |
| Vd _{ss} (ml) | 4.0 ± 0.3 | 5.5 ± 0.5* |
| MRT (min) | 14.2 ± 1.2 | 11.7 ± 1.3 |
| t _{1/2} (min) | 10.6 ± 0.9 | 9.0 ± 0.9 |
| r ² | 0.994 ± 0.002 | 0.995 ± 0.001 |

Values are expressed as mean ± SE (n=10). AUC is the area under the plasma concentration-time curve, CL is the total clearance, V₁ is the volume of central compartment, Vd_{ss} is the volume of distribution steady-state, MRT is the mean residence time, t_{1/2} is the terminal half-life, and r² is the coefficient of determination. *P<0.05, **P<0.01, ***P<0.001.

Table 6.2. Renal pharmacokinetics of carnosine in Pept2^{+/+} and Pept2^{-/-} mice after a 1 nmol/g intravenous bolus dose of drug

| Parameter | Pept2^{+/+} | Pept2^{-/-} |
|--------------------------|----------------------------|----------------------------|
| CL _R (μl/min) | 11.5 ± 4.3 | 206 ± 16 *** |
| GFR (μl/min) | 250 | 250 |
| fu | 1.0 | 1.0 |
| fe ³⁰ | 0.023 ± 0.005 | 0.50 ± 0.03*** |
| ER | 0.06 ± 0.02 | 0.81 ± 0.08*** |
| F | 0.94 ± 0.02 | 0.19 ± 0.08*** |
| F ₁ | 0.19 ± 0.08 | 0.19 ± 0.08 |
| F ₂ | 0.92 ± 0.02 | 0 |
| %PEPT1 | 16.9 ± 8.1 | 100 |
| %PEPT2 | 83.1 ± 7.2 | 0 |

Values are expressed as mean ± SE (n=7). CL_R is the renal clearance, GFR is the glomerular filtration rate (values taken from references 14, 15), fu is the fraction unbound in plasma, fe³⁰ is the fraction excreted unchanged in the urine over 30 min, ER is the excretion ratio, F is the fraction of available dipeptide reabsorbed, F₁ is the fraction of available dipeptide reabsorbed by PEPT1, F₂ is the fraction of available dipeptide reabsorbed by PEPT2, %PEPT1 is percentage of reabsorbed carnosine that occurs via PEPT1, and PEPT2 is percentage of reabsorbed carnosine that occurs via PEPT2. ***P<0.001.

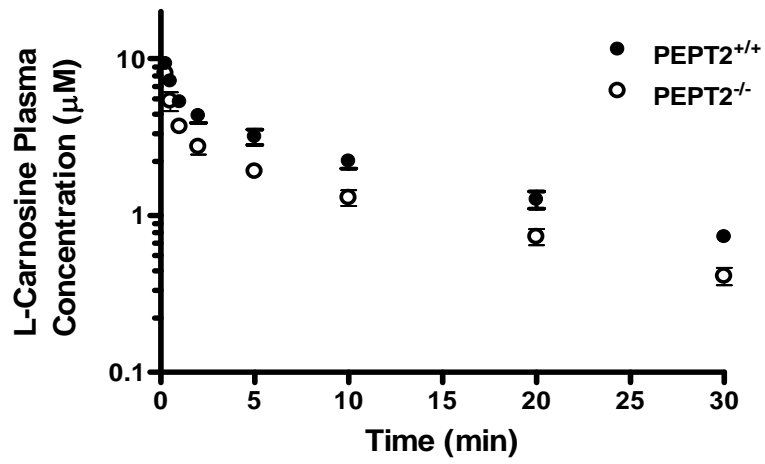


Figure 6.1. Plasma concentration-time profiles of carnosine in *Pept2*^{+/+} and *Pept2*^{-/-} mice after a nmol/g intravenous bolus dose of drug (mean ± SE, n=10).

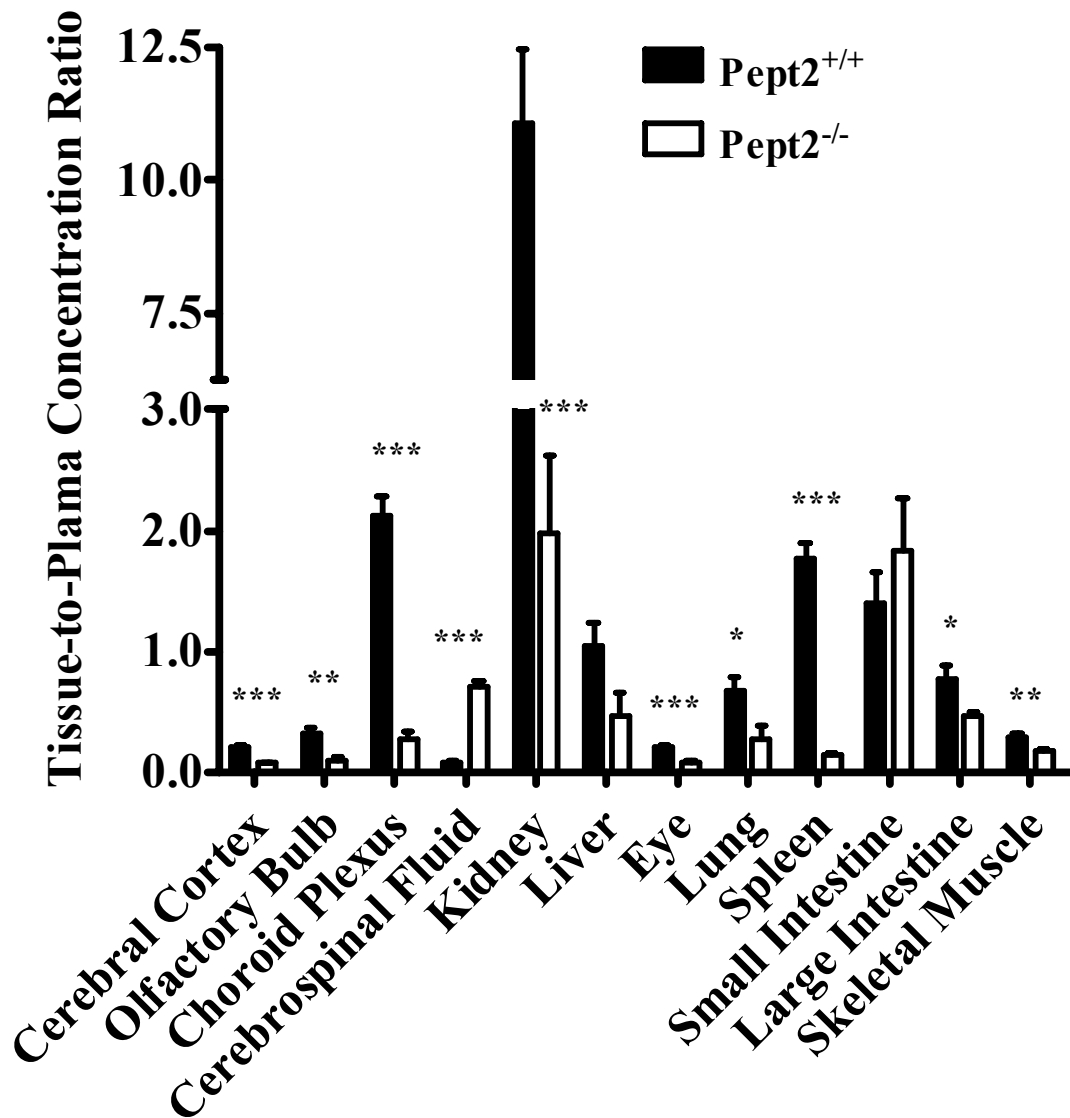


Figure 6.2. Tissue-to-plasma concentration ratios of carnosine in *Pept2*^{+/+} and *Pept2*^{-/-} mice, 30 min after a 1 nmol/g intravenous bolus dose of drug (mean ± SE, n=7).

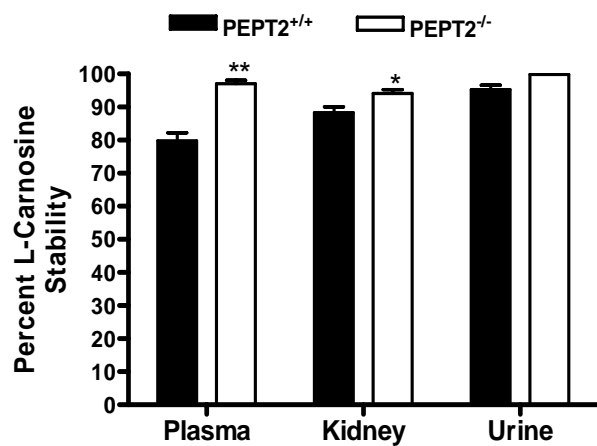


Figure 6.3. Stability of carnosine in plasma, kidney, and urine samples from Pept2^{+/+} and Pept2^{-/-} mice, 30 min after a 1 nmol/g intravenous bolus dose of drug (mean ± SE, n=4).

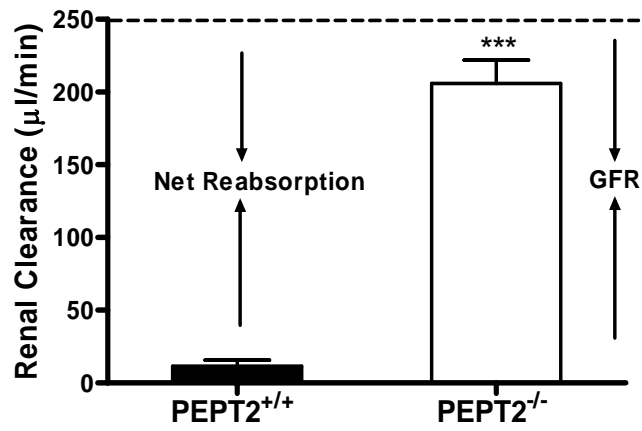


Figure 6.4. Renal clearance of carnosine in *Pept2*^{+/+} and *Pept2*^{-/-} mice after a 1 nmol/g intravenous bolus dose of drug (mean ± SE, n=7). The estimated GFR of 250 μl/min is indicated by a dashed line.

References

- Berger U, Hediger M. Distribution of peptide transporter PEPT2 mRNA in the rat nervous system. *Anat Embryol* 199; 439-449 (1999).
- Biffo S, Grillo M, Margolis FL. Cellular localization of carnosine-like and anserine-like immunoreactivities in rodent and avian central nervous system. *Neuroscience* 35: 637-651 (1990).
- Bröer S. Amino acid transport across mammalian intestinal and renal epithelia. *Physiol Rev* 88: 249-286 (2008).
- Daniel H, Rubio-Aliaga I. An update on renal peptide transporters. *Am J Physiol Renal Physiol* 284: F885-F892 (2003).
- Döring F, Walter J, Will J, Focking M, Boll M, Amasheh S, Clauss W, Daniel H. Delta-aminolevulinic acid transport by intestinal and renal peptide transporters and its physiological and clinical implications. *J Clin Invest* 101: 2761-2767 (1998).
- Flancbaum L, Fitzpatrick J, Brotman D, Marcoux A, Kasziba E, Fisher H. The presence and significance of carnosine in histamine-containing tissues of several mammalian species. *Agents Actions* 31: 190-196 (1990).
- Fujii T, Takaoka M, Muraoka T, Kurata H, Tsuruoka N, Ono H, Kiso Y, Tanaka T, Matsumura Y. Preventive effect of L-carnosine on ischemia/reperfusion-induced acute renal failure in rats. *Eur J Pharmacol* 474: 261-267 (2003).
- Harding J, Margolis FL. Denervation in the primary pathway of mice.III. Effect of enzymes of carnosine metabolism. *Brain Res* 110: 351-360 (1976).
- Hartman P, Hartman Z, Ault KT. Scavenging of singlet molecular oxygen by imidazole compounds: high and sustained activities of carboxy terminal histidine dipeptides and exceptional activity of imidazole-4-acetic acid. *Photochem Photobiol* 51: 59-66 (1990).
- Hu Y, Ocheltree SM, Xiang J, Keep RF, Smith DE. Glycyl-L-glutamine disposition in rat choroid plexus epithelial cells in primary culture: Role of PEPT2. *Pharm Res* 22: 1281-1286 (2005).
- Hu Y, Shen H, Keep RF, Smith, DE. Peptide transporter 2 (PEPT2) expression in brain protects against 5-aminolevulinic acid neurotoxicity. *J Neurochem* 103: 2058-2065 (2007).
- Janssen B, Hohenadel D, Brinkkoetter P, Peters V, Rind N, Fischer C, Rychlik I, Cerna M, Romzova M, de Heer E, Baelde H, Bakker SJ, Ziric M, Rondeau E, Mathieson P, Saleem MA, Meyer J, Köppel H, Sauerhoefer S, Bartram CR, Nawroth P, Hammes HP, Yard BA, Zschocke J, van der Woude FJ. Carnosine as a protective factor in diabetic nephropathy: association with a leucine repeat of the carnosinase gene CNBP1. *Diabetes* 54: 2320-2327,(2005).
- Kurata H, Fujii T, Tsutsui H, Katayama T, Ohkita M, Takaoka M, Tsuruoka N, Kiso Y, Ohno Y, Fujisawa Y, Shokoji T, Nishiyama A, Abe Y, Matsumura Y. Renoprotective effects of L-carnosine on ischemia/reperfusion-induced renal injury in rats. *J Pharmacol Exp Ther* 319: 640-647(2006).
- Levy G. Effect of plasma protein binding on renal clearance of drugs. *J Pharm Sci* 69: 482-483 (1980).

Margolis FL, Grillo M. Inherited differences in mouse kidney carnosinase activity. *Biochem Genet* 22: 441-451, (1984).

Margolis F, Grillo M, Grannot N, Farbman A. Purification, characterization and immunocytochemical localization of mouse kidney carnosinase. *Biochim Biophys Acta* 744: 237-248, (1983).

Ocheltree SM, Shen H, Hu Y, Keep RF, Smith DE. Role and relevance of peptide transporter 2 (PEPT2) in the kidney and choroid plexus: in vivo studies with glycylsarcosine in wild-type and PEPT2 knockout mice. *J Pharmacol Exp Ther* 35: 240-247, (2005).

Quinn P, Boldyrev A, Formzuyk V. Carnosine: its properties, functions and potential therapeutic applications. *Mol Aspects Med* 13: 379-444, (1992).

Rejanikant G, Zemke D, Senut M, Frenkel M, Chen A, Gupta R, Majid A. Carnosine is neuroprotective against focal cerebral ischemia in mice. *Stroke* 38: 3023-3031, (2007).

Shen H, Ocheltree SM, Hu Y, Keep RF, Smith DE. Impact of genetic knockout of PEPT2 on cefadroxil pharmacokinetics, renal tubular reabsorption, and brain penetration in mice. *Drug Metab Disp* 35: 1209-1216, (2007).

Shen H, Smith DE, Keep RF, Brosius FC. Immunolocalization of the proton-coupled oligopeptide transporter PEPT2 in developing rat brain. *Mol Pharm* 1: 248-256, (2004).

Shen H, Smith DE, Keep RF, Xiang J, Brosius III FC. Targeted disruption of the PEPT2 gene markedly reduces dipeptide uptake in the choroid plexus. *J Biol Chem* 278: 4786-4791(2003).

Shen H, Smith DE, Yang T, Brosius FC. Localization of PEPT1 and PEPT2 proton-coupled oligopeptide transporter mRNA and protein in rat kidney. *Am J Physiol* 276: F658-F665 (1999).

Stvolinsky S, Kukley M, Dobrota D, Matejovicova M, Tkac I, Boldyrev A. Carnosine: An endogenous neuroprotector in the ischemic brain. *Cell Mol Neurobiol* 19: 45-56, (1999).

Terada T, Sawada K, Irie M, Saito H, Hashimoto Y, Inui K. Structural requirements for determining the substrate affinity of peptide transporters PEPT1 and PEPT2. *Pflugers Arch* 440: 679-84 (2000).

Teuscher N, Shen H, Shu C, Xiang J, Keep RF, Smith DE. Carnosine uptake in rat choroid plexus primary cell cultures and choroid plexus whole tissue from PEPT2 null mice. *J Neurochem* 89: 375-382 (2004).

CHAPTER 7

CONCLUSION TO PART II

Major Findings

The PEPT2 knockout mouse has become an important tool to evaluate the evolving role and relevance of this transporter in drug disposition, dynamics and toxicity. Although disruption of the PEPT2 gene itself does not result in obvious phenotypic changes in the knockout mouse, our studies emphasize the fact that challenging the knockout in a certain manner may bring about phenotypic abnormalities. This study and others conducted in our lab have challenged the PEPT2 knockout model with various substrates of physiological, pharmacological and toxicological relevance, and have consistently demonstrated the dual action of this transporter with respect to its apical localization in kidney and choroid plexus epithelial cells. The results have clearly shown that *in vivo*: 1) PEPT2 effluxes carnosine from the CSF into choroid plexus, thereby affecting regional disposition in the brain; and 2) PEPT2 reabsorbs carnosine from renal tubular fluid, thereby affecting systemic pharmacokinetics and exposure. It also appears that the regional effect of PEPT2 in limiting exposure of L-carnosine to the CSF (and presumably ISF) of brain may be of more importance than its effect in increasing systemic exposure. These findings may have implications on the reported neuroprotective and neuromodulatory effects of L-carnosine, however, further studies will be needed to assess if PEPT2- mediated changes in disposition of L-carnosine translate directly into significant changes in its pharmacodynamics

Proposed Future Studies

Future studies should aim to further investigate how PEPT2-induced changes in regional disposition of carnosine in the kidney and brain affect its pharmacodynamics. For example, carnosine can be administered in wild-type and Pept2 knockout mice induced with cerebral ischemia to determine the effect of PEPT2 on the neuroprotective action of carnosine. Based on our results, PEPT2 should significantly reduce the neuroprotective effects of carnosine in the brain while facilitating the reno-protective activity of the dipeptide in an ischemia/reperfusion-induced acute renal failure mouse model.

Future studies should further investigate the proposed transporter-metabolic interaction of PEPT2 and carnosinase by conducting metabolic stability studies of carnosine in wild-type and PEPT2 knockout mice in which the enzyme carnosinase is inhibited. Such a study would provide definitive evidence of how PEPT2 may increase exposure of peptide substrates to intracellular peptidases.

APPENDIX A

ROLE AND RELEVANCE OF PEPT2 IN DRUG DISPOSITION, DYNAMICS, AND TOXICITY

Introduction

Heterogeneity of Proton-Coupled Oligopeptide Transporters (POTs)

a) Molecular Biology of POTs

The superfamily of POTs is characterized by the ability to transport small peptides and peptide-mimetic molecules across biological membranes.^{1,2)} Uptake of peptides into epithelial cells by these transporters is driven by an inwardly-directed proton gradient and negative membrane potential. In mammals, the POT family consists of four members: PEPT1 (*SLC15A1*), PEPT2 (*SLC15A2*), PHT1 (*SLC15A4*) and PHT2 (*SLC15A3*) which vary in size from 572-729 amino acids and contain 12 transmembrane domains, with the N- and C-termini facing the cytosol. PEPT1 was the first mammalian POT cloned, using expression-cloning strategies from a rabbit intestinal cDNA library.³⁾ PEPT2 was next identified and cloned from a human kidney cDNA library⁴⁾. The more recent members PHT1⁵⁾ and PHT2⁶⁾ were cloned from a rat brain cDNA library. These transporters differ from PEPT1 and PEPT2 in that they recognize the amino acid L-histidine as a substrate. While both PEPT1 and PEPT2 have high inter-species homology (about 80% in rat, rabbit, human, and mouse), the sequence homology between these transporters for a given species is low (about 50%).⁷⁾ Rat PHT1 and PHT2 have an amino acid identity of

about 50%, but they show little sequence homology to either PEPT1 or PEPT2 (less than 20%).

PEPT1 and PEPT2 proteins are believed to share a high degree of overlapping substrate specificity, possessing the capability for sequence-independent transport of 400 different dipeptides and 8000 different tripeptides. It is unclear whether or not the PHT1 and PHT2 proteins can transport the same spectrum of di-/tripeptides. However, the ability of PHT1/PHT2 to transport L-histidine marks a distinct difference in functionality from PEPT1/PEPT2. Since a three-dimensional structure of the transporter proteins has yet to be developed, no precise pharmacophore model is currently available. However, preferred configurations and conformational features of PEPT1 and PEPT2 substrates include: 1) a peptide backbone of 2-3 amino acid residues, 2) both a free amino acid and carboxy terminus with the free amino group in the α or β positions, 3) the presence of hydrophobic sidechains, and 4) stereoselectivity with L-amino acids and trans-conformers being preferred. It must be noted that these are not absolute criteria and some notable exceptions have been reported in the literature.^{1,2,8)}

b) Expression of POTs

Several studies have shown unique tissue distribution and expression patterns for the different POTs. PEPT1 protein is localized in the brush border (apical) membrane of absorptive epithelia cells of the small intestine⁹⁾ and the kidney.^{10,11)} Intestinal PEPT1 is confined to duodenum, jejunum and ileum of the small intestine, while renal PEPT1 is localized predominantly in S1 segments of early convoluted proximal tubule (i.e., pars convoluta).¹⁰⁾ PEPT1 mRNA is expressed at lower levels in the liver and pancreas.^{3,12)}

PEPT2 exhibits a different tissue expression pattern compared to PEPT1.^{4,13)} In kidney, immunolocalization studies show it is localized predominantly in S3 segments of latter proximal tubule (i.e., pars recta)¹⁰⁾. PEPT2 mRNA also exhibits strong levels of expression in the brain, lung and mammary gland, with weaker signals detected in the pancreas, skeletal muscle, heart, liver, spleen and colon.¹⁴⁾ In brain, PEPT2 mRNA has been specifically localized to astrocytes, subependymal cells, ependymal cells and epithelial cells of the choroid plexus.¹⁵⁾ With immunohistochemistry, PEPT2 protein has been found in astrocytes, ependyma and choroid plexus epithelium, as well as in some neurons.¹⁶⁾ The same study also found that PEPT2 expression in cerebral cortex (probably astrocytic) decreased with age. The choroid plexus epithelium is the site of the blood-cerebrospinal fluid barrier (BCSFB) and the presence of PEPT2 at that barrier has been demonstrated by immunoblot^{17,18)} and functional analyses.¹⁸⁻²⁰⁾ PEPT2 appears to be absent at the blood-brain barrier of cerebral capillaries.¹⁶⁾ Immunoblots show that PEPT2 protein is expressed in whole brain homogenates¹⁶⁾ as well as in peripheral nervous system glial cells.²¹⁾ In the eye, *in situ* hybridization studies have localized PEPT2 mRNA to the retina.¹⁵⁾ In the lung, PEPT2 protein was expressed in alveolar type II pneumocytes, bronchial epithelium, and endothelium of small vessels.²²⁾ Relatively less is known about the expression and distribution of PHT1 and PHT2. PHT1 mRNA has been found in the brain and eye, particularly in the choroid plexus and retina.⁵⁾ PHT2 transcripts were expressed primarily in the lymphatic system, lung, and spleen and detected faintly in the brain.⁶⁾

c) *Function of POTs*

As mentioned previously, an inwardly-directed electrochemical gradient for protons provides POTs with the driving force needed for active transport of peptides and peptide-mimetic molecules across biological membranes.^{1,2)} The pH of the extracellular microenvironment, therefore, plays an important role in determining the rate of transport. This is important in the intestine and kidney where low pH microenvironments are established by ion transporters at the microvilli of apical membrane epithelia.

Due to their unique tissue distribution and expression patterns, the POTs are thought to have distinct functions *in vivo*. Being the predominant (and perhaps only) POT located on the brush border membrane of the small intestine, PEPT1, a high-capacity and low-affinity transporter, is the transporter responsible for the absorption of small peptide fragments from the digestion of dietary proteins.³⁾ It may also to be the primary transporter responsible for absorption of peptide-mimetic drugs such as some ACE inhibitors and the antiviral prodrug valacyclovir. Despite the sequential expression of PEPT1 and PEPT2 in the proximal tubule of the nephron,¹⁰⁾ recent *in vivo* studies have shown PEPT1 plays a relatively minor role in the reabsorption of a dipeptide and an aminocephalosporin from tubular fluid.^{23,24)} In contrast, these studies have shown that PEPT2, a high-affinity and low-capacity transporter, is the major player involved in the renal handling and reabsorption of peptide substrates and peptide-mimetic drugs. The localization of PEPT2 on the apical membrane of choroid plexus epithelial cells at the BCSFB is thought to facilitate its mediation of neuropeptide homeostasis and removal of neurotoxins from the brain. This localization of PEPT2 also makes it an attractive target for manipulating delivery of peptide-mimetic drugs to the brain.²⁵⁾ Because little is known about the cellular localization, tissue distribution, and transport properties of

PHT1 and PHT2, little is also known about their functional activity *in vivo*. Functional studies¹⁷⁻²⁰⁾ in the choroid plexus have failed to show inhibition of dipeptide uptake by excess L-histidine, suggesting that PHT1/PHT2 are unlikely to be involved in peptide transport at the BCSFB. Some studies suggest they may play a role in intracellular trafficking of small peptides.^{6,26)}

d) Relevance to physiology, pharmacology and toxicology

While *in vitro* studies are convenient to probe mechanism, they are limited by experimental designs that employ nonphysiologic conditions, such as the lack of an intact blood supply. Moreover, the presence of multiple transport systems with overlapping substrate specificities in a tissue or organ of interest confounds an accurate assessment of the significance of a specific transporter relative to other transporters. Studies using wild-type and knockout mice offer a unique opportunity to study the role and relevance of a particular POT under physiological *in vivo* conditions. By challenging *in vivo* knockout models, unique phenotypes can be discovered, demonstrating the role and relevance of a particular POT with respect to drug disposition, dynamics, and toxicity. The rest of this review will address *in vivo* findings of PEPT2 with respect to the three model substrates glycylsarcosine,²³⁾ cefadroxil,²⁴⁾ and 5-aminolevulinic acid²⁷⁾, and attempt to illustrate the evolving relevance of this transporter to physiology, pharmacology, and toxicology using a PEPT2 knockout mouse model developed by our laboratory.²⁸⁾

Disposition of Glycylsarcosine (GlySar)

Our first study investigated the *in vivo* pharmacokinetics, tissue distribution, and renal handling of a synthetic dipeptide following an intravenous bolus dose (0.05 $\mu\text{mol/g}$ body

weight) of [¹⁴C]GlySar in wild-type and gender-matched PEPT2 knockout mice.²³⁾ These findings showed that, in PEPT2 knockout mice, the clearance of GlySar was markedly increased (2-fold), resulting in significantly lower systemic exposure of GlySar. In addition, renal reabsorption was almost abolished and GlySar was eliminated almost exclusively by glomerular filtration. Of the 46% of GlySar reabsorbed in wild-type mice, PEPT2 accounted for 86% of this process. Null mice also had lower choroid plexus concentrations of GlySar and a 5-fold lower choroid plexus-to-cerebrospinal fluid (CSF) ratio compared with wild-type mice at 60 min. Despite a 2-fold lower systemic exposure, null mice exhibited a greater CSF/blood ratio at 60 min (0.9 versus 0.2) and area under the curve (AUC_{CSF}/AUC_{blood}) ratio over 60 min (0.45 versus 0.12), indicating that PEPT2 significantly impacts GlySar exposure in the CSF compartment.

These findings were consistent with our hypothesis that PEPT2 is the predominant peptide transporter in kidney and that it acts as an efflux transporter in the choroid plexus (clearing peptides from CSF). However the next logical step was to determine whether or not these *in vivo* results hold when PEPT2 is challenged with a substrate of pharmacologic relevance.

Disposition of Cefadroxil

Our second study investigated the *in vivo* pharmacokinetics, renal tubular reabsorption, and brain penetration of cefadroxil, a broad spectrum, first-generation aminocephalosporin antibiotic.²⁴⁾ In these experiments, [³H]cefadroxil was administered by a single intravenous bolus injection in wild-type and gender-matched PEPT2 knockout mice over a wide range of doses (i.e., 100, 50, 12.5, and 1 nmol/g body weight). Results showed that cefadroxil disposition was clearly nonlinear over the dose range studied, due

to both saturable renal tubular secretion and reabsorption of the antibiotic. After the 1 nmol/g dose of cefadroxil, PEPT2 null mice exhibited a 3-fold greater total clearance and 3-fold lower systemic concentrations of drug compared to wild-type animals. Further, the cefadroxil plasma concentrations produced at this dose (i.e., approximately 0.01-10 μ M) are clinically relevant since they are in the minimal inhibitory concentration range of most bacteria.²⁹⁾ Renal reabsorption of cefadroxil was almost completely abolished in PEPT2 null mice versus wild-type animals (i.e., 3% versus 70%, respectively; $p < 0.001$). Of the 70% of cefadroxil reabsorbed in wild-type mice, PEPT2 accounted for 95% of reabsorbed substrate. Tissue distribution studies indicated that PEPT2 had a dramatic effect on cefadroxil tissue exposure, especially in brain where the CSF-to-blood concentration ratio of cefadroxil was 6-fold greater in PEPT2 null mice compared with wild-type animals.

The results were consistent with our hypothesis that PEPT2 significantly limits the exposure of cefadroxil in CSF, despite its role in increasing systemic exposure of the cephalosporin by renal reabsorption. Thus, cefadroxil (and possibly other aminocephalosporins) may be ineffective in the treatment of meningitis, at least in part, because of PEPT2-mediated efflux of antibiotic from CSF, thereby resulting in sub-therapeutic levels of drug at its active site. However, while the results were encouraging, a question that remained unanswered was whether or not PEPT2-mediated changes in drug disposition would result in significant changes to the pharmacological or toxicological effect of a drug.

Disposition and Neurotoxicity of 5-Aminolevulinic Acid (ALA)

Our third study investigated the role of PEPT2 in modulating ALA concentrations in the CSF and brain, and whether or not these changes would translate into greater neuroprotection *in vivo* against challenge doses of ALA, an endogenous heme precursor. ALA was chosen for study because of its known neurotoxicity in patients with hepatic porphyria³⁰⁻³²⁾ or lead toxicity³³, and because it is a PEPT2 substrate.^{14,17,34)} Studies below report the PEPT2-mediated changes in ALA pharmacokinetics and pharmacodynamics under different experimental conditions.

Preliminary studies were first performed to probe the pharmacokinetics of [¹⁴C]ALA after an intravenous bolus dose of drug (10 nmol/g body weight) in gender-matched wild-type and PEPT2 knockout mice²⁷⁾. Results indicated that PEPT2 knockout mice had a 2-fold higher clearance resulting in a 2-fold lower systemic exposure. Despite the reduction in systemic concentrations of ALA, knockout mice showed a 5-fold greater concentration of drug in CSF, an 8-fold greater CSF/blood concentration ratio, and significantly lower concentrations of drug in choroid plexus. These results are very consistent with that of GlySar and cefadroxil, as described previously and in Figure 1. As shown in this figure, the CSF-to-plasma ratios increased to a similar extent for GlySar, cefadroxil, and ALA in PEPT2 knockout mice as compared to wild-type animals. Similar reductions in the choroid plexus-to-CSF ratio were also observed in PEPT2 null vs. wild-type mice for all three PEPT2 substrates. These findings underscore the impact of PEPT2 in limiting exposure of these substrates to the CSF compartment and emphasize the directionality of PEPT2 transport from CSF into the choroid plexus epithelium *in vivo*.

With respect to pharmacodynamics, PEPT2 had a major impact on the ability of PEPT2 null mice to survive the toxic insult of a single high dose of ALA (4000 mg/kg s.c.).²⁷⁾ The time at which 50% of the animals died was 21 hr in wild-type mice as compared to only 4 hr in null mice ($p < 0.001$), providing strong evidence that PEPT2 confers a neuroprotective advantage against the toxicity of ALA. Further evidence of a neuroprotective role of PEPT2 was demonstrated under chronic dosing conditions of ALA (500 mg/kg s.c. each day) for 7 days, where wild-type mice showed no sign of a reduced ability to maintain balance on a rotating rod while for PEPT2 knockout mice, rotary rod times were progressively lower in response to chronic ALA administration.²⁷⁾ Neuromuscular dysfunction in the null mice was particularly evident after 4 days of ALA dosing, and balance times were reduced to 58% of control values at 7 days. This finding was even more obvious when chronic dosing conditions of ALA (100 mg/kg s.c. each day) were examined for 30 days. Specifically, by 30 days, wild-type mice had balance times that were 91% of control values while PEPT2 knockout mice had balance times that were only 60% of control values. Two-way ANOVA showed these correlations were highly significant as a function of both time and genotype ($p < 0.001$ for both factors). These differences could not be explained by plasma concentrations as there was little difference in the systemic exposure of ALA (after a single dose of 100 mg/kg s.c.) in wild-type and PEPT2 null mice. In contrast, the CSF concentrations were 8- and 30-fold greater in PEPT2 null mice at 30 min and 240 min ($p < 0.001$ for both times), respectively, indicating that the observed pharmacodynamic differences between genotypes were the result of differences in brain, and not systemic, levels of ALA. Moreover, the results are clinically relevant since chronic dosing of ALA at 100 mg/kg s.c. produced plasma

concentrations (i.e. $\sim 23 \mu\text{M}$, on average) which are similar to those observed in patients during acute attacks of porphyria (i.e. 2-13 μM).³¹⁾

These findings are novel in that they demonstrate not only a neuroprotective phenotype for the POT family member PEPT2, but that PEPT2-mediated effects on disposition in the brain translate into significant changes in toxicity.²⁷⁾ This phenomenon demonstrates the ability of a transporter to modulate drug effects beyond the conventional role of mediating drug disposition. The ability of PEPT2 to limit ALA exposure in CSF suggests that it may act as a secondary genetic modifier in the sensitivity of the brain to diseases such as hepatic porphyria or to environmental challenges such as lead poisoning. Figure 2 shows a proposed model of ALA neurotoxicity and the protective role of PEPT2 in reducing ALA concentrations in CSF and the interstitial fluid (ISF) surrounding parenchymal cells. As a result of higher ALA concentrations in the ISF of PEPT2 knockout mouse (or in conditions where choroid plexus expression of PEPT2 is reduced), there would be more interactions of this neurotoxin with extracellular receptors (e.g., glutamatergic or GABAergic receptors^{30,35)}), leading to an increased risk of toxicity. This scenario was demonstrated phenotypically as reduced survival and balancing times in our transgenic PEPT2 null mice.

Translation to humans

Translation of the role and relevance of PEPT2 in drug disposition, dynamics, and toxicity from the mouse to human will depend on four important factors: 1) the degree of inter-species sequence homology between mouse and human PEPT2 protein, 2) the conservation of PEPT2 transport functionality between these species; 3) the concordance

in cellular localization, expression levels and tissue distribution patterns of PEPT2 in both species; and 4) the concordance in cellular localization, expression levels and distribution patterns of other transporters with overlapping substrate specificities to PEPT2. These criteria, with the exception of criterion 4, have been tested when comparing the human and monkey peptide transporters, PEPT1 and PEPT2.³⁶⁾ As mentioned previously, the sequence homology between the mouse and human PEPT2 is high at about 80%. The molecular and structural features of the POT superfamily is highly conserved³⁷⁾ and studies have shown the ability of human cell lines expressing PEPT2 to transport the same range of substrates as mouse PEPT2.³⁸⁻⁴⁰⁾ Moreover, the apical localization of PEPT2 in the kidney^{38,41)} and lung⁴²⁾ cells of human has been shown indicating the same directionality of transport. Further studies, however, will be needed to demonstrate the inter-species concordance in expression levels and tissue distribution patterns of PEPT2. Since more than one transporter may affect the tissue distribution and organ elimination of a drug, additional studies will need to be performed to probe the influence of transporters with overlapping substrate specificity.

Pharmacogenomic Implications

As the PEPT2 transporter is continued to be challenged with various substrates or conditions, more phenotypes will be elucidated, further demonstrating the relevance of PEPT2 in mediating drug disposition, dynamics, and toxicity. To the extent that more PEPT2-mediated therapeutic agents are discovered, the transporter will become an important target for manipulating the delivery of drugs to intended sites of action (e.g., the brain), or manipulating the overall kinetic, dynamic, or toxic profiles of drugs. What is less clear, however, is the extent to which genetic variants of PEPT2 exist in the human

population, and whether or not these variants may lead to functional polymorphisms in drug disposition, dynamics, and toxicity.

A few investigators have reported that certain genetic variants of human PEPT2 (hPEPT2) may lead to functional polymorphisms in transport. For example, Terada et al.⁴³⁾ showed that a single amino acid substitution (Arg57His) of hPEPT2 caused the complete loss of functional activity when expressed in *Xenopus* oocytes or HEH293 cells, in spite of PEPT2 having a conserved protein expression at the plasma membrane. This phenotype, although believed to be rare in humans, is analogous to our PEPT2 knockout mouse. Pinsonneault et al.⁴⁴⁾ conducted a haplotype analysis of 27 single nucleotide polymorphisms of hPEPT2 and found two main variants containing several phased amino acid substitutions (i.e., hPEPT2*1 and hPEPT2*2; about 45% each), being present in all ethnic groups tested. They found that CHO cells, transfected with both variants, displayed similar V_{max} values for GlySar but significantly different values for K_m (83 μ M vs. 233 μ M for hPEPT2*1 and hPEPT2*2, respectively). The two haplotypes also differed in their pH sensitivity of GlySar uptake. While these two *in vitro* studies^{43,44)} point to an attenuation (or complete abolition) of PEPT2-mediated transport in some groups, the *in vivo* relevance of these genetic variants in the human population remains unclear. Further studies will be needed to determine the frequency and phenotypic significance of these (and other) genetic polymorphisms in PEPT2.

Conclusions

The PEPT2 knockout mouse has become an important tool to evaluate the evolving role and relevance of this transporter in drug disposition, dynamics and toxicity.

Although disruption of the PEPT2 gene itself does not result in obvious phenotypic changes in the knockout mouse, our studies emphasize the latent fact that challenging the knockout in a certain manner may bring about phenotypic abnormalities. Our studies have challenged the PEPT2 knockout model with various substrates of physiological, pharmacological and toxicological relevance, and have consistently demonstrated the dual action of this transporter with respect to its apical localization in kidney and choroid plexus epithelial cells. The results have clearly shown that *in vivo*: 1) PEPT2 effluxes GlySar, cefadroxil and ALA from the CSF into choroid plexus, thereby affecting regional disposition in the brain; and 2) PEPT2 reabsorbs these substrates from renal tubular fluid, thereby affecting systemic pharmacokinetics and exposure. It also appears that the regional effect of PEPT2 in limiting exposure of substrates to the CSF and ISF of brain may be of more importance for some compounds than its effect in increasing systemic exposure. Specifically, in the case of ALA, the modulation of regional brain disposition by PEPT2 translates directly into significant changes in neurotoxicity.

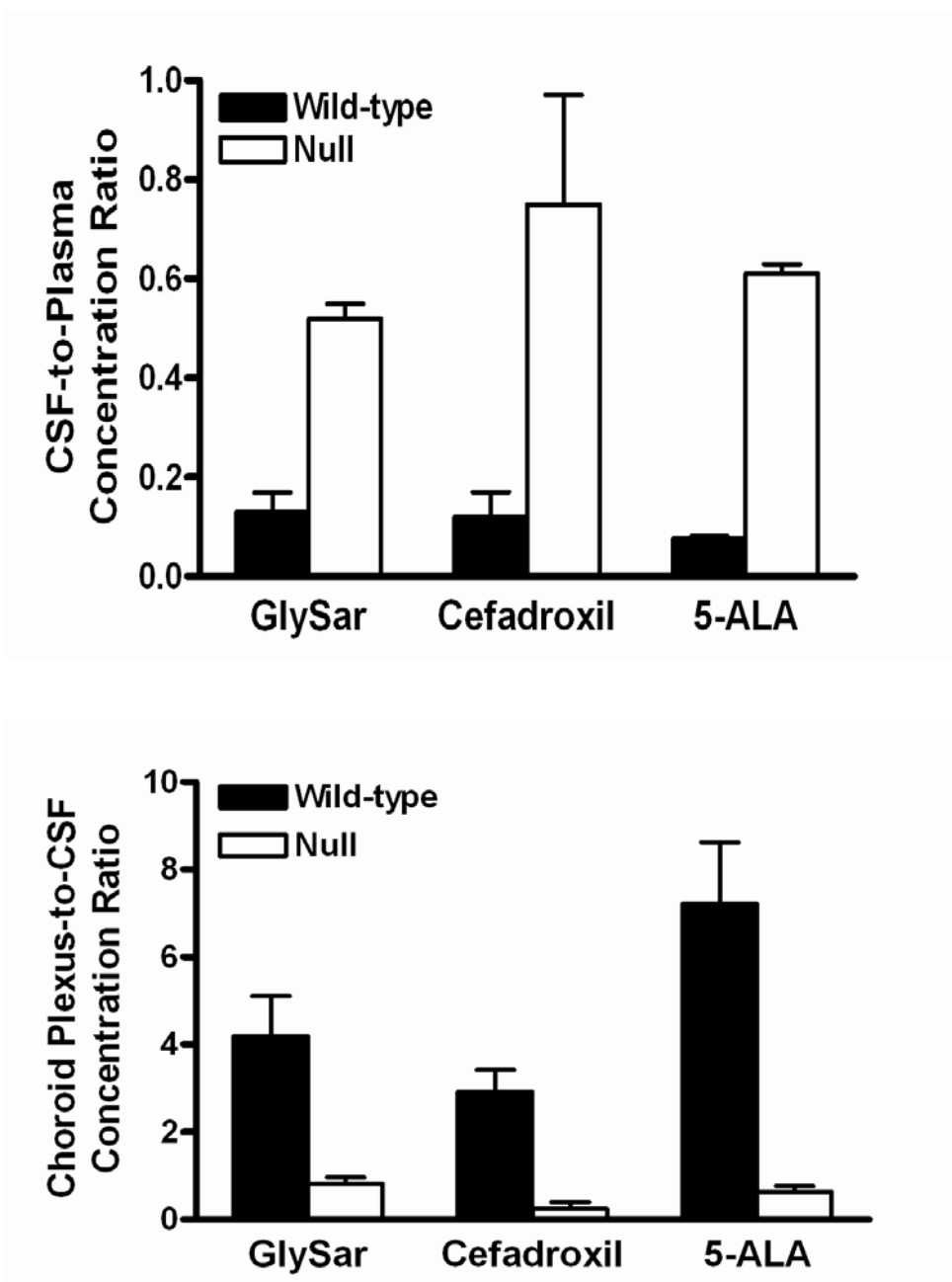


Figure A.1. Top panel: cerebrospinal fluid (CSF)-to-plasma concentration ratios in PEPT2 null mice were 4.2, 5.6 and 7.3 times that of values in wild-type mice for glycylsarcosine (GlySar), cefadroxil and 5-aminolevulinic acid (ALA), respectively. Bottom panel: choroid plexus-to-CSF concentration ratios in PEPT2 null mice were 0.3, 0.07 and 0.09 times that of values in wild-type mice for GlySar, cefadroxil and ALA, respectively. Samples were obtained 60 min after dosing GlySar (50 nmol/g body weight)²³, 120 min after dosing cefadroxil (1 nmol/g body weight)²⁴, and 60 min after dosing ALA (10 nmol/g body weight).²⁷

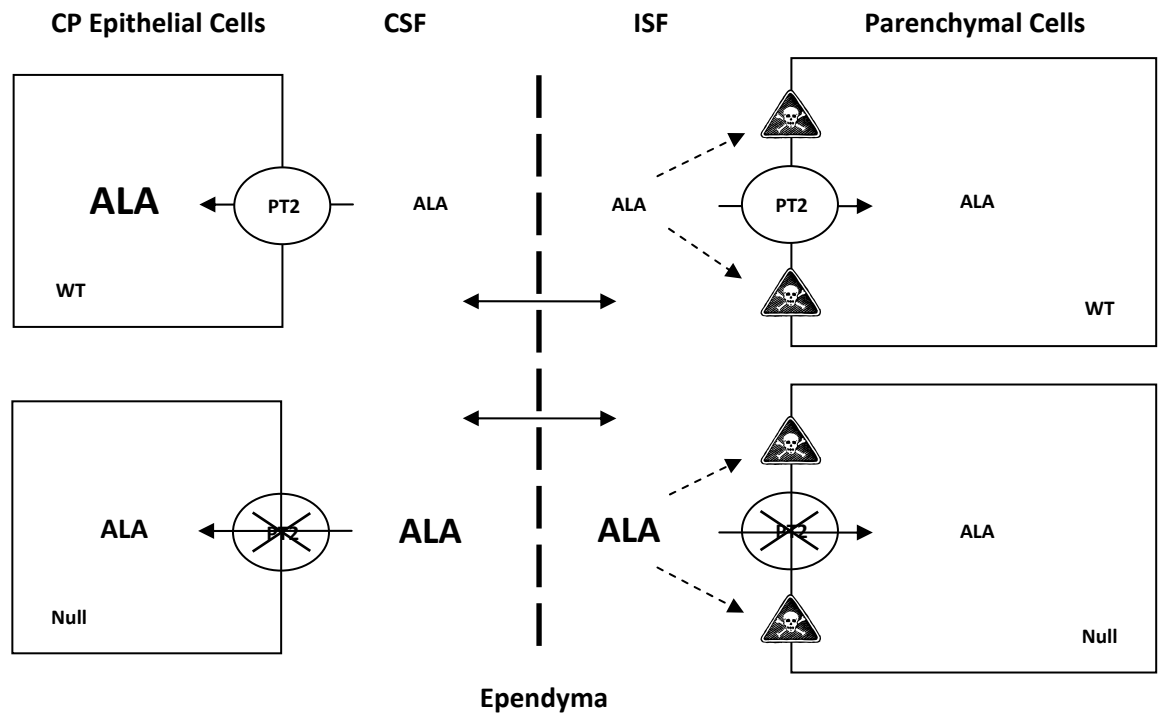


Figure A.2 Schematic of how the proton-coupled oligopeptide transporter SLC15A2 (PEPT2 displayed as PT2) affects the distribution of 5-aminolevulinic acid (ALA) in different compartments of the brain.²⁷⁾ In particular, the loss of PEPT2 results in substantially lower concentrations of ALA in choroid plexus (CP) epithelial cells, and substantially higher concentrations of ALA in cerebrospinal fluid (CSF) and interstitial fluid (ISF) surrounding the parenchymal cells. As a result of the higher concentrations of ALA in ISF, there may be more interactions with extracellular receptors, thereby, leading to an increased risk of neurotoxicity (as displayed by the “skull and crossbones” symbol). The top-half of the figure represents a scenario in wild-type (WT) mice while the bottom-half of the figure represents a scenario in PEPT2-deficient (Null) mice.

References

- 1) Daniel, H. and Kottra, G.: The proton oligopeptide cotransporter family SLC15 in physiology and pharmacology. *Pflugers Arch.*, **447**: 610-618 (2004).
- 2) Herrera-Ruiz, D. and Knipp, G.T.: Current perspectives on established and putative mammalian oligopeptide transporters. *J. Pharm. Sci.*, **92**: 691-714 (2002).
- 3) Fei, Y., Kanai, Y., Boron, W.F. and Heidiger, M.A.: Expression cloning of a mammalian proton-coupled oligopeptide transporter. *Nature (Lond)*, **368**: 563-566 (1994).
- 4) Lui, W., Liang, R., Ganapathy, V. and Leibach, F.H.: Molecular cloning of PEPT2, a new member of the H⁺/peptide cotransporter family from human kidney. *Biochem. Biophys. Acta.*, **1235**: 461-466 (1995).
- 5) Yamashita, T., Shimada, S., Tagaki, T. and Tohyama, M.: Cloning and functional expression of a brain peptide/histidine transporter. *J Biol. Chem*, **272**: 10205-10211 (1997).
- 6) Sakata, K., Yamashita, T., Maeda, M. and Shimada, S.: Cloning of a lymphatic peptide/histidine transporter. *J. Biochem.*, **356**: 53-60 (2001).
- 7) Botka, C., Wittig, T., Graul, R., Nielson, C., Amidon, G. and Sade'e, W.: Human proton/oligopeptide transporter (POT) genes: identification of putative human genes using bioinformatics. *AAPS Pharm. Sci.*, **2**: 1-22 (2000).
- 8) Rubio-Aliaga, I. and Daniel, H.: Mammalian peptide transporters as targets for drug delivery. *Trends pharmacol. Sci.*, **23**: 434-440 (2002).
- 9) Ogihara, H., Saito, H., Shin, B.C., Terado, T., Takenoshita, S., Nagamachi, Y., Inui, K. and Takata, K.: Immunolocalization of H⁺/peptide cotransporter in rat digestive tract. *Biochem. Biophys. Res. Commun.*, **220**: 848-52 (1996).
- 10) Shen, H., Smith, D.E., Yang, T. and Brosius, F.: Localization of PEPT1 and PEPT2 proton-coupled oligopeptide transporter mRNA and protein in rat kidney. *Am. J. Physiol.*, **276**: F658-F665 (1999).
- 11) Terada, T., Saito, H. and Mukai, M.: Recognition of β -lactam antibiotics by rat peptide transporters, PEPT1 and PEPT2 in LLC-PK cells. *Am. J. Physiol.*, **273**: F706-F711 (1997).
- 12) Gonzalez, D.E., Covitz, K. and Sadée, W.: An oligopeptide transporter is expressed at high levels in the pancreatic carcinoma cell lines AsPc-1 and Capan-2. *Cancer. Res.*, **58**: 519-525 (1998).
- 13) Boll, M., Herget, M., Wagener, M., Weber, W.M., Markovich, D., Biber, J., Clauss, W., Murer, H. and Daniel, H.: Expression cloning and functional characterization of the kidney cortex high-affinity proton-coupled peptide transporter. *Proc. Natl. Acad. Sci. USA*, **93**: 284-289 (1996).
- 14) Doring, F., Walter, J., Will, J., Focking, M., Boll, M., Amasheh, S., Clauss, W. and Daniel, H.: Delta-aminolevulinic acid transport by intestinal and renal peptide transporters and its physiological and clinical implications. *J Clin. Invest.*, **101**: 2761-2767 (1998).
- 15) Berger, U. and Hediger, M.: Distribution of peptide transporter PEPT2 mRNA in the rat nervous system. *Anat. Embryol.*, **199**: 439-449 (1999)

- 16) Shen, H., Smith, D.E., Keep, R.F. and Brosius, F.C.: Immunolocalization of the proton-coupled oligopeptide transporter PEPT2 in developing rat brain. *Mol. Pharm.*, **1**: 248-256 (2004).
- 17) Novotny, A., Xiang, J., Stummer, W., Teuscher, N.S., Smith, D.E. and Keep, R.: Mechanisms of 5-aminolevulinic acid uptake at the choroid plexus. *J. Neurochem.*, **75**: 321-328 (2000).
- 18) Shu, C., Shen, H., Keep, R.F. and Smith, D.E.: Role of PEPT2 in peptide/mimetic trafficking at the blood-cerebral fluid barrier: studies in rat choroid plexus epithelial cells in primary culture. *J. Phar. Exp. Ther.*, **301**: 820-829 (2002).
- 19) Teuscher, N.S., Novotny, A., Keep R.F., and Smith, D.E.: Functional evidence for the presence of PEPT2 in rat choroid plexus: Studies with glycylsarcosine. *J. Pharmacol. Exp. Ther.*, **294**: 494-499 (2000).
- 20) Teuscher, N.S., Keep, R.F. and Smith, D.E.: PEPT2-mediated uptake of neuropeptides in rat choroid plexus. *Pharm. Res.*, **18**: 807-813 (2001).
- 21) Groneberg D.A., Doring, F., Nickolaus, M., Daniel, H. and Fischer, A.: Expression of PEPT2 peptide transporter mRNA and protein in glial cells of rat dorsal root ganglia. *Neurosci. Lett.*, **304**: 181-4 (2001).
- 22) Groneberg, D.A., Nickolaus, M., Springer, J., Doring, F., Daniel, H. and Fischer, A.: Localization of the peptide transporter PEPT2 in the lung: implications for pulmonary oligopeptide uptake. *Am. J. Pathol.*, **158**: 707-714 (2001).
- 23) Ocheltree, M., Shen, H., Hu, Y., Keep, R.F. and Smith, D.E.: Role and relevance of peptide transporter 2 (PEPT2) in the kidney and choroid plexus: in vivo studies with glycylsarcosine in wild-type and PEPT2 knockout mice. *J. Pharmacol. Exp. Ther.*, **35**: 240-247 (2005).
- 24) Shen, H., Ocheltree, S., Hu, Y., Keep, R.F. and Smith, D.E.: Impact of genetic knockout of PEPT2 on cefadroxil pharmacokinetics, renal tubular reabsorption, and brain penetration in mice. *Drug Metab. & Disp.*, **35**: 1209-1216 (2007).
- 25) Smith, D.E., Johanson, C.E. and Keep, R.F.: Peptide and peptide analog transport systems at the blood-CSF barrier. *Adv. Drug Deliv. Rev.*, **56**: 1765-1791 (2004).
- 26) Ocheltree, M., Keep, R.F., Shen, H., Yang, D., Hughes, B. and Smith, D.E.: Preliminary investigation into the expression of proton-coupled oligopeptide transporters in neural retina and retinal pigment epithelium (RPE): lack of functional activity in RPE plasma membranes. *Pharm. Res.*, **20**: 1364-1372 (2003).
- 27) Hu, Y., Shen, H., Keep, R.F., and Smith, D.E.: Peptide transporter 2 (PEPT2) expression in brain protects against 5-aminolevulinic acid neurotoxicity. *J. Neurochem.*, **103**: 2058-2065 (2007).
- 28) Shen H, Smith D, Keep R, Xiang J, Brosius III FC.: Targeted disruption of the PEPT2 gene markedly reduces dipeptide uptake in the choroid plexus. *J. Biol. Chem.*, **278**: 4786-4791 (2003).
- 29) Courtieu, L. and Drugeon, H.: Compared sensitivities of 532 bacterial strains to six cephalosporins. *Int. J. Clin. Pharmacol. Res.*, **3**: 195-201 (1983).
- 30) Anderson, E., Sassa, A., Bishop, F. and Desnick, J.: Disorders of heme biosynthesis: X-linked sideroblastic anemia and the porphyrias, in *The Metabolic & Molecular Bases of Inherited Disease* (Scriver, R., Beaudet, L., Sly, S. and Valle, D.), pp 2991-3062. McGraw-Hill, New York (2001).

- 31) Lindberg, P., Martini, R., Baumgartner, M., Erne, B., Borg, J., Zielasek, J., Ricker, K., Steck, A., Toyka, K.V. and Meyer U.A.: Motor neuropathy in porphobilinogen deaminase-deficient mice imitates the peripheral neuropathy of human acute porphyria. *J. Clin. Invest.*, **103**: 1127-1134 (1999).
- 32) Albers, W. and Fink, K.: Porphyrinic neuropathy. *Muscle Nerve*, **30**: 410-422 (2004)
- 33) Klassen, D.: Heavy metals and heavy-metal antagonists, in *Goodman & Gilman's The Pharmacological Basis of Therapeutics* (Brunton, L., Lazo, S. and Parker, L., eds), pp 1753-1775. Mcgraw-Hill, New York.
- 34) Ocheltree, M., Shen, H., Hu, Y., Xiang, J., Keep, R.F. and Smith, D.E.: Role of PEPT2 in the choroid plexus uptake of glycylsarcosine and 5-aminolevulinic acid: studies in wild-type and null mice. *Pharm. Res.*, **21**: 1680-1685 (2004)
- 35) Adhikari, A., Penatti, C.A., Resende, R., Ulrich, H., Britto, G. and Bechara, H.: 5-Aminolevulinate and 4, 5-diox-ovalerate ions decrease GABA_A receptor density in neuronal cells, synaptosomes and rat brain. *Brain Res.*, **1093**: 95-104 (2006).
- 36) Zhang, E., Emerick, R., Pak, Y., Wrighton, S. and Hillgren, K.: Comparison of human and monkey peptide transporters: PEPT1 and PEPT2. *Mol. Pharmaceutics*, **1**: 201-210 (2004).
- 37) Fei, J., Ganapathy, V. and Leibach, F.: Molecular and structural features of the proton-coupled oligopeptide transporter superfamily. *Prog. Nucleic Acid Res. & Mol. Biol.*, **58**: 239-61 (1998).
- 38) Ganapathy, M., Brandsch, M., Prasad, P., Ganapathy, V. and Leibach, F.: Differential recognition of β -lactam antibiotics by intestinal and renal peptide transporters, PEPT1 and PEPT2. *J. Biol. Chem.*, **270**: 25672:25677 (1995).
- 39) Biegel, A., Knutter, I., Hartrodt, B., Gabauer, S., Theis, S., Luckner, P., Kottra, G., Rastetter, M., Zebisch, K., Thondorf, I., Daniel, H., Neubert, K. and Brandsch, M.: The renal type H⁺/peptide symporter PEPT2: structure-affinity relationships. *Amino Acids*, **31**: 137-156 (2006).
- 40) Sugawara, M., Huang, W., Fei, Y., Leibach, F., Ganapathy, V. and Ganapathy, M.: Transport of valganciclovir, a ganciclovir prodrug, via peptide transporters PEPT1 and PEPT2. *J. Pharm. Sci.*, **89**: 781-789 (2000).
- 41) Ramamoorthy, S., Liu, W., Ma, Y., Yang-Feng, T., Ganapathy, V. and Leibach, F.: Proton/peptide cotransporter (PEPT2) from human kidney: functional characterization and chromosomal localization. *Biochimica. et. Biophysica. Acta.*, **1240**: 1-4 (1995).
- 42) Bahadurri, P., D'Souza, V., Pinsonneault, J., Sade'e, W., Bao, S., Knoell, D. and Swaan, P.: Functional characterization of the peptide transporter PEPT2 in primary cultures of human upper airway epithelium. *Am. J. Resp. Cell & Mol. Biol.*, **32**: 319-25 (2005).
- 43) Terada, T., Irie, M., Okuda, M. and Inui, K.: Genetic variant Arg57His in human H⁺/peptide cotransporter 2 causes a complete loss of transport function. *Biochem. Biophys. Res. Commun.*, **316**: 416-420 (2004).
- 44) Pinsonneault, J., Nielsen, U. and Sadée, W.: Genetic variants of the human H⁺/dipeptide transporter PEPT2: analysis of haplotype functions. *J. Pharmacol. Exp. Ther.*, **311**: 1088-1096.

Appendix B

NONMEM control streams for paroxetine, atomoxetine, lorazepam, and olanzapine PK models

Atomoxetine PK Control Stream

```
$PROB pkatom lcompt no tlag
$INPUT STUD NMID=ID AGE WGT HT GEN HORM RACE DOSE AMT NTIM TIME DAY
CONC=DV SCR CLCR EVID MDV TXT PER
$DATA pop_pk_atomoxetine.csv IGNORE=#
$SUBS ADVAN=2 TRANS=2 INFN=infn.ci.txt
$PK
  TVCL = THETA(1)
  CL   = TVCL * EXP(ETA(1))
  TVV  = THETA(2)*(1-THETA(6))*(1-GEN))
  V    = TVV * EXP(ETA(2))
  TVKA = THETA(3)
  KA   = TVKA * EXP(ETA(3))
  K=CL/V
  KA=KA
  S2=V/1000
$ERROR
  IPRED=F ;INDIVIDUAL PREDICTION
  W=((THETA(4)**2)*(F**2)+THETA(5)**2)**0.5 ;1=Additive and F (or
IPRED)=Constant CV
  IRES=DV-IPRED ;INDIVIDUAL RESIDUAL
  IWRES=IRES/W
  Y = IPRED+W*EPS(1)
$THETA (0 15 50) ; CL TH1
        (0 100 2000) ; V TH2
        (0 3 15) ; KA TH3
        ;(0 0.4 2) ; ALAG1 TH4
        (0 0.2)
        (0 5)
        (0 0.1)

$OMEGA BLOCK(2)
  0.3
  0.01 0.3
$OMEGA BLOCK(1)
  0.3
$SIGMA (1 FIXED)
$EST METHOD=1 INTERACTION SIGDIGITS=3 MAXEVAL=9999 PRINT=5 POSTHOC
NOABORT MSFO=MSF1
$COV PRINT=E
$TABLE NMID CL V KA DOSE WGT GEN CLCR AGE RACE HT HORM ETA(1)
ETA(2) ETA(3) NOPRINT ONEHEADER FIRSTONLY FILE=pk_atom_l2a.tab
$TABLE NMID MDV CL V KA DOSE WGT GEN CLCR AGE RACE HT HORM
TIME IPRED IRES IWRES NOPRINT ONEHEADER FILE=pk_atom_l2.tab
$SCAT DV VS PRED IPRED UNIT
```

NONMEM Control Stream for Paroxetine PK

```
Paroxetine PK Output
$PROB 01 One-Compartment Model with tlag
$INPUT STUD NMID=ID AGE WGT HT GEN HORM RACE DOSE AMT NTIM TIME DAY
CONC=DV SCR CLCR EVID MDV TXT PER
$DATA pop_pk_paroxetine.csv IGNORE=#
$SUBS ADVAN=2 TRANS=2 INFN=infn.ci.txt
```

```

$PK
TVCL = THETA(1)
CL   = TVCL * EXP(ETA(1))
TVV  = THETA(2)
V    = TVV * EXP(ETA(2))
TVKA = THETA(3)
KA   = TVKA * EXP(ETA(3))
TVLAG= THETA(4)
ALAG1= TVLAG
K=CL/V
KA=KA
S2=V/1000
$ERROR
IPRED=F ;INDIVIDUAL PREDICTION
W=((THETA(5)**2)*(F**2)+THETA(6)**2)**0.5 ;l=Additive and F (or
IPRED)=Constant CV
IRES=DV-IPRED ;INDIVIDUAL RESIDUAL
IWRES=IRES/W
Y = IPRED+W*EPS(1)
$THETA (0 100) ; CL TH1
        (0 1000) ; V TH2
        (0 0.1) ; KA TH3
        (0 0.4 1) ; ALAG1 TH4
        (0 0.25) ; TH(5)
        (0 0.1) ; TH(6)
$OMEGA 0.3 0.3 0.01
$SIGMA (1 FIXED)
$EST METHOD=1 INTERACTION SIGDIGITS=3 MAXEVAL=9999 PRINT=5 POSTHOC
NOABORT MSFO=MSF1
$COV PRINT=E
$TABLE NMID MDV TIME NTIM CL V KA DOSE WGT GEN CLCR RACE AGE ETA(1) ETA(2)
ETA(3) NOPRINT ONEHEADER FIRSTONLY FILE=pk_paro_16A.tab
$TABLE NMID MDV TIME NTIM CL V KA DOSE WGT GEN CLCR RACE AGE IPRED IRES IWRES WRRES RES
NOPRINT ONEHEADER FILE=pk_paro_16.tab
$SCAT DV VS PRED IPRED UNIT

```

NONMEM Control Stream for Lorazepam PK

```

$PROB 04 Test 2 COMP Model without Tlag and etas on v3

$INPUT STUD NMID=ID AGE WGT HT GEN HORM RACE DOSE AMT NTIM TIME DAY

CONC=DV SCR CLCR EVID MDV TXT PER

$DATA pop_pk_lorazepam.csv IGNORE=#

$SUBS ADVAN=4 TRANS=4 INFN=ininci.txt
$PK

TVCL = THETA(1)+THETA(6)*(CLCR-105)
CL   = TVCL * EXP(ETA(1))

TVV  = THETA(2)+THETA(7)*(WGT-75)
V2   = TVV * EXP(ETA(2))

TVKA = THETA(3)
KA   = TVKA* EXP(ETA(4))

Q = THETA(4)
V3= THETA(5)* EXP(ETA(3))

K=CL/V2
K23 = Q/V2
K32 = Q/V3
KA=KA

```

```

S2=V2/1000
$ERROR

IPRED=F          ;INDIVIDUAL PREDICTION
W=THETA(8)*(F)   ;l=Additive and F (or IPRED)=Constant CV
IRES=DV-IPRED   ;INDIVIDUAL RESIDUAL
IWRES=IRES/W

Y = IPRED+W*EPS(1)

$THETA (0 4 15)   ; CL TH1
        (0 50 100) ; V TH2
        (0 1 5)   ; KA TH3
        (0 11 20) ; Q TH4
        (0 37 100) ; V3 TH5
        (0 0.01); TH6 CRCL ON CL
        (0 0.7) ; TH7 WGT ON V
        (0 0.25); TH8
$OMEGA 0.3 0.3 0.3 0.3
$SIGMA (1 FIXED)
$EST METHOD=1 INTERACTION SIGDIGITS=3 MAXEVAL=9999 PRINT=5 POSTHOC
NOABORT MSFO=MSF1
$COV PRINT=E
$TABLE NMID CL V2 KA Q V3 DOSE WGT GEN CLCR AGE RACE HT HORM ETA(1)
ETA(2) ETA(3) ETA(4) IPRED IRES NOPRINT ONEHEADER FIRSTONLY
FILE=pk_lorA_28.tab
$TABLE NMID MDV CL V2 KA Q V3 DOSE WGT GEN CLCR AGE RACE HT HORM
TIME IPRED IRES IWRES NOPRINT ONEHEADER FILE=pk_lor_28.tab
$SCAT DV VS PRED IPRED UNIT

```

NONMEM Control Stream for Olanzapine PK

```

$PROB 14b (Model 14) FINAL Model Calc WRES
$INPUT STUD NMID=ID AGE WGT HT GEN HORM RACE DOSE AMT NTIM TIME DAY
CONC=DV SCR CLCR EVID MDV TXT PER
$DATA pop_pk_olanzapine.csv IGNORE=#
$SUBS ADVAN=4 TRANS=4 INFN=infnci.txt
$PK
TVCL = THETA(1)
CL = TVCL * EXP(ETA(1))
TVV = THETA(2)*(1-THETA(7))*(1-GEN))
V2 = TVV * EXP(ETA(2))
KA = THETA(3)
Q = THETA(4) * EXP(ETA(3))
TVV3 = THETA(5)
V3= TVV3 * EXP(ETA(4))
ALAG1 = THETA(6)
K=CL/V2
K23 = Q/V2
K32 = Q/V3
KA=KA
S2=V2/1000
$ERROR
IPRED=F          ;INDIVIDUAL PREDICTION
W=((THETA(8)**2)*(F**2)+THETA(9)**2)**0.5 ;l=Additive and F (or
IPRED)=Constant CV
IRES=DV-IPRED   ;INDIVIDUAL RESIDUAL
IWRES=IRES/W
Y = IPRED+W*EPS(1)
$THETA (0 15 50)   ; CL TH1
        (0 300 2000) ; V TH2
        (0 0.1 3)   ; KA TH3
        (0 20 50)   ; Q TH4
        (0 600 2000) ; V3 TH5
        (0 0.4 2)   ; ALAG TH6
        (0 0.1 0.8) ; TH7 GDR on V
        (1)         ; TH8 Factor for WRES
        (0.2)       ; TH9 Factor for WRES
$OMEGA 0.3 0.3 0.1 0.1

```

```
$SIGMA 1
$EST METHOD=1 INTERACTION SIGDIGITS=3 MAXEVAL=9999 PRINT=5 POSTHOC
NOABORT MSFO=MSF1
$COV
$TABLE ONEHEADER NMID TIME NTIM CL V2 KA V3 Q ALAG1 DOSE WGT GEN CLCR
AGE ETA(1) ETA(2) ETA(3) ETA(4) MDV IPRED IWRES NOPRINT FILE=pk_olan_14c.tab
$SCAT DV VS PRED IPRED UNIT
```

Appendix C

NONMEM control streams of lorazepam sleepiness and dizziness categorical models

Lorazepam Sleepiness Categorical Model

```
$PROB SRDEQ Lorazepam sleepiness model
$INPUT STUD NMID=ID DOSE DAY=DROP NTIM=TIME SQTM RESP=DV
MV3=MDV TPK=DROP CON2 ICL IV1 IKA IQ IV2 AGE WGT HT=DROP GEN
RACE CRCL
$DATA MOE.csv IGNORE=#
$PRED
;*****PHARMACODYNAMIC MODEL*****
;*****
; Define Equations for PK in Central and Effect Comp
  K10 = ICL/IV1
  K12 = IQ/IV1
  K21 = IQ/IV2
  KKK1 = (K12 + K21 + K10)
  KKK2 = K21*K10
  ALPH = (KKK1+(KKK1**2-4*KKK2)**0.5)/2
  BETA = (KKK1-(KKK1**2-4*KKK2)**0.5)/2
  TI = TIME
  IF (TI.LE.0) TI=0
  AAA = IKA*DOSE*1000/IV1
  BBB = (K21-ALPH)/((ALPH-BETA)*(ALPH-IKA))
  CCC = (BETA-K21)/((ALPH-BETA)*(BETA-IKA))
  DDD = (K21-IKA)/((ALPH-IKA)*(BETA-IKA))
  KE0 = THETA(7)
  AAA2 = AAA*KE0
  BBB2 = BBB/(KE0-ALPH)
  CCC2 = CCC/(KE0-BETA)
  DDD2 = DDD/(KE0-IKA)
  EEE = (K21-KE0)/((ALPH-KE0)*(BETA-KE0)*(IKA-KE0))

  CONC = AAA*(BBB*EXP(-ALPH*TI)+CCC*EXP(-BETA*TI)+DDD*EXP(-IKA*TI))

SUM1=BBB2*EXP(-ALPH*TI)
SUM2=CCC2*EXP(-BETA*TI)
SUM3=DDD2*EXP(-IKA*TI)
SUM4=EEE*EXP(-KE0*TI)

CE=AAA2*(SUM1+SUM2+SUM3+SUM4)

; Define Parameters and Equation for Drug Effect

SLOPE = THETA(6)
DRUG = SLOPE*CE
; Define Parameters and Equation for Placebo Effect
EST=MIXEST
IF (MIXNUM.EQ.1) THEN
  PLAC=0
ELSE
  PLAC= THETA(8)*(EXP(-THETA(10)*TIME)-EXP((-THETA(10)*230)*TIME))
ENDIF

; Define Different Intercepts for n-1 scores

B1 = THETA(1)
```



```

B2 = B1 + THETA(2)
B3 = B2 + THETA(3)
B4 = B3 + THETA(4)
B5 = B4 + THETA(5)

; Define logits for Score 0, 1, 2
; (Y=>1, Y=>2)
A1 = B1 +DRUG+PLAC+ETA(1)
A2 = B2 +DRUG+PLAC+ETA(1)
A3 = B3 +DRUG+PLAC+ETA(1)
A4 = B4 +DRUG+PLAC+ETA(1)
A5 = B5+DRUG+PLAC+ETA(1)
C1 = EXP(A1)
C2 = EXP(A2)
C3 = EXP(A3)
C4 = EXP(A4)
C5 = EXP(A5)

; Define Probability for Each Score
; (Y=>0, Y=>1, Y=>2)
P1 = C1/(1+C1) ; Probability of Score=>1
P2 = C2/(1+C2) ; Probability of Score=>2
P3 = C3/(1+C3) ; Probability of Score=>3
P4 = C4/(1+C4) ; Probability of Score=>4
P5 = C5/(1+C5) ; Probability of Score=>4

PR0 = 1-P1 ; Probability of Score=0
PR1 = P1-P2 ; Probability of Score=1
PR2 = P2-P3 ; Probability of Score=2
PR3 = P3-P4 ; Probability of Score=3
PR4 =P4-P5 ; Probability of Score=4
PR5 = 1-(PR0+PR1+PR2+PR3+PR4) ; Probability of Score=5

; Expected Score OR Predicted Score
;ESCR = 4*PR4+3*PR3+2*PR2+1*PR1
; Select Appropriate P(Y=m)
IF (DV.EQ.5) Y=PR5
IF (DV.EQ.4) Y=PR4
IF (DV.EQ.3) Y=PR3
IF (DV.EQ.2) Y=PR2
IF (DV.EQ.1) Y=PR1
IF (DV.EQ.0) Y=PR0
$MIX
NSPOP=2
P(1)=THETA(9)
P(2)=1-P(1)

$THETA (-2) ; THETA2 B1
$THETA (-2) ; THETA3 B2
$THETA (-2) ; THETA4 B3
$THETA (-2) ; THETA5 B4
$THETA (-2) ; THETA6 B4
$THETA (0.2) ; SLOPE
$THETA (3) ; KEO
$THETA (3) ; PLAC
$THETA (0 0.5 1) ; PROP
$THETA (0.1) ; PROP
;$THETA (1) ; PROP

$OMEGA 1
$COV PRINT=E
$ESTIMATION MAXEVAL=9999 PRINT=5 METHOD=COND LAPLACE LIKELIHOOD
NOABORT MSFO=MSF1
$TABLE ONEHEADER FIRSTONLY STUD NMID NTIM DOSE
ETA(1) P1 P2 P3 P4 PR0 PR1 PR2 PR3 PR4
NOPRINT FILE=lor.srdeq.9.tab

```

B) Lorazepam Dizziness Categorical Model

```

$PROB SRDEQ PK/PD Model of Dizziness
;BOTH TREATMENT AND PLACEBO DATA WITH PK POSTHOC
$INPUT STUD NMID=ID DOSE DAY=DROP NTIM=TIME SQTM=DROP DIZZ=DV
MV9=MDV TPK=DROP CON2 ICL IV1 IKA IQ IV2 AGE WGT HGT GEN
RACE CRCL

$DATA dizziness.data.csv

$PRED

;*****PHARMACODYNAMIC MODEL*****
;*****

; Define Equations for PK in Central and Effect Comp
K10 = ICL/IV1
K12 = IQ/IV1
K21 = IQ/IV2

KKK1 = (K12 + K21 + K10)
KKK2 = K21*K10

ALPH = (KKK1+(KKK1**2-4*KKK2)**0.5)/2
BETA = (KKK1-(KKK1**2-4*KKK2)**0.5)/2

TI = TIME
IF (TI.LE.0) TI=0

AAA = IKA*DOSE*1000/IV1
BBB = (K21-ALPH)/((ALPH-BETA)*(ALPH-IKA))
CCC = (BETA-K21)/((ALPH-BETA)*(BETA-IKA))
DDD = (K21-IKA)/((ALPH-IKA)*(BETA-IKA))

CONC = AAA*(BBB*EXP(-ALPH*TI)+CCC*EXP(-BETA*TI)+DDD*EXP(-IKA*TI))

; Define Parameters and Equation for Drug Effect

SLOPE = THETA(1)

DRUG = SLOPE*CONC

; Define Parameters and Equation for Placebo Effect

EST=MIXEST
IF (MIXNUM.EQ.1) THEN
  PLAC=0
ELSE
  PLAC= THETA(5)*(EXP(-THETA(7)*TIME)-EXP(-THETA(8)*TIME))

ENDIF

; Define Different Intercepts for n-1 scores

B1 = THETA(2)
B2 = B1 + THETA(3)
B3 = B2 + THETA(4)

; Define logits for Score 0, 1, 2
; (Y=>1, Y=>2)

A1 = B1 + DRUG +PLAC+ETA(1)

```

```

A2 = B2 + DRUG +PLAC+ETA(1)
A3 = B3 + DRUG +PLAC+ETA(1)

C1 = EXP(A1)
C2 = EXP(A2)
C3 = EXP(A3)

; Define Probability for Each Score
; (Y=>0, Y=>1, Y=>2)

P1 = C1/(1+C1) ; Probability of Score=>1
P2 = C2/(1+C2) ; Probability of Score=>2
P3 = C3/(1+C3) ; Probability of Score=>3

PR0 = 1-P1 ; Probability of Score=0
PR1 = P1-P2 ; Probability of Score=1
PR2 = P2-P3 ; Probability of Score=2
PR3 = 1-(PR0+PR1+PR2) ; Probability of Score=3

; Expected Score OR Predicted Score
;ESCR = 4*PR4+3*PR3+2*PR2+1*PR1

; Select Appropriate P(Y=m)

IF (DV.EQ.3) Y=PR3
IF (DV.EQ.2) Y=PR2
IF (DV.EQ.1) Y=PR1
IF (DV.EQ.0) Y=PR0

$MIX
NSPOP=2
P(1)=THETA(6)
P(2)=1-P(1)

$THETA (0 0.2) ; THETA1 SLOPE
$THETA (-5) ; THETA2 B1
$THETA (-3) ; THETA3 B2
$THETA (-1) ; THETA4 B3
$THETA (0 5) ; Plac
$THETA (0 0.5 1) ;PROPORTION nrsp
$THETA (0.1)
$THETA (1)

$OMEGA 1
$COV PRINT=E
$ESTIMATION MAXEVAL=9999 PRINT=5 METHOD=COND LAPLACE LIKELIHOOD
NOABORT MSFO=MSF1
$TABLE ONEHEADER FIRSTONLY STUD NMID NTIM DOSE CON2
P1 P2 P3 PR0 PR1 PR2 PR3 ETA(1)
NOPRINT FILE=LOR.DIZZ.16.TAB

```

Appendix D

NONMEM control stream of VAS Sleepiness model

```
$PROB vas 01 Initial Model

$INPUT STUD NMID=ID TPK=DROP CON2 ICL IV1 IKA IQ IV2 AGE WGT HT=DROP
GEN HORM=DROP RACE=DROP DOSE TXT=DROP NTIM=TIME DAY CLCR VAS1 ADJ
LOGT=DV MV1=MDV

$DATA vas_finalmodel.csv IGNORE=#

$PRED

;*****PHARMACODYNAMIC MODEL*****
;*****

K10 = ICL/IV1
K12 = IQ/IV1
K21 = IQ/IV2

KKK1 = (K12 + K21 + K10)
KKK2 = K21*K10

ALPH = (KKK1+(KKK1**2-4*KKK2)**0.5)/2
BETA = (KKK1-(KKK1**2-4*KKK2)**0.5)/2

TI = TIME
IF (TI.LE.0) TI=0

AAA = IKA*DOSE*1000/IV1
BBB = (K21-ALPH)/((ALPH-BETA)*(ALPH-IKA))
CCC = (BETA-K21)/((ALPH-BETA)*(BETA-IKA))
DDD = (K21-IKA)/((ALPH-IKA)*(BETA-IKA))

KE0 = THETA(4)*EXP(ETA(3))

AAA2 = AAA*KE0
BBB2 = BBB/(KE0-ALPH)
CCC2 = CCC/(KE0-BETA)
DDD2 = DDD/(KE0-IKA)
EEE = (K21-KE0)/((ALPH-KE0)*(BETA-KE0)*(IKA-KE0))

CONC = AAA*(BBB*EXP(-ALPH*TI)+CCC*EXP(-BETA*TI)+DDD*EXP(-IKA*TI))

SUM1=BBB2*EXP(-ALPH*TI)
SUM2=CCC2*EXP(-BETA*TI)
SUM3=DDD2*EXP(-IKA*TI)
SUM4=EEE*EXP(-KE0*TI)

CE=AAA2*(SUM1+SUM2+SUM3+SUM4)
```

```

BSL = THETA(1) * EXP(ETA(1))
SLOPE=THETA(2)*EXP(ETA(2))
DRUG=SLOPE*CE

PLAC =THETA(3)*EXP(ETA(4))*(EXP(-THETA(5)*TIME)-EXP(-((THETA(5)*1.5)*TIME)))

IF (TIME.EQ.0) THEN
F=BSL
ELSE
F=BSL+DRUG+PLAC
ENDIF
  IPRED=F          ;INDIVIDUAL PREDICTION
  IRES=DV-IPRED   ;INDIVIDUAL RESIDUAL
  W=1             ; 1=Additive and F (or IPRED)=Constant CV
  IWRES = IRES/W

  Y =F+EPS(1)

$THETA (-3)      ; BSL
$THETA (0.1)    ;SLOPE
$THETA (-5); PLAC
$THETA (3); Keo
$THETA (0 0.01);
;$THETA (0 1)

$OMEGA 0.01 0.01 0.01 0.01

$SIGMA 1

$EST METHOD=1 INTERACTION SIGDIGITS=3 MAXEVAL=9999 PRINT=5
  POSTHOC NOABORT MSFO=MSF1
$COV PRINT=E
$TABLE ONEHEADER NMID NTIM TIME DOSE CONC BSL
WRES IWRES IPRED IRES NOPRINT FILE=vas_7aaaa.tab
$SCAT DV VS PRED IPRED UNIT

```

Appendix E

SPLUS nonparametric bootstrap code

```
data1<-read.table("C:\\nmv\\LOR.SLEEP.SRDEQ\\MOE.csv",sep=",",skip=1)
#there are 20 subjects simple PK data
sam<-seq(1,20,1)
for (j in 1:1000) {
  BGSB<-NULL
  for (i in 1:20) { lucky<-sample(sam,size=1,replace=T)+1000
    data2<-data1[data1[,2]==lucky,]
    data2[,2]<-i
    BGSB<-rbind(BGSB,data2)
  }
  exportData(BGSB,
file="c:\\nmv\\LOR.SLEEP.SRDEQ\\dumby.csv",colNames=F,quote=F)
  dos(paste("nmfe5 cl.txt rl.txt"),multi=F,output=F)
}
```

Appendix F

Categorical sleepiness simulation code (SPLUS)

```
## filter micha file with bootstrap parameters
tab<-importData("nadia.txt",type="ASCII",stringsAsFactors=F)
tab2<-tab[tab$Col1==0,c(1:14)]
tab3<-tab2[tab2$Col2==0,c(1:14)]
tab32<-tab3[tab3$Col14!=0,]
tab4<-tab32[c(4:14)]

##Get dummy file
data<-importData("dumby1.csv",type="ASCII", stringsAsFactors=F)
nr<-nrow(data)
names(data)<-c("STUD","ID", "DOSE", "TIME", "DV", "MDV", "ICL", "IV1", "IKA",
"IQ", "IV2")
BGSH<-NULL
##NESTED LOOP
##LOOP OVER MICHA FILE (OUTER LOOP)
## LOOP WITHIN STUDY (INNER LOOP)
for(i in 1:250){
  #i<-1
  #get row i of micha
  vec<-tab4[i,]
  names(vec)<-
c("th1","th2","th3","th4","th5","th6","th7","th8","th9","th10",
"om11")
  temp<-matrix(NULL,ncol=7,nrow=400)
  for (j in 1:nr){
    if (j==1) {oldid<- -1}
    ##subject level stuff
    if (data[j,2]!=oldid) {
      test1<-runif(1,0,1)
      eta<-rnorm(1,0,sd=sqrt(vec$om11))
    }
    #j<-1
    K10<- data$ICL[j]/data$IV1[j]
    K12<- data$IQ[j]/data$IV1[j]
    K21<- data$IQ[j]/data$IV2[j]
    KKK1<- (K12 + K21 + K10)
    KKK2<- K21*K10
    ALPH <- (KKK1+(KKK1**2-4*KKK2)**0.5)/2
    BETA<- (KKK1-(KKK1**2-4*KKK2)**0.5)/2
    TI<- data$TIME[j]
    if (TI<=0) { TI==0}
    AAA<- data$IKA[j]*data$DOSE[j]*1000/data$IV1[j]
    BBB <- (K21-ALPH)/((ALPH-BETA)*(ALPH-data$IKA[j]))
    CCC <- (BETA-K21)/((ALPH-BETA)*(BETA-data$IKA[j]))
    DDD <- (K21-data$IKA[j])/((ALPH-data$IKA[j])*(BETA-data$IKA[j]))
    CONC<- AAA*(BBB*exp(-ALPH*TI)+CCC*exp(-BETA*TI)+DDD*exp(-
data$IKA[j]*TI))
    KE0<-vec$th7
    AAA2 <- AAA*KE0
    BBB2 <- BBB/(KE0-ALPH)
    CCC2<- CCC/(KE0-BETA)
```

```

        DDD2 <- DDD/(KE0-data$IKA[j])
        EEE <- (K21-KE0)/((ALPH-KE0)*(BETA-KE0)*(data$IKA[j]-KE0))
        SUM1<-BBB2*exp(-ALPH*TI)
        SUM2<-CCC2*exp(-BETA*TI)
        SUM3<-DDD2*exp(-data$IKA[j]*TI)
        SUM4<-EEE*exp(-KE0*TI)
        CE<-AAA2*(SUM1+SUM2+SUM3+SUM4)
        SLOPE<-vec$th6
        DRUG<-SLOPE*CE
PLAC<-as.numeric(test1<=vec$th9)*0+as.numeric(test1>vec$th9)*vec$th8*(exp(-
vec$th10*data$TIME[j])-exp(-vec$th10*230*data$TIME[j]))
        MIXNUM<-
as.numeric(test1>vec$th9)+1

        B1<-vec$th1
        B2<- B1 + vec$th2
        B3<- B2 + vec$th3
        B4<- B3 + vec$th4
        B5<- B4 + vec$th5
        # ; Define logits for

Score 0, 1, 2

        # ; (Y=>1, Y=>2)
        A1<- B1 + DRUG +PLAC+eta
        A2<- B2 + DRUG +PLAC+eta
        A3<- B3 + DRUG +PLAC+eta
        A4<- B4 + DRUG +PLAC+eta
        A5<- B5 + DRUG +PLAC+eta
        C1<-exp(A1)
        C2<-exp(A2)
        C3<-exp(A3)
        C4<-exp(A4)
        C5<-exp(A5)
        #; Define Probability for

Each Score

        #; (Y=>1, Y=>2, Y=>3)
        P1<- C1/(1+C1) #;

Probability of Score=>1

        P2<- C2/(1+C2) #;

Probability of Score=>2

        P3<- C3/(1+C3) #;

Probability of Score=>3

        P4<- C4/(1+C4) #;

Probability of Score=>4

        P5<- C5/(1+C5) #;

Probability of Score=>5

        PR0<- 1-P1 # ;

Probability of Score=0

        PR1<- P1-P2 # ;

Probability of Score=1

        PR2<- P2-P3 # ;

Probability of Score=2

        PR3<- P3-P4 # ;

Probability of Score=3

        PR4<- P4-P5 # ;

Probability of Score=4

        PR5<- 1-

        (PR0+PR1+PR2+PR3+PR4)

        #MAKE DATA
        temp[j,1]<-data$ID[j]
        temp[j,2]<-data$DOSE[j]
        temp[j,3]<-data$TIME[j]
        temp[j,4]<-eta
        temp[j,5]<-MIXNUM
        test2<-runif(1,0,1)

```



```

0}
{temp[j,6]<-1}
{temp[j,6]<-2}
{temp[j,6]<-3}
test2>P5) {temp[j,6]<-4}
{temp[j,6]<-5}

if (test2>P1) {temp[j,6]<-
if (test2<=P1 && test2>P2)
if (test2<=P2 && test2>P3)
if (test2<=P3 && test2>P4)
if (test2<=P4 &&
if (test2<=P5)
temp[j,7]<-i

        oldid<-data[j,2]
    }

    BGSJ<-rbind(BGSJ,temp)
}

#get observed
ppcinc <-NULL
sum<-0
for (i in 1:400) {
    if (i==1) {oldid<- -1}
    if (data$ID[i]!=oldid) {ind<-0}
    if (data$DV[i]>0 && ind==0) {ind<-1
        sum<-sum+1
    }
    oldid<-data$ID[i]
}
ppcinc[1]<-sum
#Get simulated values
for (j in 1:50) {

    temp<-BGSJ[BGSJ[,7]==j,]
    sum<-0
    for (i in 1:400) {
        if (i==1) {oldid<- -1}
        if (temp[i,1]!=oldid) {ind<-0}
        if (temp[i,6]>0 && ind==0) {ind<-1
            sum<-sum+1
        }
        oldid<-temp[i,1]
    }
    ppcinc[j+1]<-sum

}

#Here is one way to make pictures your model passes this worthless check!
hist(ppcinc[2:51])
segments(ppcinc[1],0,ppcinc[1],20)

#PPC Number 3 Proportion with any AE>=2

#get observed
ppcinc2 <-NULL
sum<-0
for (i in 1:400) {
    if (i==1) {oldid<- -1}
    if (data$ID[i]!=oldid) {ind<-0}
    if (data$DV[i]>1 && ind==0) {ind<-1

```

```

sum<-sum+1
}

oldid<-data$ID[i]
}
ppcinc2[1]<-sum
#Get simulated values
for (j in 1:50) {

temp<-BGS[BGS[,7]==j,]
sum<-0
for (i in 1:400) {
if (i==1) {oldid<- -1}
if (temp[i,1]!=oldid) {ind<-0}
if (temp[i,6]>1 && ind==0) {ind<-1
sum<-sum+1
}

oldid<-temp[i,1]
}
ppcinc2[j+1]<-sum

}

hist(ppcinc2[2:51])
segments(ppcinc2[1],0,ppcinc2[1],20)

#The model does well here too!
##P>=2
ppcinc2 <-NULL
sum<-0
for (i in 1:400) {
if (i==1) {oldid<- -1}
if (data$ID[i]!=oldid) {ind<-0}
if (data$DV[i]>1 && ind==0) {ind<-1
sum<-sum+1
}

oldid<-data$ID[i]
}
ppcinc2[1]<-sum
#Get simulated values
for (j in 1:50) {

temp<-BGS[BGS[,7]==j,]
sum<-0
for (i in 1:400) {
if (i==1) {oldid<- -1}
if (temp[i,1]!=oldid) {ind<-0}
if (temp[i,6]>1 && ind==0) {ind<-1
sum<-sum+1
}

oldid<-temp[i,1]
}
ppcinc2[j+1]<-sum

}

hist(ppcinc2[2:51])
segments(ppcinc2[1],0,ppcinc2[1],20)
help(density)

####PPC 4 (Maximum Expected Score)
par(mfrow=c(2,2))
#get observed
data1<-data[data$DOSE==2,c(1:11)]

```

```

ppc3 <-NULL
coll<-NULL
maxsc<-0
sum<-0
for (i in 1:200) {
  if (i==1) {oldid<- 1001}
  #if new subject write max score for previous subject, reset
  maxscore
  if (data1$ID[i]!=oldid && i>1) {
    sum<-sum+1
    coll[sum]<-maxsc
    maxsc<-0
    oldid<-data1$ID[i]
  }
  if (data1$DV[i]>maxsc && data1$ID[i]==oldid) {
    maxsc<-data1$DV[i]
  }
  oldid<-data1$ID[i]
  #handle last subject
  if (i==200) {
    sum<-sum+1
    coll[sum]<-maxsc
  }
}
#the missing dv generates a character vector so change it to numeric
ppc3[1]<-mean(as.numeric(coll))
#Get simulated values
BGSH1<-BGSH[BGSH[,2]==2,]
for (j in 1:250) {
  temp<-BGSH1[BGSH1[,7]==j,]
  coll<-NULL
  maxsc<-0
  sum<-0
  for (i in 1:200) {
    if (i==1) {oldid<- 1001}
    if (temp[i,1]!=oldid && i>1) {
      sum<-sum+1
      coll[sum]<-maxsc
      maxsc<-0
      oldid<-temp[i,1]
    }
    if (temp[i,6]>maxsc && temp[i,1]==oldid) {
      maxsc<-temp[i,6]
    }
    oldid<-temp[i,1]
    #handle last subject
    if (i==200) {
      sum<-sum+1
      coll[sum]<-maxsc
    }
  }
  ppc3[1+j]<-mean(as.numeric(coll))
}
hist(ppc3[2:251], xlab="Max Score", col=6, main="Lorazepam Sleepiness")
segments(ppc3[1],0,ppc3[1],80)

```

```

#AUEC
#get observed
ppc4 <-NULL
coll<-NULL
auc<-0
sum<-0
#subset those with dose>0
data1<-data[data$DOSE>0,]
ul<-nrow(data1)
for (i in 1:ul) {
  if (i==1) {oldid<- 1001
             oldtime<-0
             oldae<-as.numeric(data1$DV[i])
             }
  #if new subject write auc for previous subject, reset auc
  if (data1$ID[i]!=oldid && i>1) {
    sum<-sum+1
    coll[sum]<-auc
    auc<-0
    oldid<-data1$ID[i]
  }
  if (data1$ID[i]==oldid && data1$TIME[i]>0) {
    auc<-
auc+1/2*(oldae+as.numeric(data1$DV[i]))*(data1$TIME[i]-oldtime)
  }

  oldid<-data1$ID[i]
  oldtime<-data1$TIME[i]
  oldae<-as.numeric(data1$DV[i])
  #handle last subject
  if (i==ul) {
    sum<-sum+1
    coll[sum]<-auc
  }
}
#the missing dv generates a character vector so change it to numeric
ppc4[1]<-mean(as.numeric(coll))
#Get simulated values
for (j in 1:250) {

  temp<-BGSH[BGSH[,7]==j,]
  temp1<-temp[temp[,2]>0,]
  coll<-NULL
  auc<-0
  sum<-0

  for (i in 1:ul) {
    if (i==1) {oldid<- 1001
              oldtime<-0
              oldae<-as.numeric(temp1[i,6])
              }
    if (temp1[i,1]!=oldid && i>1) {
      sum<-sum+1
      coll[sum]<-auc
      auc<-0
      oldid<-temp1[i,1]
    }

    if (temp1[i,3]>0 && temp1[i,1]==oldid) {
      auc<-
auc+1/2*(oldae+as.numeric(temp1[i,6]))*(temp1[i,3]-oldtime)
    }
  }
}

```

```

        oldid<-temp1[i,1]
        oldtime<-temp1[i,3]
        oldae<-temp1[i,6]
        #handle last subject
        if (i==ul) {
            sum<-sum+1
            coll[sum]<-auc
        }
    }
    ppc4[1+j]<-mean(as.numeric(coll))

}
hist(ppc4[2:251],xlab="AUEC", col=6)
segments(ppc4[1],0,ppc4[1],80)

par(mfrow=c(2,1))
#PI treatment

bill<-matrix(NULL,nrow=10,ncol=5)
#observed data first
data2<-data[data$DOSE>0,]
ul<-nrow(data2)
sum<-0
times<-unique(data2$TIME)
for (k in times) {
    data3<-data2[data2$TIME==k,]
    sum<-sum+1
    #populate times
    bill[sum,1]<-times[sum]
    #populate observed
    bill[sum,2]<-mean(as.numeric(data3$DV))
    #bill[sum,2]<-quantile(probs=0.5,as.numeric(data3$DV))
}

#now for simulations
#loop over studies
#j<-1
#make big matrix cols=time rows = simnum
store<-matrix(NULL,nrow=250,ncol=10)
for (j in 1:250) {temp<-BGS[BGS[,7]==j,]
    temp1<-temp[temp[,2]>0,]
    sum<-0
    for (k in times) {
        temp2<-temp1[temp1[,3]==k,]
        sum<-sum+1
        store[j,sum]<-mean(temp2[,6])
    }
}

#now combine results
#put mean of simulations in billshit
sum<-0
for (b in times) {
    sum<-sum+1
    bill[sum,3]<-mean(store[,sum])
    #bill[sum,3]<-quantile(probs=0.5,store[,sum])
}
}

```

```

#lower quantile
sum<-0
for (b in times) {
  sum<-sum+1
  bill[sum,4]<-quantile(probs=0.1,store[,sum])
}
#what could be more fun?
sum<-0
for (b in times) {
  sum<-sum+1
  bill[sum,5]<-quantile(probs=0.9,store[,sum])
}

# PI placebo
moe<-matrix(NULL,nrow=10,ncol=5)
#observed data first
data2<-data[data$DOSE==0,]
ul<-nrow(data2)
sum<-0
times<-unique(data2$TIME)
for (k in times) {
  data3<-data2[data2$TIME==k,]
  sum<-sum+1
  #populate times
  moe[sum,1]<-times[sum]
  #populate observed
  moe[sum,2]<-mean(as.numeric(data3$DV))
  #bill[sum,2]<-quantile(probs=0.5,as.numeric(data3$DV))
}

#now for simulations
#loop over studies
#j<-1
#make big matrix cols=time rows = simnum
store<-matrix(NULL,nrow=250,ncol=10)
for (j in 1:250) {temp<-BGSH[BGSH[,7]==j,]
  temp1<-temp[temp[,2]==0,]
  sum<-0
  for (k in times) {
    temp2<-temp1[temp1[,3]==k,]
    sum<-sum+1
    store[j,sum]<-mean(temp2[,6])
  }
}

#now combine results
#put mean of simulations in bill
sum<-0
for (b in times) {
  sum<-sum+1
  moe[sum,3]<-mean(store[,sum])
  #bill[sum,3]<-quantile(probs=0.5,store[,sum])
}

#lower quantile
sum<-0
for (b in times) {
  sum<-sum+1
  moe[sum,4]<-quantile(probs=0.1,store[,sum])
}

```

```

    }

#what could be more fun?
sum<-0
  for (b in times) {
    sum<-sum+1
    moe[sum,5]<-quantile(probs=0.9,store[,sum])

    }

  graphsheet()
  plot(bill[,1],bill[,2],type="n",xlab="Time", ylab="Observed SRDEQ Score and
  Prediction Intervals",ylim=c(0,4))
  points(bill[,1],bill[,2],col=1,type="p",pch=16)
  points(bill[,1],bill[,3],col=1,type="l")
  points(bill[,1],bill[,4],col=1,type="l")
  points(bill[,1],bill[,5],col=1,type="l")
  polygon(c(bill[,1], rev(bill[,1])), c(bill[,4], rev(bill[,5])),col=4,
  density=20)

  points(moe[,1],moe[,2],col=1,type="p")
  points(moe[,1],moe[,3],col=1,type="l")
  points(moe[,1],moe[,4],col=1,type="l")
  points(moe[,1],moe[,5],col=1,type="l")

  polygon(c(bill[,1], rev(bill[,1])), c(bill[,4], rev(bill[,5])),col=4,
  density=20)
  polygon(c(moe[,1], rev(moe[,1])), c(moe[,4], rev(moe[,5])),col=4, density=20)

  key(corner=c(1,1), text=list(c("Lorazepam Sleepiness","Placebo Sleepiness")),
  lines=list(type="p",col=1,pch=c(16,1),transparent=T, border=T))

```

APPENDIX G

Categorical dizziness simulation code (SPLUS)

```
#Get Micha Filter Junk
tab<-importData("micha2.txt", type="ASCII",stringsAsFactors=F)
tab2<-tab[tab$Col1==0,c(1:12)]
tab3<-tab2[tab2$Col2==0,c(1:12)]
tab32<-tab3[tab3$Col12!=0,]
tab4<-tab32[,c(4:12)]
#Get dummy
data<-importData("dummy2.csv", type="ASCII",stringsAsFactors=F)
nr<-nrow(data)
names(data)<-c("STUD", "ID", "DOSE", "TIME", "DV", "MDV", "ICL", "IV1", "IKA",
  "IQ", "IV2")
BGSH<-NULL
#loop over micha
#LEVEL=STUDY
for (i in 1:350){

  #i<-10
  #Get row i of micha
  vec<-tab4[i,]
  names(vec)<-
c("th1", "th2", "th3", "th4", "th5", "th6", "th7", "th8", "om11")
  temp<-matrix(NULL,ncol=7,nrow=400)
  for (j in 1:nr) {
    if (j==1) {oldid<- -1}
    #subject level stuff
    if (data[j,2]!=oldid) {
      test1<-runif(1,0,1)
      eta<-
rnorm(1,0,sd=sqrt(vec$om11))
      }
      #j<-1
      K10<-
      data$ICL[j]/data$IV1[j]
      K12<-
      data$IQ[j]/data$IV1[j]
      K21<-
      data$IQ[j]/data$IV2[j]
      KKK1<- (K12 + K21 + K10)
      KKK2<- K21*K10
      ALPH <- (KKK1+(KKK1**2-
4*KKK2)**0.5)/2
      BETA<- (KKK1-(KKK1**2-
4*KKK2)**0.5)/2
      TI<- data$TIME[j]
      if (TI<=0) { TI==0}
      AAA<-
      data$IKA[j]*data$DOSE[j]*1000/data$IV1[j]
      BBB <- (K21-ALPH)/((ALPH-
BETA)*(ALPH-data$IKA[j]))
      CCC <- (BETA-K21)/((ALPH-
BETA)*(BETA-data$IKA[j]))
```



```

DDD <- (K21-
data$IKA[j])/((ALPH-data$IKA[j])*(BETA-data$IKA[j]))
CONC<- AAA*(BBB*exp(-
ALPH*TI)+CCC*exp(-BETA*TI)+DDD*exp(-data$IKA[j]*TI))
SLOPE<-vec$th1
DRUG<-SLOPE*CONC
PLAC<-
as.numeric(test1<=vec$th6)*0+as.numeric(test1>vec$th6)*vec$th5*(exp(-
vec$th7*data$TIME[j])-exp(-vec$th8*data$TIME[j]))
MIXNUM<-
as.numeric(test1>vec$th6)+1

B1<-vec$th2
B2<- B1 + vec$th3
B3<- B2 + vec$th4
# ; Define logits for

# ; (Y=>1, Y=>2)
A1<- B1 + DRUG +PLAC+eta
A2<- B2 + DRUG +PLAC+eta
A3<- B3 + DRUG +PLAC+eta

C1<-exp(A1)
C2<-exp(A2)
C3<-exp(A3)
#; Define Probability for

#; (Y=>1, Y=>2, Y=>3)
P1<- C1/(1+C1) #;
P2<- C2/(1+C2) #;
P3<- C3/(1+C3) #;
PR0<- 1-P1 # ;
PR1<- P1-P2 # ;
PR2<- P2-P3 # ;
PR3<- 1-(PR0+PR1+PR2)
#Make data
temp[j,1]<-data$ID[j]
temp[j,2]<-data$DOSE[j]
temp[j,3]<-data$TIME[j]
temp[j,4]<-eta
temp[j,5]<-MIXNUM
test2<-runif(1,0,1)
if (test2>P1)
{temp[j,6]<-0}
if (test2<=P1 && test2>P2)
{temp[j,6]<-1}
if (test2<=P2 && test2>P3)
{temp[j,6]<-2}
if (test2<=P3)
{temp[j,6]<-3}
temp[j,7]<-i

oldid<-data[j,2]
}

BGSH<-rbind(BGSH,temp)
}

```

```

#PPC Number 3 Proportion with any AE

#get observed
ppcinc <-NULL
sum<-0
for (i in 1:400) {
  if (i==1) {oldid<- -1}
  if (data$ID[i]!=oldid) {ind<-0}
  if (data$DV[i]>0 && ind==0) {ind<-1
                              sum<-sum+1
                              }
  oldid<-data$ID[i]
}
ppcinc[1]<-sum
#Get simulated values
for (j in 1:50) {

  temp<-BGS[BGS[,7]==j,]
  sum<-0
  for (i in 1:400) {
    if (i==1) {oldid<- -1}
    if (temp[i,1]!=oldid) {ind<-0}
    if (temp[i,6]>0 && ind==0) {ind<-1
                                sum<-sum+1
                                }
    oldid<-temp[i,1]
  }
  ppcinc[j+1]<-sum

}
#Here is one way to make pictures your model passes this worthless check!
hist(ppcinc[2:51])
segments(ppcinc[1],0,ppcinc[1],20)

#PPC Number 3 Proportion with any AE>=2

#get observed
ppcinc2 <-NULL
sum<-0
for (i in 1:400) {
  if (i==1) {oldid<- -1}
  if (data$ID[i]!=oldid) {ind<-0}
  if (data$DV[i]>1 && ind==0) {ind<-1
                              sum<-sum+1
                              }
  oldid<-data$ID[i]
}
ppcinc2[1]<-sum
#Get simulated values
for (j in 1:50) {

  temp<-BGS[BGS[,7]==j,]
  sum<-0
  for (i in 1:400) {
    if (i==1) {oldid<- -1}
    if (temp[i,1]!=oldid) {ind<-0}
    if (temp[i,6]>1 && ind==0) {ind<-1
                                sum<-sum+1
                                }
    oldid<-temp[i,1]
  }
  ppcinc2[j+1]<-sum
}

```

```

    }
hist(ppcinc2[2:51])
segments(ppcinc2[1],0,ppcinc2[1],20)

#The model does well here too!

#PPC Number ? Average (over subjects) maximum (within subject) score

#get observed

  #get observed
data1<-data[data$DOSE==2,c(1:11)]
ppc3 <-NULL
coll<-NULL
maxsc<-0
sum<-0
for (i in 1:200) {
  if (i==1) {oldid<- 1001}
  #if new subject write max score for previous subject, reset
  maxscore
  if (data1$ID[i]!=oldid && i>1) {
    sum<-sum+1
    coll[sum]<-maxsc
    maxsc<-0
    oldid<-data1$ID[i]
  }
  if (data1$DV[i]>maxsc && data1$ID[i]==oldid) {
    maxsc<-data1$DV[i]
  }

  oldid<-data1$ID[i]
  #handle last subject
  if (i==200) {
    sum<-sum+1
    coll[sum]<-maxsc
  }
}
#the missing dv generates a character vector so change it to numeric
ppc3[1]<-mean(as.numeric(coll))
#Get simulated values
BGSH1<-BGSH[BGSH[,2]==2,]
for (j in 1:300) {

  temp<-BGSH1[BGSH1[,7]==j,]
  coll<-NULL
  maxsc<-0
  sum<-0

  for (i in 1:200) {
    if (i==1) {oldid<- 1001}
    if (temp[i,1]!=oldid && i>1) {
      sum<-sum+1
      coll[sum]<-maxsc
      maxsc<-0
      oldid<-temp[i,1]
    }
    if (temp[i,6]>maxsc && temp[i,1]==oldid) {
      maxsc<-temp[i,6]
    }

    oldid<-temp[i,1]
  }
}

```

```

        #handle last subject
        if (i==200) {
            sum<-sum+1
            coll[sum]<-maxsc
        }
    }
    ppc3[1+j]<-mean(as.numeric(coll))

}
hist(ppc3[2:301], xlab="Max Score", col=6, main="Lorazepam Dizziness")
segments(ppc3[1],0,ppc3[1],80)

#PPC Number ? average AUC (over subjects)

#get observed
ppc4 <-NULL
coll<-NULL
auc<-0
sum<-0
#subset those with dose>0
data1<-data[data$DOSE>0,]
ul<-nrow(data1)
for (i in 1:ul) {
    if (i==1) {oldid<- 1001
                oldtime<-0
                oldae<-as.numeric(data1$DV[i])
            }
    #if new subject write auc for previous subject, reset auc
    if (data1$ID[i]!=oldid && i>1) {
        sum<-sum+1
        coll[sum]<-auc
        auc<-0
        oldid<-data1$ID[i]
    }
    if (data1$ID[i]==oldid && data1$TIME[i]>0) {
        auc<-
        auc+1/2*(oldae+as.numeric(data1$DV[i]))*(data1$TIME[i]-oldtime)
    }

    oldid<-data1$ID[i]
    oldtime<-data1$TIME[i]
    oldae<-as.numeric(data1$DV[i])
    #handle last subject
    if (i==ul) {
        sum<-sum+1
        coll[sum]<-auc
    }
}
#the missing dv generates a character vector so change it to numeric
ppc4[1]<-mean(as.numeric(coll))
#Get simulated values
for (j in 1:300) {

    temp<-BGS[BGS[,7]==j,]
    temp1<-temp[temp[,2]>0,]
    coll<-NULL
    auc<-0
    sum<-0

    for (i in 1:ul) {

```

```

        if (i==1) {oldid<- 1001
                    oldtime<-0
                    oldae<-as.numeric(temp1[i,6])
                }
        if (temp1[i,1]!=oldid && i>1) {
                    sum<-sum+1
                    coll[sum]<-auc
                    auc<-0
                    oldid<-temp1[i,1]
                }
        if (temp1[i,3]>0 && temp1[i,1]==oldid) {
                    auc<-
auc+1/2*(oldae+as.numeric(temp1[i,6]))*(temp1[i,3]-oldtime)
                }

        oldid<-temp1[i,1]
        oldtime<-temp1[i,3]
        oldae<-temp1[i,6]
        #handle last subject
        if (i==ul) {
            sum<-sum+1
            coll[sum]<-auc
        }
    }
    ppc4[1+j]<-mean(as.numeric(coll))

}
hist(ppc4[2:301],xlab="AUEC", col=6)
segments(ppc4[1],0,ppc4[1],80)

#PIs ## Treatment

bill<-matrix(NULL,nrow=10,ncol=5)
#observed data first
data2<-data[data$DOSE>0,]
ul<-nrow(data2)
sum<-0
times<-unique(data2$TIME)
for (k in times) {
    data3<-data2[data2$TIME==k,]
    sum<-sum+1
    #populate times
    bill[sum,1]<-times[sum]
    #populate observed
    bill[sum,2]<-mean(as.numeric(data3$DV))
    #bill[sum,2]<-quantile(probs=0.5,as.numeric(data3$DV))
}

#now for simulations
#loop over studies
#j<-1
#make big matrix cols=time rows = simnum
store<-matrix(NULL,nrow=300,ncol=10)
for (j in 1:300) {temp<-BGSH[BGSH[,7]==j,]
    temp1<-temp[temp[,2]>0,]
    sum<-0
    for (k in times) {
        temp2<-temp1[temp1[,3]==k,]
        sum<-sum+1
    }
}

```

```

                                store[j,sum]<-mean(temp2[,6])
                                }
                                }
#now combine results
#put mean of simulations in bill
sum<-0
for (b in times) {
    sum<-sum+1
    bill[sum,3]<-mean(store[,sum])
    #bill[sum,3]<-quantile(probs=0.5,store[,sum])

}

#lower quantile
sum<-0
for (b in times) {
    sum<-sum+1
    bill[sum,4]<-quantile(probs=0.1,store[,sum])

}

sum<-0
for (b in times) {
    sum<-sum+1
    bill[sum,5]<-quantile(probs=0.9,store[,sum])

}

### PI placebo
moe<-matrix(NULL,nrow=10,ncol=5)
#observed data first
data2<-data[data$DOSE==0,]
ul<-nrow(data2)
sum<-0
times<-unique(data2$TIME)
for (k in times) {
    data3<-data2[data2$TIME==k,]
    sum<-sum+1
    #populate times
    moe[sum,1]<-times[sum]
    #populate observed
    moe[sum,2]<-mean(as.numeric(data3$DV))
    #bill[sum,2]<-quantile(probs=0.5,as.numeric(data3$DV))

}

#now for simulations
#loop over studies
#j<-1
#make big matrix cols=time rows = simnum
store<-matrix(NULL,nrow=300,ncol=10)
for (j in 1:300) {temp<-BGS[BGS[,7]==j,]
    temp1<-temp[temp[,2]==0,]
    sum<-0
    for (k in times) {
        temp2<-temp1[temp1[,3]==k,]
        sum<-sum+1
        store[j,sum]<-mean(temp2[,6])
    }

}

```

```

#now combine results
#put mean of simulations in bill
sum<-0
for (b in times) {
  sum<-sum+1
  moe[sum,3]<-mean(store[,sum])
  #bill[sum,3]<-quantile(probs=0.5,store[,sum])

}

#lower quantile
sum<-0
for (b in times) {
  sum<-sum+1
  moe[sum,4]<-quantile(probs=0.1,store[,sum])

}

#what could be more fun?
sum<-0
  for (b in times) {
    sum<-sum+1
    moe[sum,5]<-quantile(probs=0.9,store[,sum])

  }

  graphsheet()
  plot(bill[,1],bill[,2],type="n",xlab="Time", ylab="Observed and Prediction
Intervals",ylim=c(0,4))
points(bill[,1],bill[,2],col=1,type="p",pch=16)
points(bill[,1],bill[,3],col=1,type="l")
points(bill[,1],bill[,4],col=1,type="l")
points(bill[,1],bill[,5],col=1,type="l")
polygon(c(billshit[,1], rev(bill[,1])), c(bill[,4], rev(bill[,5])),col=4,
density=20)
lines=list(type="p",col=1,pch=c(1,16),transparent=T, border=T)

points(bill[,1],moe[,2],col=1,type="p")
points(bill[,1],moe[,3],col=1,type="l")
points(bill[,1],moe[,4],col=1,type="l")
points(bill[,1],moe[,5],col=1,type="l")

polygon(c(bill[,1], rev(bill[,1])), c(moe[,4], rev(moe[,5])),col=4, density=20)
key(corner=c(1,1), text=list(c("Lorazepam Dizziness","Placebo Dizziness")),
lines=list(type="p",col=1,pch=c(16,1),transparent=T, border=T))

#stop here

```

Appendix H

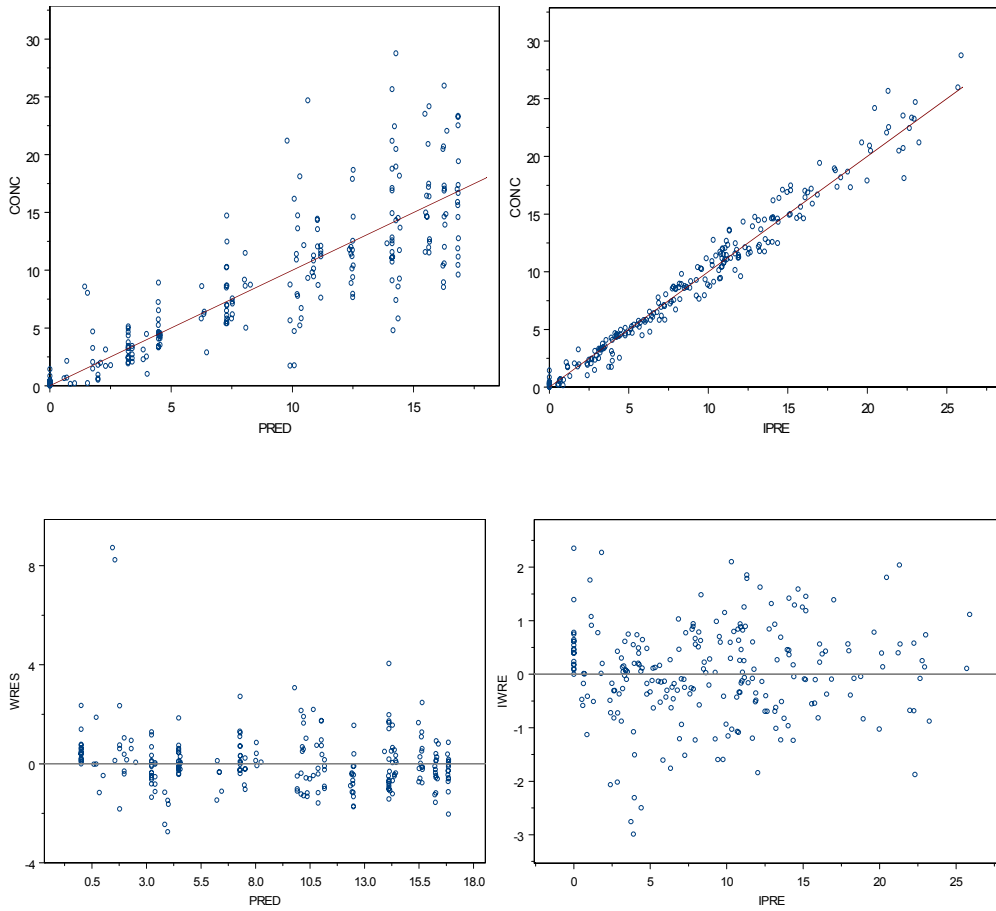
Table of final PK parameter estimates of four study CNS drugs

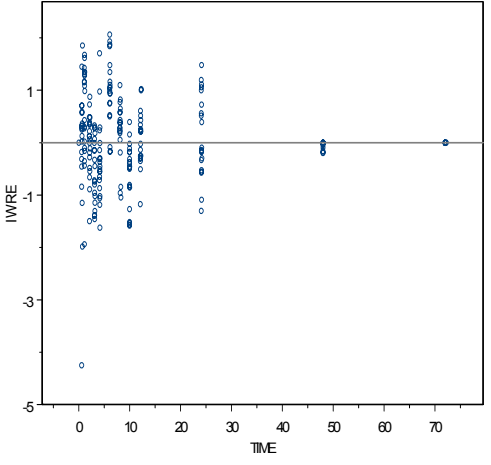
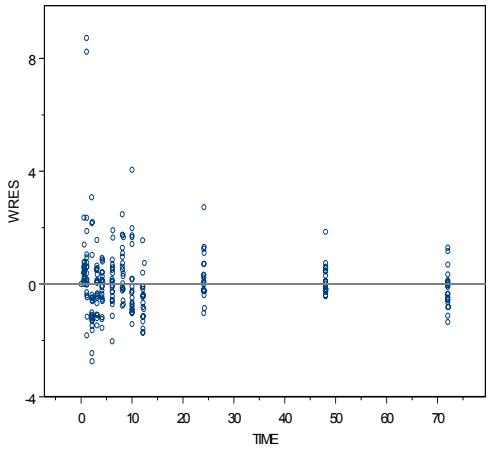
| Drug | Parameter | Mean | 95% CI | HV(%CV) | 95% CI |
|--------------------|-----------------------|-------------|---------------|----------------|---------------|
| Olanzapine | | | | | |
| | CL/F (L/min) | 13.4 | 11.26-15.54 | 22 | |
| | V1/F (L) | 321 | 227.6-414.4 | 80.7 | |
| | V2/F (L) | 684 | 511.2-856.8 | 44.6 | |
| | Ka (h ⁻¹) | 0.12 | .091-0.15 | | |
| | Q (L/min) | 33.2 | 28.32-38.08 | 18.8 | |
| | Tlag (h) | 0.94 | 0.87-1.01 | | |
| Lorazepam | | | | | |
| | CL/F (L/min) | 4.02 | 3.55 - 4.45 | 25.6 | 12.2 - 39 |
| | V1/F (L) | 26.3 | 19.12 - 33.48 | 34.1 | 13.6 - 54.6 |
| | V2/F (L) | 58.4 | 52.1 - 64.7 | | |
| | Ka (h ⁻¹) | 0.5 | 0.34 - 0.66 | 13.3 | 6 - 20.6 |
| | Q (L/min) | 16.4 | 13.92 - 18.88 | | |
| Paroxetine | | | | | |
| | CL/F (L/min) | 96.6 | | 65 | |
| | V1/F (L) | 1200 | | 19 | |
| | Ka (h ⁻¹) | 0.14 | | 59 | |
| | Tlag (h) | 0.46 | | | |
| Atomoxetine | | | | | |
| | CL/F (L/min) | 26.4 | 21.94-30.86 | 36.3 | 16.5-56.1 |
| | V1/F (L) | 134 | 115.04-152.96 | 16 | 3.7-28.3 |
| | Ka (h ⁻¹) | 3.16 | 1.31-5.01 | 108.6 | 36.4-180.8 |

Appendix I

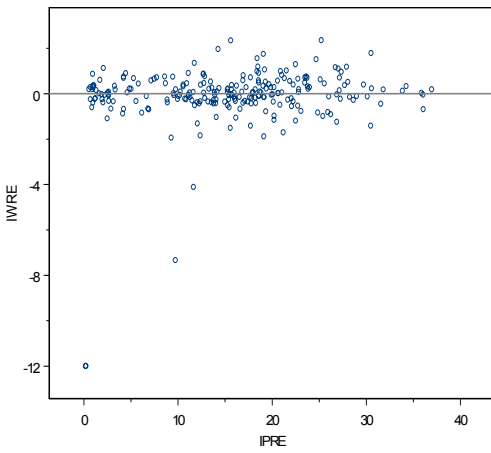
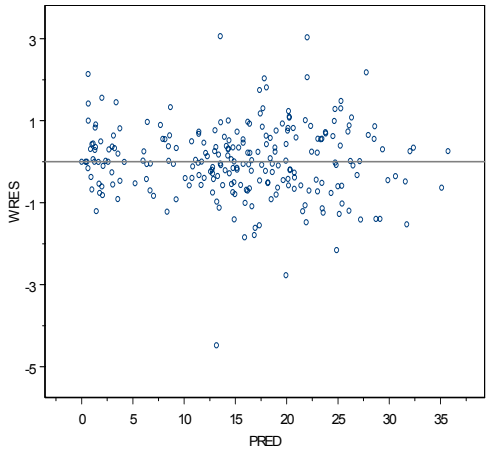
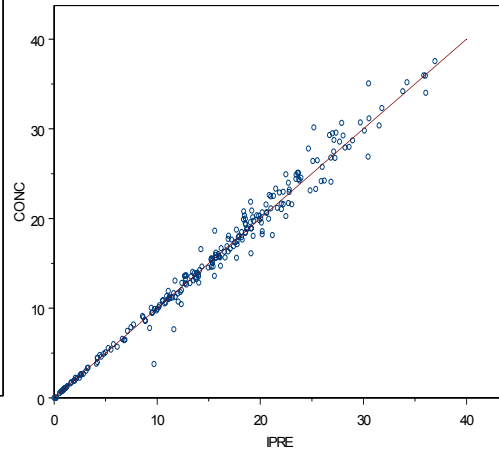
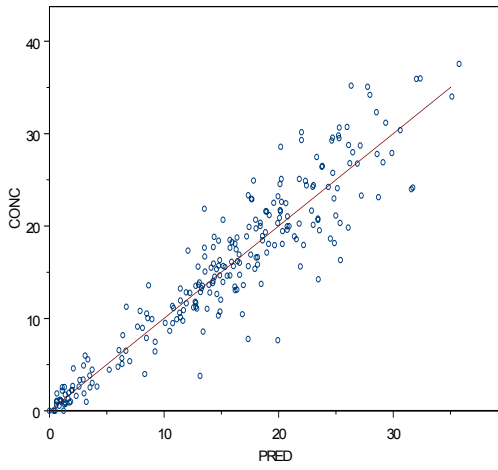
PK model goodness-of-fit plots

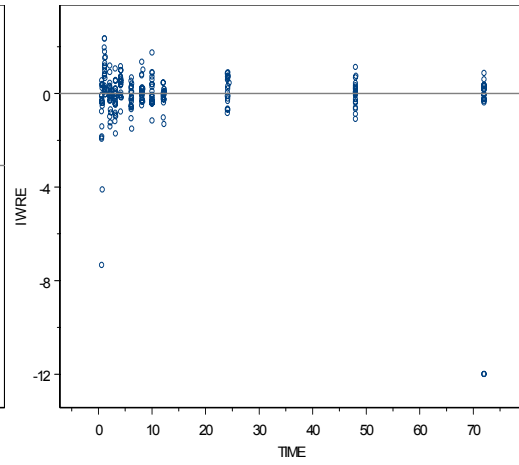
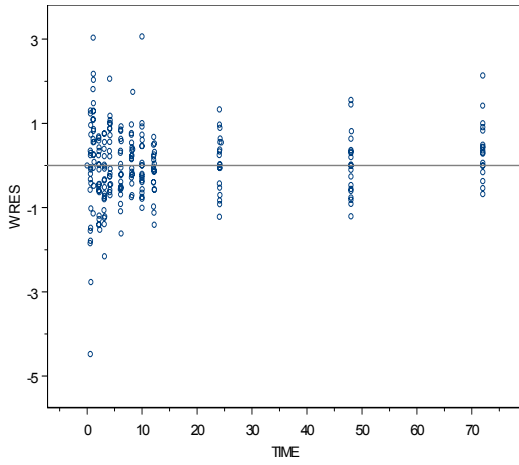
A. Olanzapine



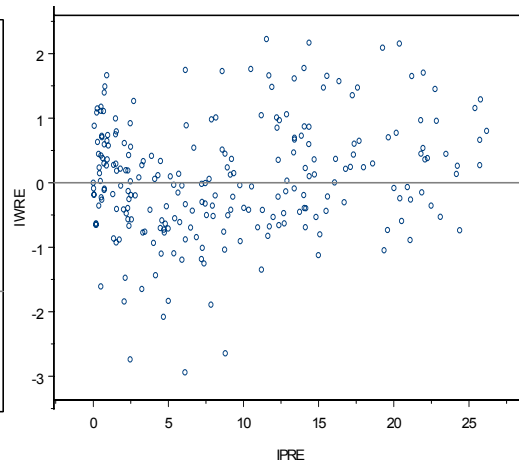
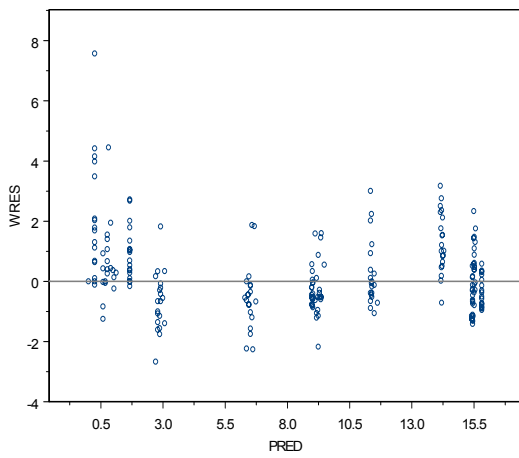
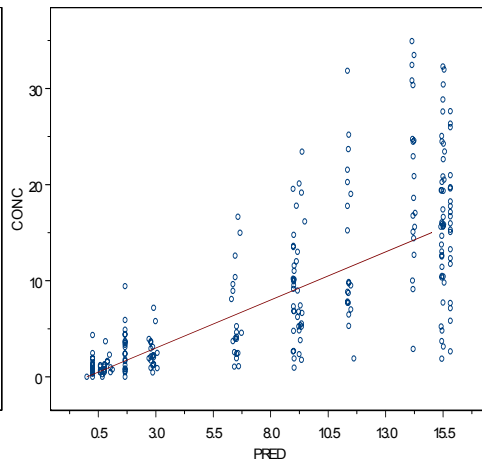
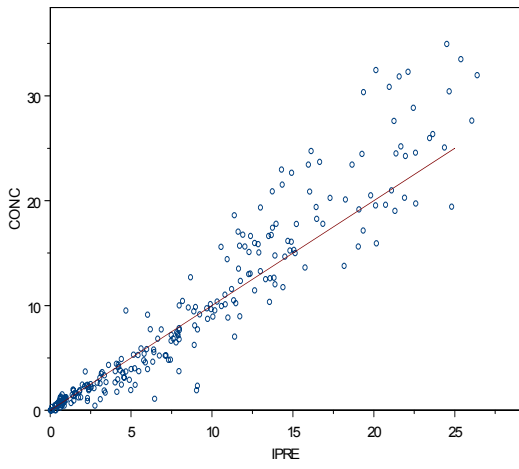


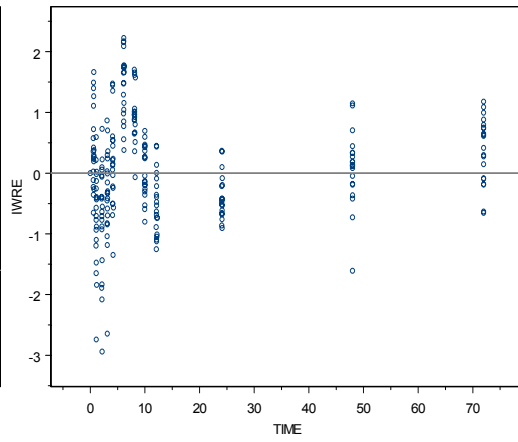
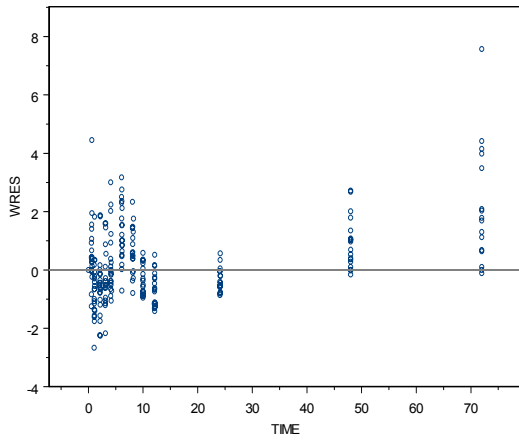
B. Lorazepam





C. Paroxetine





D) Atomoxetine

